PHOTOMETRIC AND FUNDAMENTAL PLANE STUDIES OF GALAXIES

Thesis submitted to
Cochin University of Science and Technology
in partial fulfillment of the requirements
for the award of the degree of

DOCTOR OF PHILOSOPHY

Ravikumar C D
Department of Physics
Cochin University of Science and Technology
Kochi - 682022

April 2004

If we knew what it was we were doing, it would not be called research, would it?
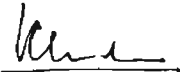
Albert Einstein

Dedicated to Amma, Achan & Ajit.

CERTIFICATE

Certified that the work presented in this thesis is a bonafide work done by Mr. Ravikumar C D, under my guidance in the Department of Physics, Cochin University of Science and Technology and that this work has not been included in any other thesis submitted previously for the award of any degree.
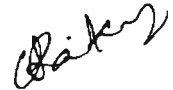
Kochi

April 15, 2004

Dr. V. C. Kuriakose

(Supervising Guide)

DECLARATION

I hereby declare that the work presented in this thesis is based on the original work done by me under the guidance of Dr. V. C. Kuriakose, Professor, Department of Physics, Cochin University of Science and Technology and has not been included in any other thesis submitted previously for the award of any degree.

Kochi

April 15, 2004

Ravikumar C D

Contents

List of Figures

List of Tables

Acknowledgements

From my childhood days I was charmed by the beauty of starry nights and was lead to the wonderful world of constellations and stories related to that. During my graduate studies, this 'attraction' towards the heavenly bodies were shaping into a deep desire to do research in Astrophysics and was very lucky to get an opportunity to work with Professor Kuriakose after my MSc. His timely advice and able guidance coupled with deep thinking were always encouraging and supportive. I remain deeply indebted to him for all that I could learn from him.

Right from the very first visit, my association with IUCAA had immensely benefitted me. Let me take this opportunity to express my deep sense of gratitude to Professor Ajit Kembhavi, who took a keen personal interest in moulding the study carried out in this thesis. I am deeply indebted to him for his excellent guidance and support I enjoyed during my PhD. I would also like to express my gratitude to Mrs. Asha Kembhavi and Anirudh Kembhavi for their affection and warm hospitality extended to me during my 'many extended visits' at IUCAA. It was during one of such visits Parihar and Yogesh introduced me to the world of galaxies and the data reduction using IRAF and many thanks to both of them for their enthusiasm and patience shown towards me. Interactions with M. K. Patil also helped me a lot in understanding the intricacies involved in the data

reduction.

I wish to thank Professor Dadhich, Director, IUCAA for his kind words and the personal interest he had shown towards me. Many thanks to Professor J.V Narlikar, former Director, for his kind encouragement. I would like to thank Professors Sanjeev Dhurandhar and T. Padmanabhan for the many discussions during my PhD. Special thanks to Srianand, Ramaprakash and Ranjeev for always providing a helping hand (or two!), be it a problem on science or sports or trekking! Words are insufficient to express my gratitude to my dear friends Sudhanshu, Anand, Jatush, Param, Anoop, Nandan, Niranjan, Ujjaini, Atul, Ahuja, Abhishek, Ali, Amir and others for the warm and cordial friendship extended to me. The excellent computing and library facilities at IUCAA were really a boon for carrying out my thesis work. Many special thanks to Sarah, Anjali, Manisha, Neelam, Neelima, Hemand, Sandeep, Vijay and Sasikant for all their helps. I would also like to thank Lata, Ratna, Susan and Rajesh for their help and hospitality making my stay at IUCAA really pleasant. Once again, I thank all at IUCAA for their memorable association with me during my PhD.

My sincere thanks to Professor B. Mobasher, for providing data upon which this thesis is based, and for his suggestions and inspiring discussions at various stages of this work. I would also like to acknowledge the many fruitful discussions with Professors S. K. Pandey, Tushar Prabhu, G. C. Anupama, U. C. Joshi and Mark Whittle which helped me understand things better.

Let me express my sincere thanks to Professor K. P. Vijayakumar, Head of the Department of Physics (DoP) and to Professors and former Heads of DoP, Babu Joseph, Sabir, Rajappan Nair and Elizabeth Mathai for kindly providing the necessary facilities for my research work. Many thanks are also due to Dr. Ramesh Babu, Dr. M. R. Anantharaman, Dr. B. Pradeep and Dr. S. Jayalekshmi for the lively discussions they shared with me. I

Ravikumar C D

Preface

Determining the morphological parameters that describe galaxies has always been a challenging task. The studies on the correlations between different photometric as well as spectroscopic parameters of the galaxies help in understanding their structure, properties of the stars and gas which constitute the galaxy, the various physical and chemical processes which determine the properties, and galaxy formation and evolution. In the last few decades, the advent of Charge Coupled Devices (CCDs) and near infrared arrays have provided quick and reliable digitized data acquisition, in the optical and near infrared bands. This has provided an avalanche of data, which can be processed using sophisticated image analysis techniques to obtain information about the morphology of galaxies. The photometric analysis performed in this thesis involve the extraction of structural parameters of early type galaxies imaged in the near infrared K (2.2μm) band, obtaining correlations between these parameters and using them to constrain the large scale properties of galaxies.

Chapter 1 starts with a general introduction to galaxies. The various classification schemes used to characterise different types of elliptical, spiral, lenticular and irregular galaxies, along with the theories proposed for their formation and evolution are described briefly there.

Chapter 2 deals with the surface brightness analysis of galaxies. In general, a galaxy contains two distinct components; a spheroidal bulge and a circular flattened disk of stars. In the case of elliptical galaxies the bulge dominates the disk. We describe in this chapter Fourier techniques which are used to obtain model independent surface brightness profiles along the major axis of galaxies, and present examples of the application of the technique to ellipticals. We consider various descriptions of brightness profiles, like the de Vaucouleurs and Sersic laws, and King's models which have been used for elliptical galaxies and the bulges of spiral galaxies. We then consider the brightness distributions of disks of spiral galaxies, and bulge-to-disk ratios and other such parameters which are important for the phenomenological descriptions of the large scale structure of galaxies.

We then move to discuss the two dimensional bulge disk decomposition algorithm, *fitgal*, which we have used in our work to determine the photometric parameters that describe the galaxy. The method involves building two dimensional image models that conform to the observed light profiles and comparing these with observed images of galaxies. For the simulation of galaxy images, the projected bulge component is represented either by the de Vaucouleurs' law or by the more general Sersic law. The surface brightness profile for the disk component, is assumed to be exponential. The accuracy and reliability of the procedure is discussed at the end of this chapter.

We next describe the data and observation for our sample in **Chapter 3**. The galaxies in this sample were observed earlier using the United Kingdom Infra-red Telescope (UKIRT). K band images for 21 galaxies from Abell 2199 and 17 galaxies from Abell 2634 were obtained, using 256×256 infra-red array detector with a total exposure time of nine minutes for each galaxy have been made available to us. In this chapter we determine the morphological parameters for the galaxies in our sample assuming de

Vaucouleurs' law to the surface brightness profiles. Detailed study on the quality of the fit suggests that not all galaxies in our sample is represented by de Vaucouleurs law. The famous correlations Kormendy, Faber-Jackson and fundamental plane relations are obtained for this sample. Comparison with similar studies showed that these planar relations are indistinguishable from that obtained for a sample of ellipticals in Coma cluster. Finally we proceed further to determine the dependence of M/L on the structural parameters, using the fundamental plane.

In **Chapter 4** we have determined the structural parameters assuming the Sersic law to the surface brightness profiles. By comparing the fits, we show that using the Sersic law provides better fits to the observed light distribution of the bulges than the de Vaucouleurs law. We also show assuming the structural homology, which is usually done by fixing a de Vaucouleurs law surface brightness profile to the galaxy, actually causes systematic and serious under- or over-estimation of the structural parameters.

We further explore the various correlations that have been reported in the literature with the specific interest to see whether there is any deviations induced by the assumption of homology in the luminosity distribution (i. e. , using de Vaucouleurs profiles for all galaxies). We examine the Faber-Jackson, Kormendy and the fundamental plane (FP) relations and we note that though the assumption of de Vaucouleurs profiles causes systematic, and sometimes serious, under or over-estimation of parameters, that is not reflected in these correlations, at least for this sample. The FP relation is studied in detail for environmental effects and for determining the dependence of mass-to-light (M/L) ratio on the structural parameters.

In **Chapter 5** we use the parameters extracted from the Sersic fits to obtain the photometric plane (PP) for our sample. We then explore the possibility of a correlation between the Sersic index n and central velocity dispersion σ for the galaxies. We find that there is no significant $n - \sigma$ cor-

relation for our sample. We also find that deviations from the photometric plane correlates well with the central velocity dispersion showing that there exists a hyper plane (HP) involving the four parameters that define the FP and PP. The existence of such an hyper plane has not been reported earlier and is a major result of this thesis.

We then show that the two lower dimensional planes, FP and PP can be derived from this hyper plane. We also show that the PP forms a simple projection of the hyper plane, in which the displacements along the $\log \sigma$ axis is not taken in to account of. The difference in the surface brightness term used in FP and HP, makes the comparative study a little difficult. However, we hope the smaller scatter in the HP, will be useful in simulations intending to study the formation and evolution of early type galaxies. We then deduce the dependence of M/L on Sersic parameter n along with other structural parameters.

We note that the bulges of spiral galaxies obey the same FP and HP for ellipticals, at least in the local Universe. The velocity dispersion, unlike the photometric parameters, becomes really difficult to measure for distant galaxies. Hence we explore the possibility of predicting velocity dispersion, from FP and HP. From the calculated velocity dispersions we further predict the mass of the super-massive black holes present in the cores of these galaxies. This estimation of the mass of the black hole is an indirect method but has the advantage of being faster as no spectroscopy is involved.

In Chapter 6 we discuss the main results and conclusion of this thesis. Future plans for the extension of this work are also mentioned in this chapter.

List of papers published/presented/communicated:

1. Presented a paper titled 'Disks in elliptical galaxies', at the 25th International School for Young Astronomers' held at Chiang Mai University, Chiang Mai, Thailand, during January 3-22, 2001.

2. Presented a paper on 'Systematics in Galaxies' at the IUCAA workshop on 'Structure and Dynamics of Galaxies' held at Pt. Ravishankar Shukla University, Raipur during September 27-30, 2001.

3. Presented a paper at Inter University Centre for Astronomy and Astrophysics (IUCAA), Pune on 'Clusters of Galaxies', on the occasion of National Science Day, on February 28, 2002.

4. Presented a paper on 'Estimation of super-massive black holes across the Hubble sequence', at the International Conference on Gravitation and Cosmology (ICGC-2004) held at Cochin University of Science & Technology, Kochi, India, during January 5-10, 2004.

5. 'The Hyper Plane for early type galaxies', C D Ravikumar, A Kembhavi, B Mobasher and V C Kuriakose. (Submitted to APJL).

6. Photometry of E and S0 galaxies in Abell 2199 & 2634-Data and bulge-disk decomposition results', C D Ravikumar, A Kembhavi, B Mobasher and V C Kuriakose. (To be communicated)

7. 'Fundamental plane for early type galaxies in Abell 2199 and 2634', B Mobasher, C D Ravikumar, A Kembhavi and V C Kuriakose. (To be submitted).

Chapter 1

Introduction and Thesis Outline

Galaxies are the basic building blocks of the Universe containing vast collection of stars that are held together by mutual gravitational attraction. Apart from stars, which form the bulk of .ts luminous matter, a galaxy consists of gas and dust. Some galaxies contain at their centers, bright point-like objects called active galactic nuclei (AGNs). An AGN can, in some extreme cases, become so bright that it even out-shines the host galaxy itself. Various recent observations provide evidence to suggest that almost all galaxies contain a supermassive black hole at their centers. There are many reasons to believe that the luminous mass in a galaxy is only a small fraction of its total gravitating mass. The unseen mass, the nature of which is yet to be known, is termed as the dark matter. In this chapter we provide a general introduction to the subject matter of the thesis, surface photometry of galaxies, starting with a description of early observations on galaxies and their classification by Hubble. Then we discuss briefly a few

galaxy formation and evolution scenarios in relation to the observations. We conclude this chapter by giving a broad outline of the thesis.

1.1   Detection of Galaxies

The French astronomer Charles Messier first noticed in 1780 fuzzy and patchy extended objects in the night sky. He called them *nebulae*, many of which were later identified as galaxies, and constructed a catalogue of 103 members. Later the German born English astronomer William Herschel built a 4-ft aperture reflecting telescope (the largest at that time) and using it, he and his sister Caroline made a catalogue of more than 2000 nebulae. His son John expanded and compiled this into the *General Catalogue* in 1864. Since observations were not able to resolve any structure present in these galaxies, they were not given the status of isolated systems but were considered as part of our own *Milky Way*. Later observations using photographic imaging revealed many features of galaxies. Studying the luminosity variations of Cepheid stars in the outer regions of the Andromeda Nebula, Hubble (1922) was able to show that the distance to the nebula was many times larger than the known extent of the Milky Way and established that the nebula had size and luminosity comparable to the Milky Way, and led to the understanding that galaxies are stellar systems comparable to the Milky Way. Slipher (1914) first reported the existence of *redshift* in the wavelengths of the absorption lines in the spectra of galaxies. Hubble (1929) investigated this effect further and discovered that almost all galaxies in his sample were receding from us, with velocities proportional to the distance to them. This led to the idea of an expanding Universe.
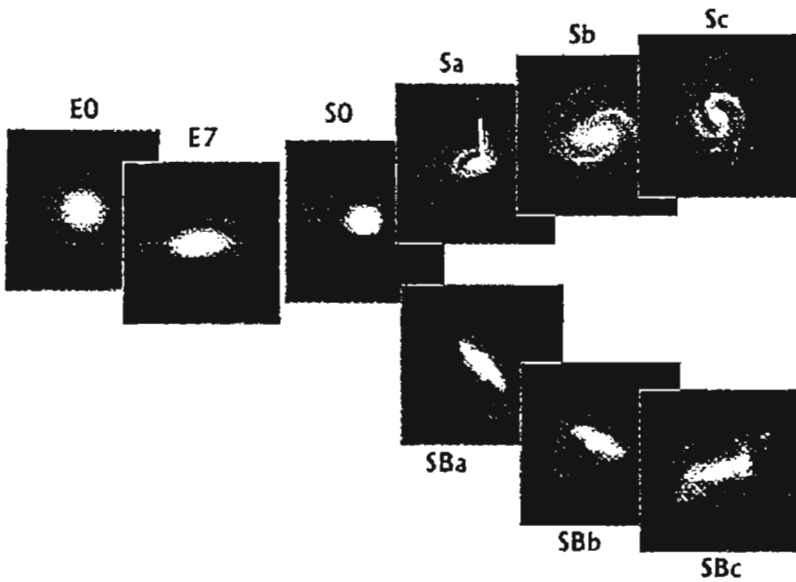
Figure 1.1: Hubble's classification of galaxies. The ellipticals and lenticulars are shown edge-on while the spirals are shown face-on. Source: http://www.astro.princeton.edu/~frei/Gcat_htm.

1.2   Classification of Galaxies

In the 1930s Hubble introduced his classification scheme for galaxies based on their apparent morphology, which is still used today, with some modifications. Hubble recognised three main classes of galaxies: ellipticals, lenticulars and spirals. Galaxies that would not fit in these main types were considered as irregulars. The simple form of his classification is shown in Figure 1.1. When Hubble proposed his classification scheme (Hubble 1926, 1930, 1936), he thought that it might represent an evolutionary sequence with galaxies evolving from ellipticals to form spirals. But for various rea-
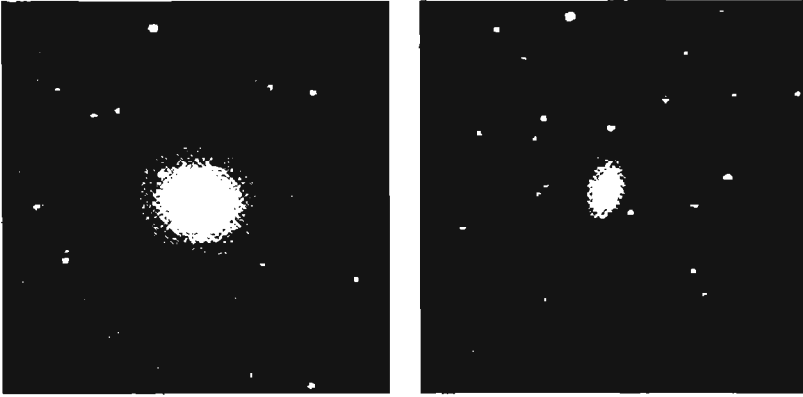
Figure 1.2: Appearance of elliptical galaxies: the galaxy M105 on the left is an example of an E1 galaxy. A more elongated E5 galaxy, M59 is shown on the right side.

sons this is not believed to be true today.

In Hubble's tuning fork diagram elliptical galax es are placed at the left side. These elliptical galaxies are the simplest systems of stars, being smooth and structureless in their luminosity profile. Ellipticals, in general, lack cool gas and hence possess few young blue stars.

The elliptical galaxies are further classified according to their apparent elongation, and are designated En, where n is an integer describing the apparent axial ratio (b/a) through the formula $n = 10[1 - (b/a)]$. Ellipticals with higher elongations than E6 are rare. Figure 1.2 shows examples of E1 and E5 galaxies.

Ellipticals, as a class, spread over a large range in luminosity and size. They predominate in rich clusters of galaxies, and the largest of them, the *cD galaxies*, are found in the densest parts of those clusters. These cD galaxies may become 100 times more luminous than the Milky Way, and can extend to hundreds of kiloparsecs. Normal or *giant* ellipticals have luminosities a few times that of the Milky Way, with characteristic sizes of

tens of kiloparsecs. The stars in these bright ellipticals show little organised motion, like rotation. The orbits of stars are oriented randomly and they do not share a common axis of rotation.

On the other hand, the stars in less luminous elliptical galaxies have more rotation and less random motion. Often there are signs of a disk embedded within the spheroidal body. Fainter ones, with luminosities ~ 0.01 of that of the Milky Way, comprise of rare compact ellipticals, diffuse dwarf elliptical (dE) galaxies and even less luminous dwarf spheroidal (dSph) galaxies.

Elliptical galaxies have more complicated structures than was initially thought. Apart from being *oblate*, with two axes equal and longer than the third or *prolate* where the two axes are equal and shorter than the third, there is evidence for ellipticals, from their intensity contours, to be *triaxial* in which all the axes are different in length from one another.

Spiral galaxies are placed on the right side of the tuning fork diagram and are characterized by the existence of central bulge and a thin disk with spiral arms in the outer parts. Hubble developed the spiral classification depending on three parameters: (1) the size of the bulge relative to the disk length, (2) the tightness of the winding of the spiral arms, and (3) the degree of resolution of the spiral arms. Spiral galaxies are denoted as S, with subdivisions a, b and c, for galaxies ranging from those with big bulges and less defined spiral arms, to those with small bulges and well defined spiral arms as shown in the upper right side of Figure 1.1. The spiral arms contain large collections of bright hot O and B stars and the dusty gas out of which these stars form, while the bulges possess relatively older stars. Two different types of normal spiral galaxies are shown in Figure 1.3. Typically nearly 75% of the blue light comes from the disks. The ratio of luminosity of disk to that of bulge (D/B) varies with the Hubble type: the later the spiral type the greater the ratio is. For an Sb galaxy the (D/B)
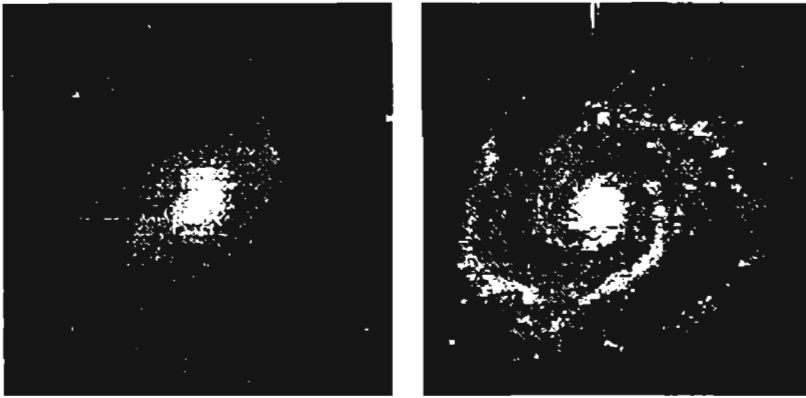
Figure 1.3: Examples of spiral galaxies: On the left the galaxy M96 is shown. This is the brightest in the Leo I group of galaxies and is classified as Sa. On the right the famous whirlpool galaxy, which is classified as Sc, is shown.

ratio is around 3 and for Sd galaxies it can reach as high as 100.

Hubble noted the presence of elongated, bar-shaped stellar configurations in some spiral galaxies and denoted these by SB, with subdivisions like the normal spiral galaxies. Nearly half of all spiral and lenticular galaxies show a central linear bar. Barred spiral galaxies are shown on the lower arm of the Hubble's tuning fork diagram.

Lenticular galaxies resemble ellipticals in their central regions but are surrounded by a structureless flattened rotating disk of stars. These are designated as $S0$. They resemble ellipticals in lacking extensive gas and dust and in preferring regions densely populated by galaxies. At the same time, they resemble spirals in possessing a thin and fast-rotating stellar disk. It may be noted that the presence of lenticular galaxies makes the transition from Ellipticals to Spirals a continuous one. This means that there are S0 galaxies with high ellipticities (E7) which can be identified either as ellipticals or as spirals. There exist lenticulars with a central
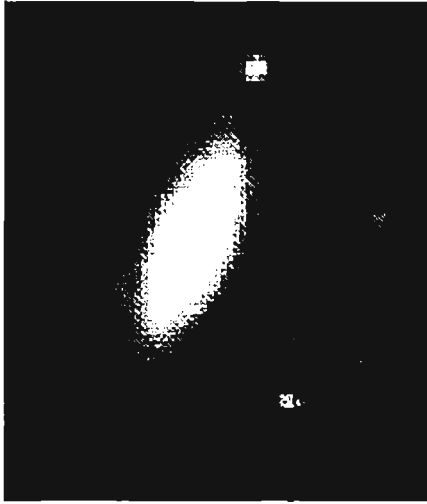
Figure 1.4: NGC 3115. This is the famous spindle galaxy classified as S0. The galaxy is seen edge-on and could easily be mistaken for an elliptical galaxy.

elongated bar and these are designated as SB0.

Hubble classified asymmetrical galaxies into *irregulars*. He noticed two types of irregular galaxies: *Irr I galaxies* that lack symmetry or well defined spiral arms but display bright knots that contain O and B stars and *Irr II galaxies* that are asymmetrical objects having rather smooth images. However, he found it difficult to accommodate these galaxies in his evolutionary scheme, that galaxies form as ellipticals and evolve to the Spirals with the lenticulars being the intermediate stage.

Later astronomers in general considered Hubble's original classification scheme satisfactory, except for some modifications like the one introduced by de Vaucouleurs (1959) to include substructures like *rings* and *lenses*. de Vaucouleurs felt, like many others, that Hubble's division of the spirals and

irregulars were incomplete and inadequate to describe the many features displayed by these types. He argued for additional spiral classes Sd, Sm and Im, as an extension to the Hubble scheme. The Sd class provided extension to Hubble's Sc galaxies and contained some more extreme objects which were originally classified as Irr I in Hubble's scheme. The Sm and Im classes contain the rest of Irr I galaxies. The 'm' in these types stands for systems similar to the Large Magellanic Cloud which is classified SBm by de Vaucouleurs.

Even though Hubble's nomenclature is still used, his concept of galaxy evolution is not considered completely correct. On the contrary, simulations suggest that spirals can merge together to form ellipticals (Schweizer 1982; Barnes & Hernquist 1992). There are reasons to believe from observations that interactions between galaxies can change their morphology and that ellipticals on merging can form spirals as well (see for e. g. Larsen 1990 and the references therein).

1.3   Structural Parameters of Galaxies

As we can see from the discussion in the previous section, the spheroidal bulge and the flattened disk form the two important components of galaxies. Initially the flattening of elliptical galaxies was attributed to the rotation of stars about the polar axis (Osterbrock 1960). Later it was shown that the rotational velocity of elliptical galaxies were insufficient to support the flattening (Bertola & Capacciolli 1975; Illingworth 1977). Detailed studies on the stellar motion suggested that ellipticals are supported against gravitational collapse by the anisotropic random velocities of stars (Binney 1976). The bulges of spiral galaxies are similar in their properties to ellipticals (Khosroshahi et al. 2000) though they are less flattened. The disks, on the other hand, are highly flattened systems supported by more

ordered rotation of stars. The existence of two distinct types suggests the possibility of two scenarios for the formation of galaxies. The two processes have to be equally important as the total mass contained in the spheroidal bulges and the disks are roughly the same (Schechter & Dressler 1987).

The classical, and the simplest, view suggests that galaxies form from large, nearly uniform rotating clouds that collapse under gravity (see Larsen 1990 for a review and the references therein). Such a collapse is able to account for the formation of galactic disks, but it can not directly account for the properties of spheroidal systems like the halo of our Galaxy. However, using models of protogalaxies containing many smaller clouds with large random motions, it was possible to construct structures that resemble many of the observed properties of galaxies (Larsen 1969, 1975) and galaxies with both bulge and disk components (Carlberg 1984).

Toomre (1977) suggested formation of galaxies through mergers of smaller galaxies which forms the hierarchical merging scenario (White & Rees 1978; Silk 1978; Tinsley & Larsen 1979). In this view the dynamical friction acting on the two galaxies during a close and violent tidal encounter (Binney & Tremaine 1994) disrupts any preexisting disks and largely randomizes the stellar motions to form elliptical galaxies.

As already mentioned, galaxies contain different morphological components to varying strengths and their study is closely linked to their formation and evolution scenarios. In other words, the different components in a galaxy are pointers towards the history of the galaxy, and for a physical understanding of the formation and evolution processes of galaxies it becomes important to quantify the various components of galaxies and study their correlations along the Hubble sequence. This is achieved through the measurement of surface brightness distributions of different components in galaxies. In the next chapter we will consider detailed descriptions of the surface brightness distributions and the methods that are used to quantify

the distributions.

1.3.1   Correlations Between the Structural Parameters

Studies on correlations among the global properties of galaxies can pro-
vide valuable insights into their evolution. Correlations with parameters
that depend on distance have been effectively used to measure distances to
galaxies. Further, the existence of tight correlations between structural pa-
rameters provide the much-needed constraints on theories of galaxy forma-
tion. Ellipticals were considered the simplest of systems amongst different
types of galaxies because of their smooth and feature-less luminosity distri-
butions, and were subjected to detailed photometric as well as spectroscopic
studies. The discovery of the colour- magnitude effect (Baum 1959) was
used for measuring relative distances of galaxies and clusters (Sandage 1972;
Visvanathan & Sandage 1977; Sandage & Visvanathan 1978a, 1978b). Fur-
ther, the small scatter in the relation was used to constrain the time-scales
for formation of elliptical galaxies (Bower, Lucey & Ellis 1992). Similarly,
the correlation between luminosity and velocity dispersion (Faber & Jack-
son 1976) was used as a distance indicator (Tonry & Davis 1981; Dressler
1984). Kormendy (1977b) demonstrated that a correlation exists between
surface brightness and effective radius, which in turn suggested that more
luminous ellipticals have lower surface brightnesses. All these correlations
have *cosmic scatter*: the scatter of the points about the mean relations
is larger than that can be accounted by measurement errors alone. Sub-
sequent studies found that elliptical galaxies lie on a *fundamental plane*
within a three-dimensional space defined by the observables: a charac-
teristic surface brightness, half-light radius and central velocity dispersion
(Dressler et al. 1987a,b; Djorgovski & Davis 1987). The various bivariate
correlations like color-magnitude, Faber-Jackson and Kormendy relations
form projections of this fundamental plane (FP). The existence of the FP

was soon interpreted as providing a strong constraint on the mass-to-light ratio (M/L) of elliptical galaxies, going by some simple assumptions regarding the structure and stability of the stellar systems (Djorgovski & Davis 1987).

By studying large populations of galaxies one hopes to understand the effect of environment on the wide range of morphologies. When reliable observations of galaxies were made, it was found that galaxies in clusters are much more likely to be ellipticals or S0s than are those in the field (e. g. Hubble & Humason 1931). This suggested that environmental factors play an important role in determining the morphology of a galaxy.

Oemler (1974) found that the fraction of ellipticals in a cluster of galaxies correlates with the morphology of the cluster - a cluster with a large elliptical fraction, $f(E)$, tends to have a more regular, symmetric appearance, often with a giant cD galaxy at the centre, while a cluster with small value of $f(E)$ generally has less organised appearance. Oemler also discovered the morphology-radius relation that the projected number density of spirals *increases* with radial distance R in the inner parts of clusters. Allowing for projection effects, these observations suggested a pronounced lack of spiral galaxies near the cores of regular clusters. Similarly, Melnick & Sargent (1977) found that the number density of S0s becomes increasingly dominant near the cluster center. By studying large samples of galaxies Dressler (1980) confirmed the morphology -radius correlations. However, Dressler concluded that correlations involving R are not the fundamental ones, and that galaxy type is really determined by the local density of galaxies. Dressler argued that the morphology-density relation is more fundamental than the morphology-radius relation. Beers & Tonry (1986) showed that the projected number density N is a monotonic function of R, with $N \propto R^{-1}$ over a large range of radii in many clusters. Such a close relationship between N and R implies that if morphology is correlated with

R, so it is with N and vice-versa. Hence it is extremely difficult to ascertain which of these relations is more fundamental and one has to wait until understanding of the underlying physical mechanism is improved.

Another important planar relation reported in the literature is the photometric plane (Khosroshahi et al. 2000a, 2000b), a correlation between the three purely photometric parameters that define the intensity distribution of galaxies. Studying a sample of ellipticals and bulges of *early*-type spirals Khosroshahi et al. (2000b) reported that though the Kormendy relation for the two components showed marked difference they co-existed on the photometric plane. This led to the suggestion of a common scenario for the formation of these components. As in the case of the fundamental plane, the observed tightness of photometric plane also can be used to provide a strong constraint on the bulge formation scenarios.

The physical basis for both these planar relations still remains unclear. Assuming that elliptical galaxies behave as spherical, isotropic one component systems in hydrostatic equilibrium with constant specific entropy, Lima Neto et al. (1999) presented theoretical arguments for the so called *entropic plane*, a planar relation involving only photometric parameters, but failed to match it with observation. Márquez et al. (2000), using the same sample of Lima Neto et al. (1999), came to the conclusion that galaxies may not have a constant entropy, but a value which increases with galaxy luminosity. This idea is supported by simulations of galaxy formation through hierarchical merging, as one expects the level of entropy to increase on merging.

Though both entropic and photometric planes are constituted from purely photometric parameters, it has not been possible to establish a direct connection between the two planes, mainly due to the difference in the definition of the parameters which are involved in the relations. One may hope that as models of galaxy formation and evolution advance, they will

shed more light on the physical origin of these planar relations.

1.4 Present Work

We use detailed near infra-red surface photometry of 35 early type galaxies from two rich clusters, Abell 2199 and Abell 2634, to extract the morphological parameters. The Abell galaxies were observed at the United Kingdom Infra-Red Telescope (UKIRT) during August 7-9, 1995. The galaxies were compiled from the sample in Lucey et al. (1997) taking care that reliable velocity dispersion measurements were available for the selected galaxies.

It was de Vaucouleurs (1948) who noticed that the logarithmic intensity of an elliptical falls as $r^{1/4}$ and this empirical law named after him was extensively used to describe the light distribution in elliptical galaxies and in bulges of spiral galaxies (de Vaucouleurs 1959). However, as more and more accurate data and image processing techniques became available, thanks to the advent of more efficient Charge Coupled Devices (CCDs) and sophisticated algorithms running on fast computers, systematic deviations from the $r^{1/4}$ law for ellipticals were found (Michard 1985; Schombert 1986; van den Bergh 1989; Bingelli & Cameron 1991). Sersic (1968) proposed the generalized $r^{1/n}$ law, with n as a free parameter to describe the intensity distribution in elliptical galaxies and bulges of S0 galaxies (Caon, Capaccioli & D'Onofrio 1993), as well as in the bulges of spiral galaxies (e.g. Andredakis, Peletier, & Balcells 1995). The Sersic index, n, was reported to correlate with effective radius and the total galaxy luminosity.

We have obtained the global photometric parameters for the Abell galaxies in our sample applying de Vaucouleurs' and Sersic laws separately to the surface brightness profiles. We achieve this using an algorithm developed by Wadadekar et al. (1999). Our work has shown that Sersic law always fits better the observed profiles than de Vaucouleurs' law. In addi-

tion to that, we show that serious and systematic under- or over-estimation of the structural parameters are made by enforcing the luminosity structural homology for galaxies, which has been done through the assumption of de Vaucouleurs' law in the literature.

We further explore various correlations existing between the global morphological parameters with special attention given to the comparison of scaling relations for the parameters extracted from the two different intensity profiles. We find that even though the Sersic law fits better to the observed profiles, there is no noticeable change in the Kormendy, Faber-Jackson and fundamental plane relations by moving from de Vaucouleurs' to Sersic fits.

By studying the scatter in the fundamental and photometric plane relations we demonstrate the existence of a four dimensional hyper plane for galaxies. The well-known photometric plane forms a simple projection of the hyper plane. We also show that the fundamental plane relation can be derived from the hyper plane. Using the hyper plane relation, we analyze the dependence of M/L on the structural parameters.

The observed tightness in the fundamental and hyper plane relations is used to estimate the central velocity dispersion σ of different Hubble types of galaxies in our sample. The measurement of σ becomes extremely challenging and difficult across the galaxy sequence and especially when the galaxies are at high redshifts, and hence this method provides a cheaper and reliable way of estimating the central velocity dispersion. Finally, we provide the estimations of the masses of supermassive black holes assumed to be located at the centers of all galaxies.

Chapter 2

Surface Brightness
Distribution in Galaxies

2.1 Introduction

As we have already seen in Chapter 1, galaxies possess a wide variety of appearance, based on which Hubble constructed his famous tuning fork diagram for classifying galaxies and studying their evolution. Studying the intensity[1] distribution in galaxies could provide a tool for quantifying the morphology of galaxies. Until the advent of CCDs in the early 1980s, photographic imaging of galaxies were used for the measurement of surface brightness, which is defined as the flux received from unit solid angle of a galaxy. Photographic images have to be digitized for processing and analyzing with the help of computers. The photographic plates used for obtaining images have many disadvantages as they are plagued by low

---

[1]While describing the profiles, the terms surface brightness and intensity are used interchangeably through out this thesis.

quantum efficiency, poor linear response and small dynamic range. The advent of CCDs with their better performance due to high efficiency, larger dynamical range and ability to provide digital output directly, paved the way for faster, more effective and economical techniques to measure the surface brightness of galaxies using computers.

In this chapter we describe the various distribution laws, analytical as well as empirical, that have been employed from time to time to represent the surface brightness variations within galaxies. Then we move on to discuss various measurement techniques used for the determination of the surface brightness profile. Finally, we describe in some detail the method used in our decompositions for the extraction of structural parameters of galaxies.

2.2 Ellipticals and Bulges

Resolving individual stars in a galaxy is almost impossible for any telescope-detector combination, except for the very outer regions of nearby galaxies like Andromeda (M31). Hence, the brightness at any point in a CCD image of a galaxy consists of the sum of the intensities of unresolved stars along that line of sight, and the intensity from other sources like HI regions, supernova remnants, an active galactic nucleus etc., with the whole possibly affected by absorption due to intervening matter. The net effect of adding all these individual components is to obtain, in general, a diffuse and continuous intensity distribution in the galaxy image.

As already stated, the images of galaxies are 2D projections of 3D objects. To get a 1D profile this 2D image is further averaged, leading to some loss of information. But because of the presence of large scale regularities of their structure, this 1D profile is often enough for studying the intensity distribution within galaxies and can in fact provide a higher signal-to-noise
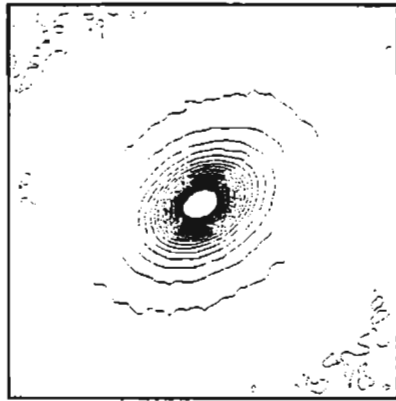
Figure 2.1: Contour plot of elliptical galaxy NGC 661 observed in R band. To a very good approximation the isophotes of elliptical galaxies have elliptical shapes, with the small-scale irregularities in contour shape being due to noise in the image.

ratio than individual pixels in the 2D image. Different mathematical representations have been used at one time or another to fit the mean surface brightness profiles. Some of these are purely empirical, while others have been motivated from theory and/or simulations.

Isophotes of spheroidal bulges (this class includes ellipticals as well as bulges of other Hubble types) are well approximated by ellipses. Figure 2.1 shows the contour plot of a nice, feature-less elliptical galaxy NGC 661, observed in Johnson R band using a 1m telescope at the Uttar Pradesh State Observatory (UPSO), Nainital. This galaxy is used for demonstrating various techniques that are described in the following sections of this chapter.

The intensity contours of both bulges and circular (flattened) disks when projected on the plane of the sky have elliptical shapes, in the most general case, with different ellipticities for these components. In the classical one-dimensional (1D) method to obtain intensity profile within a galaxy,
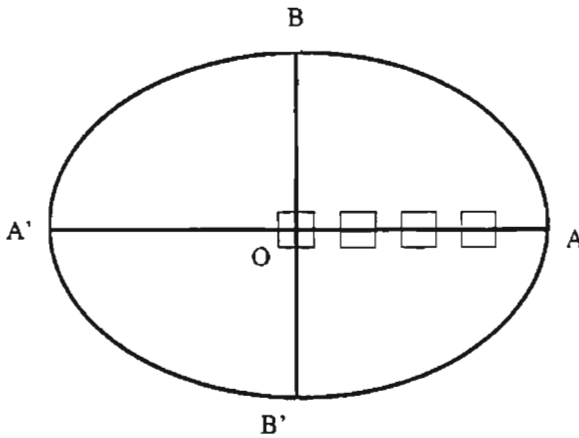
Figure 2.2: Construction of 1D intensity profile. Total intensities inside the rectangular areas selected along AA' are measured to get a 1D profile. For clarity the rectangles are shown much larger than they are in practice.

intensities were measured in small area elements along some selected axes of the galaxy, like the major axis of an elliptical galaxy (Figure 2.2). Later various algorithms that can average light along isophotes were developed to provide 1D distribution of intensities within galaxies. In galaxies with regular features, the 1D profiles are sufficient for most considerations. However, for studying small scale morphological distortions or peculiarities, it is necessary to use the full 2D image.

We shall have a look at the different model profiles proposed in the literature for quantifying the brightness distribution within galaxies, before actually discussing the various 1D and 2D methods to obtain the light profiles.

Hubble's law

The earliest and one of the simplest forms for the surface brightness, $I_b(r)$ at a radial distance r, was suggested by Reynolds (1913), as

$$I_b(r) = \frac{I_b(0)}{(1 + r/r_0)^2},$$ (2.1)

where $I_b(0)$ is the central surface brightness and r_0 is the scale radius at which the surface brightness falls to a quarter of its central value. This relation is known as *Hubble's law* for the reason that it was Hubble who used it extensively and made it popular (Hubble 1930).

Hubble's law is able to describe the surface brightness profile for most elliptical galaxies very well within specific ranges of r. However, the law predicts $I_b(r) \propto r^{-2}$ for $r \gg r_0$, which leads to non-physical infinite luminosity for galaxies.

de Vaucouleurs' law

Studying large samples of galaxies, de Vaucouleurs (1948) discovered that the surface brightness $\mu(r)$, expressed in magnitudes per square arcsec, followed an $r^{1/4}$ decrease to a remarkably good approximation. This lead to the famous relation known after him,

$$I_b(r) = I_b(0) \, e^{-7.67(r/r_e)^{1/4}}$$ (2.2)

where r_e, called the effective radius, is the semi-major axis length of the isophote within which half of the total intersity is enclosed. This de Vaucouleurs' $r^{1/4}$ law is probably the most widely used empirical relation to describe the profile for elliptical galaxies. The total light contained by the

galaxy is given by

$$B = \int_0^\infty I(r)\, 2\,\pi\, r\, dr = 7.22\,\pi\, I_b(r_e)\, r_e^2, \qquad (2.3)$$

where $I_b(r_e) \approx 2000\, I_b(0)$, is the surface brightness at r_e.

One can obtain different estimates for the effective radius by fitting surface brightness along different directions from the centre of the galaxy. In such cases, the effective radius is usually determined as the geometric mean of the major and minor axes of that elliptical isophote which contains half the total intensity of the galaxy. Figure 2.3 shows the de Vaucouleurs' fit to the elliptical galaxy NGC 661.

It is worth noting here that simulations of galaxies could actually reproduce the $r^{1/4}$ law (e. g. Schweizer 1982, Barnes 1988) in the case of relaxed galaxies with merging history. The accretion of dense satellites onto disk galaxies also settles to $r^{1/4}$ bulges (Agurri, Balcells, & Peletier 2001). However, the de-projected mass density $j(r)$, corresponding to de Vaucouleurs' law, is not analytically tractable (Young 1976). Hence the $r^{1/4}$ law is not very useful for theoretical modeling. There have been attempts to obtain density profiles that resemble the $r^{1/4}$ law or those with simpler analytic forms (e. g. Binney 1982; Bertin & Stiavelli 1984, 1989; Hernquist 1990). But implementation and extraction of structural parameters based on these analytical forms were, in general, not very convenient.

Petrosian's η Function

Petrosian introduced another way of describing the surface brightness in terms of a monotonous and dimensionless function $\eta(r)$, which is the ratio of the average surface brightness up to a radius r to the surface brightness at r.   It is a scale-independent quantity, and hence is useful in studying
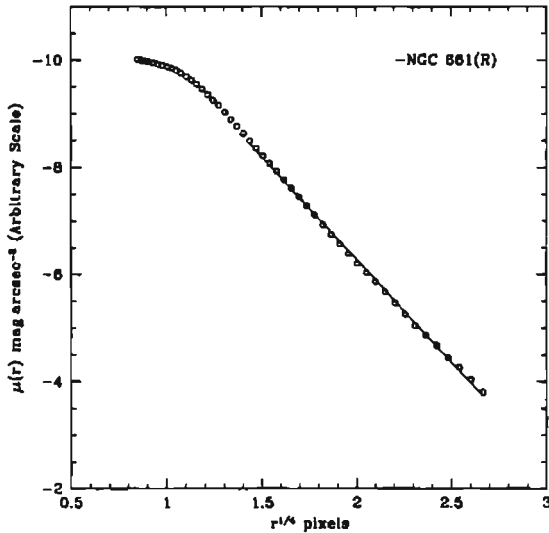
Figure 2.3: Surface brightness profile for NGC 661 observed in Johnson R band. This is a good example of a galaxy with de Vaucouleurs' profile. The open circles indicate mean surface brightness along successive isophotes, while the continuous line is a de Vaucouleurs' law fit. The curvature of the profile near the centre of the galaxy is due to the point spread function, and not an intrinsic feature of the galaxy.

the evolution of galaxies with little reference to any particular cosmological model.

Dehnen Models

As we have seen, Hubble's law incorrectly predicts infinitely large values for the luminosity of galaxies, which can not be true. Dehnen (1993) provided a family of density profiles which do not have this problem, with the three

dimensional luminosity density given as

$$j(r) = \frac{3-\gamma}{4\pi} \frac{La}{r^{\gamma}(r+a)^{4-\gamma}}.$$ (2.4)

Here L is the total luminosity, a is a characteristic scale length and γ is a constant. When γ is either integer or half integer, $j(r)$ in Equation 2.4 yields an analytically tractable projected density distribution. The model with $\gamma = 1$ is known as *Hernquist model* (Hernquist 1990) and $\gamma = 2$ gives us the *Jaffe model* (Jaffe 1983). A close approximation to the de Vaucouleurs law can be obtained by taking $\gamma = \frac{3}{2}$. Quantities like surface brightness, gravitational potential, projected velocity dispersion etc. can be derived from this law rather easily. Hence this law is employed in a number of studies involving simulation of spheroidal systems.

Sersic Profile

Almost all the two parameter functions (like Hubble's law and de Vaucouleurs' law) have the major drawback that they do not fit intensity profiles of all ellipticals completely, from the centre to all the way out to the exteriors of galaxies. Burkert (1993) showed that de Vaucouleurs' law actually describes the brightness profile well only for regions with $0.1r_e \leq r \leq 1.5r_e$. Also, analysis of high quality data with more accurate CCD surface photometric techniques showed systematic deviations from the $r^{1/4}$ profile in many galaxies (Michard 1985; Schombert 1986; van den Bergh 1989; Bingelli & Cameron 1991). These observations supported the idea of providing fitting functions that contain more than two free parameters, which are expected to yield better fits to a larger range of galaxies than those containing only two free parameters.

Sersic (1968) suggested a generalization of the $r^{1/4}$ to a $r^{1/n}$ law, with

n as a free parameter. Sersic's law is given by

$$I_b(r) = I_b(0)\, e^{-2.303\, b_n\, (r/r_e)^{1/n}} \qquad (2.5)$$

where the parameter b_n is chosen so as to keep the definition of the effective radius r_e the same as in Equation 2.2. b_n is a function of n, and its value is determined from the equation

$$P(2n, 2.303\, b_n) = 0.5, \qquad (2.6)$$

where $P(a, x) = \int_0^x e^{-t}\, t^{a-1}\, dt$ is the incomplete Gamma function (see e.g. Press et al. 1992). However, it is found that (Khosroshahi et al. 2000a) b_n can be expressed as a linear function of n, accurate to better than one part in 10^5, by

$$b_n = 0.868242n - 0.142058. \qquad (2.7)$$

The luminosity of a galaxy obeying the Sersic law is

$$B = 2\pi I_b(0)\, r_e^2\, \phi(n), \quad \phi(n) = \frac{n\,\Gamma(2n)}{(2.303 b_n)^{2n}}. \qquad (2.8)$$

This law was used to fit a sample of elliptical and S0 galaxies by Caon, Capaccioli & D'Onofrio (1993). They found that the Sersic index n is correlated with the effective radius and the total luminosity of the galaxy. Later it was noticed that the Sersic law provides good fits to the bulges of spiral galaxies too (Andredakis, Peletier & Balcells 1995; de Jong 1996; Khosroshahi et al. 2000a).

2.3   Disk Profile

Although elliptical galaxies are the simplest systems observed, even these, on careful analysis display considerable variety. In the case of spiral galaxies, the complexities involved can be great, as they contain disks with pronounced spiral structure, in addition to the bulge and/or a bar. However, averaging over the spiral structure, the light profile for the disk component of spiral galaxies is observed to be an exponential (Patterson 1940; de Vaucouleurs 1956; Freeman 1970). Similarly, disks of 30 galaxies also were fitted using the exponential profile successfully (Burstein 1979). An inner truncated exponential disk was also proposed (Kormendy 1977a), but is not widely used. The exponential law used for the disk component is

$$I_{\mathrm{d}}(r) = I_{\mathrm{d}}(0)e^{-(r/r_s)}, \qquad (2.9)$$

where $I_{\mathrm{d}}(0)$ is the disk central intensity and r_s is the disk scale length. The characteristic spiral pattern seen in the disk is averaged over in determining $I_{\mathrm{d}}(0)$ and r_s. It is generally assumed that disks are intrinsically circular and thin, and the observed ellipticity of the disk is attributed to it's inclination to the line of sight.

The total intensity enclosed by the disk is given by

$$D = \int_0^\infty I_{\mathrm{d}}(r)\, 2\pi\, r dr = 2\pi I_{\mathrm{d}}(0)\, r_{\mathrm{e}}^2. \qquad (2.10)$$

The ratio of luminosities of bulge and disc components is a parameter that is sometimes used as a quantitative measure for morphological classification of galaxies. Using a Sersic bulge and an exponential disk, we get

$$\left[\frac{B}{D}\right]_n = \frac{I_{\mathrm{b}}(0)}{I_{\mathrm{d}}(0)}\phi(n)\left(\frac{r_{\mathrm{e}}}{r_{\mathrm{d}}}\right)^2 \qquad (2.11)$$

where $\phi(n)$ is defined in Equation 2.8. For a bulge with de Vaucouleurs' law profile this relation becomes,

$$\left[\frac{B}{D}\right]_4 = 1.69 \times 10^{-3}\, \frac{I_b(0)}{I_d(0)} \left(\frac{r_e}{r_d}\right)^2 \tag{2.12}$$

For the elliptical galaxies in our sample, we have obtained the photometric structural parameters of the galaxies applying both de Vaucouleurs' and Sersic laws. There are a few S0 galaxies also in our sample, for which we have obtained a simultaneous bulge and disk model to extract the structural parameters. The details of the procedure are described later. We shall now move on to various methods that are employed in the estimation of the surface brightness profile of galaxies.

2.4 The Radial Intensity Profile

Isophotes of galaxies can be well approximated to be ellipses. The images of galaxies we obtain during observation can be regarded as the projection of 3D galaxies on to the plane of sky. The bulges of galaxies, in the most general case, are triaxial. On projection they show up as ellipses. For a triaxial ellipsoid with principal axes, $a > b > c$, the highest possible ellipticity is $1 - (c/a)$. It is noticed that the ellipticities of bulges seldom go very high (> 0.6) values.

The disks are inherently circular, and their projections on the plane of the sky again form ellipses. The ellipticity of a disk is completely determined by the orientation of the plane of the disk with the line of sight of the observer, and is given by

$$e_d = 1 - \cos i, \tag{2.13}$$

where i is the inclination angle of the disk, the angle between the line of sight and the normal to the disk plane. Hence apparent disk ellipticity can have all values between zero, when the disk is seen face on, and unity when it is seen edge on.

Due to the reasons described above, the projected galaxy image shows elliptical bulge isophotes and, in many cases, a more elliptical disk isophotes. Hence one can fit ellipses to the observed isophotes of galaxies to obtain the mean surface brightness as a function of major axis length of the isophotes. An ellipse can be fully described by five parameters, viz., length and position angle of the major axis, ellipticity and the co-ordinates of the centre of the ellipse. The idea is to fit ellipses to successive isophotes in a galaxy, and estimate the basic five parameters with the respective errors. This is most often achieved through a minimization algorithm starting from a trial ellipse. We have used the IRAF[2] task *ellipse* which follows the procedure described by Jedrzejewski (1987; See also Young 1976; Kent 1984). One begins with a trial ellipse of a given semi-major axis length. The intensity along the trial ellipse changes as one goes along it, until one reaches again the starting value. The change in intensity along the trial ellipse is therefore periodic and and it can be expanded in a Fourier series,

$$I = I_0 + \sum_{j=1}^{\infty} (A_j \sin(j\theta) + B_j \cos(j\theta)), \qquad (2.14)$$

where I_0 is the mean intensity along the ellipse, θ is the *eccentric anomaly* and A_j and B_j $(j = 1, 2, \ldots)$ are the harmonic amplitudes.

Assuming a trial ellipse with a pre-defined semi-major axis length, the coefficients of A_1, B_1, A_2 and B_2 for are determined by a least square fit

to

$$I = I_0 + A_1 \sin \theta + B_1 \cos \theta + A_2 \sin 2\theta + B_2 \cos 2\theta. \qquad (2.15)$$

Each one of the harmonic amplitudes A_1, B_1, A_2 and B_2 is related to a specific ellipse geometric parameter, their amplitude being a measure of the misalignment of the trial ellipse from the actual isophote. A correction factor is applied to the most deviant ellipse parameter to modify the trial ellipse. The algorithm picks up the largest amplitude among the four, estimates the local gradient and computes the corresponding increment in the associated ellipse parameter. That parameter is updated, and the image is re-sampled. This process is repeated until the largest harmonic amplitude has become smaller than a pre-defined threshold or a maximum number of iterations (decided by the user) is over.

On successful completion of the iterations, best fit values of the centre, ellipticity and position angle are obtained for the elliptical isophote with the pre-defined semi-major axis length, along with the mean intensity I_0.

The third and fourth harmonics are obtained using a least squares fit to

$$I = I_0 + A_3 \sin 3\theta + B_3 \cos 3\theta + A_4 \sin 4\theta + B_4 \cos 4\theta. \qquad (2.16)$$

The terms A_3, B_3, A_4 and B_4 show the deviations of the shape of the isophote from a perfect ellipse. A_3 and B_3 components give 'egg-shaped' or 'heart-shaped' isophotes respectively. But the most interesting is the B_4 coefficient. If this is negative the isophote will appear 'boxy', if positive the isophote will be 'disky' with pointed ends.

This procedure is repeated increasing the semi-major axis length, say by 10%, from one isophote to the next. This is continued till the desired outer limit of the galaxy is covered. Typically the outer limit is decided by the size of the galaxy (if it is very large) or by the noise levels (generally set by the sky brightness). It is possible with the present day CCDs to go
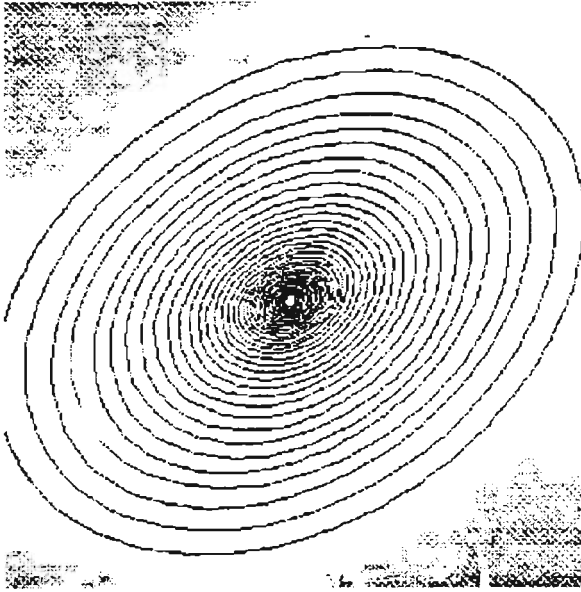
Figure 2.4: The elliptical isophotes fitted to galaxy NGC 661 by the IRAF task *ellipse*

up to a few percent or less of the sky level. The elliptical isophotes plotted over the galaxy NGC 661 are shown in Figure 2.4.

Because of the point spread function (PSF), the high central intensity of the galaxy is spread out to make the isophotes near the centre circular (providing that the PSF has a circular shape; in general the central isophotes have the shape of the PSF), irrespective of the real ellipticity of the isophotes. Hence the ellipse parameters estimated for isophotes near the centre of the galaxy are not reliable.

It is possible to have regions in the image which one does not wish to include in the fitting, like the regions contaminated by bad pixels, foreground stars or other spurious features. During the ellipse fitting, care is

taken to mask all such regions and interpolate suitably.

It is worth noting that the intensity profile estimated by *ellipse* is model independent and is a fair representation of the galaxy profile, so long as the galaxy is smooth and featureless. We have used this property for analyzing the quality of the fit obtained by de Vaucouleurs' and Sersic distributions for the intensity profile.

2.5   Decomposition of Bulges and Disks

The idea of photometric decomposition of the bulge and disk components of galaxies probably dates back to the classic work of Hubble (1926), when he constructed the Hubble sequence of galaxies. Later, Baade (1944) showed that this sequence actually had a systematic variation in terms of population of stars. This inspired the search for a quantitative analysis of the photometric distributions, providing a handful of approximations, both empirical and analytical, which we reviewed in the last few sections.

The bulge and disk components enjoyed most of the attention in photometric separation techniques (van Houten 1961; Freeman 1970). Bulge and disk intensities were separately fitted to the observed surface brightness profile taking note of the regions of dominance of these components. Yoshizawa and Wakamatsu (1975) were the first to systematically fit both the components. Simien (1989) provided a comprehensive description of various 1D decomposition techniques. The essential idea in most of these separating techniques was to obtain the 1D intensity profile and fit each component separately in the regions where it is dominant and then iterating the procedure till certain convergence criteria are met (Kormendy 1977b; Burstein 1979).

Kent (1985) introduced the idea of simultaneous fitting of bulge and disk components to major- and minor-axis profiles of galaxies obtained by fitting

ellipses to the isophotes. One major advantage of Kent's method is that it provided bulge-disk separation in a model independent way. However, his procedure was constrained by the fact that it required very different ellipticities for bulge and disk as he used the ellipticities of these components to determine the respective 1D profiles. Clearly, this method works well for edge-on galaxies where the ellipticity of the disk is much higher than that of the bulge. The technique developed by Schombert & Bothun (1987) used a similar method to get initial estimates of galaxy parameters with a standard bulge, disk and noise model. From these initial estimates bulge and disk parameters were extracted by a χ^2 fitting algorithm. Similar methods followed for the simultaneous extraction of bulge and disk components (e. g. Kodaira et al. 1987; Mahabal 1998).

The conventional one-dimensional techniques assume that the 1D profile can be extracted uniquely from galaxy images. This is not completely true as in the case of galaxies with a strong and highly inclined (viewed nearly or completely edge-on) disk. The different techniques of fitting standard laws to one-dimensional profiles extracted from galaxy images were compared in detail by Knapen & van den Kruit (1991). They noticed that the distribution of the extracted parameters vary a lot depending on the algorithm. For example, it was found that even for the same galaxy, different authors derive values for disk scale length with an average scatter as high as 23%. The existence of such large uncertainties in the extracted structural parameters poses a big hurdle in the study of structure, formation and evolution of bulge and disk of components in galaxies. Accurate and reliable estimation of structural parameters of galaxies is a prerequisite for differentiating between competing models that describe galaxy formation and evolution.

With the advent of more accurate data acquisition and high- speed reduction facilities, thanks mainly to the CCD imaging techniques, methods

that employ two-dimensional fits to broad band galaxy images have been developed (e. g., Byun & Freeman 1995; de Jong 1996; Wadadekar, Robbason & Kembhavi 1999). These methods, in general, use the information from all pixels available for the extraction of the structural parameters of galaxies. In these methods a two dimensional model image, which conforms to adopted bulge and disk intensity laws, is generated and compared on a pixel-by-pixel basis with an observed image, to determine the best values of the parameters. Accounting for the PSF effects and masking unwanted regions were additional advantages of these algorithms. These models provide a robust determination of the morphological parameters of galaxies and are increasingly being used in the literature. We describe such a complete two dimensional method, which we used for the extraction of the galaxy parameters.

2.6 The Decomposition Algorithm: *fitgal*

The decomposition procedure we use is a full 2D method that uses information from all pixels in the image. Details about the code, the reliability of extracted values and the associated errors can be had from Wadadekar et al. (1999). However, we provide a brief outline of the procedure for the sake of completeness.

The algorithm we use, *fitgal*, basically involves obtaining structural parameters of a galaxy, by simulating a 2D galaxy image similar to it with known parameters. The algorithm determines the parameters by minimizing the difference between the simulated and observed images. For this minimization, the code uses the Davidon-Fletcher-Powell variable metric algorithm included as part of MINUIT, a multi-dimensional minimization package distributed by CERN (James 1994) Here the quantity minimized is the signal-to-noise weighted χ^2-value, which provides a measure of the

quality of fit.

2.6.1 The Simulation of Galaxy Images

Using the code, it is possible to simulate a CCD image of a galaxy with desired bulge, disk and a point source components. The orientation of the galaxy can also be set separately. However, the code assumes exactly similar position angles for both bulge and the disk components. This is true in general, except for some triaxial galaxies.

The code has provisions to convolve the simulated image with a circular Gaussian PSF. Stars can be added into the image at random positions. If required, Poisson noise can be introduced before construction of the image. Any or all parameters used in the program can be modified by the user through a parameter file.

In our galaxy simulation algorithm, the intensity at any pixel, $I(x, y)$, is the sum of the intensity contributions from the bulge, disk and the sky counts. i.e.,

$$I(x, y) = I_b(x, y) + I_d(x, y) + I_{sky}(x, y) \tag{2.17}$$

where x and y are the distances from the centre of the galaxy along the major and minor axes, respectively. The projected bulge component is represented by the $r^{1/n}$ law,

$$I_b(x, y) = I_b(0) \, e^{-2.303 b_n (r_b/r_e)^{1/n}}, \tag{2.18}$$

where $I_b(0)$ is the central bulge intensity and b_n is defined as the root of Equation 2.6, involving the incomplete Gamma function. In the code this equation is solved numerically. However, a simplification can be applied here to reasonable accuracies through Equation 2.7, where b_n depends lin-

early on n. The radial distance r_b is obtained as

$$r_b = \sqrt{\frac{x^2 + y^2}{(1 - e_b)^2}}.$$ (2.19)

where e_b is the apparent ellipticity of the bulge.

The projected disk is represented by an exponential distribution with central disk intensity $I_d(0)$ and scale length r_s,

$$I_d(x, y) = I_d(0) \, e^{-r_d/r_s},$$ (2.20)

with the radial distance r_d given by

$$r_d = \sqrt{\frac{x^2 + y^2}{(1 - e_d)^2}}.$$ (2.21)

To add the sky contribution $I_{sky}(x, y)$ a constant count is added to every pixel.

The noise level in each pixel, if required, is determined in the following way. The total count in each pixel, estimated using Equation 2.17, is multiplied by the gain (electrons/ADU). A random Poisson deviate about this value is obtained. The deviate is then divided by the gain to get the total count at each pixel. Addition of stars or point source are carried out before the convolution of the image with PSF is done. Stars are placed in the frame by adding intensities to individual pixels selected at random positions. An intensity is added to the central pixel, if the presence of a point source (like the Active Galactic Nucleus) is required. Finally the convolution is performed in the Fourier domain.

2.6.2   Decomposition Procedure

To extract the structural parameters of the galaxies, the algorithm tries to minimize the difference between the model (simulated) image and the observed galaxy. The model to be fitted is constructed using the same procedure as described above, except that features like the Poisson noise, which are not the actual contributions from the galaxy, are not added to the model.

To effect the minimization of the χ^2, the counts observed in the galaxy image are compared with those predicted by the test model for each pixel. Each pixel is weighted with the variance of its associated intensity, as determined by the photon shot noise of the combined sky and galaxy counts at that pixel. This weighting scheme is chosen to give importance to pixels in proportion to their signal-to-noise ratio (S/N). This scheme makes the fit less sensitive to the contribution of the bulge in the outer region of the galaxy where the disk dominates. Thus, an effect similar to the earlier decompositions in which the disk was fitted to the outer region and the bulge to the inner region of galaxies, is obtained automatically.

As the photon shot noise obeys Poisson statistics, the variance of the count at each pixel is equal to the intensity value itself. Hence the definition of the reduced χ^2 is

$$\chi_\nu^2 = \frac{1}{\nu} \sum_{i,j} \frac{[I_m(i,j) - I_o(i,j)]^2}{I_o(i,j)}. \tag{2.22}$$

where $I_m(i,j)$ and $I_o(i,j)$ are the intensities in the pixel (i,j) of the model and observed images respectively with i and j ranging over the whole image and $\nu = [N - (\text{Number of fitted parameters})]$ is the number of degrees of freedom with N being the number of pixels in the image involved in the fit. The observed intensity count I_o, is assumed to be greater than one. It is

possible to have pixels with intensities less than unity in an observed image because of sky subtraction or other effects like bad pixels. These pixels are ignored during decomposition.

For real galaxies, the program assumes that intensity values $I_o(i, j)$, represent actual photon counts. If the image has been normalized in some way (divided by exposure time, or by the gain factor of the CCD etc.), the extracted χ^2_ν values should be multiplied by the appropriate factor to get the correct normalization.

In the most general case there are ten parameters to be fit in the scheme. These are $I_b(0)$, r_e, n, e_b, $I_d(0)$, r_s, e_d, position angle (PA), I_{sky} and the point source. Schombert & Bothun (1987) tried to fit parameters $I_b(0)$, r_e, $I_d(0)$ and r_s while Byun and Freeman (1995) and de Jong (1996) additionally fitted the parameters e_b and e_d as well.

CCD images of galaxies may contain features, such as dust lanes, foreground stars and bad pixels, that will affect the accuracy of the decomposition procedure. There is provision to provide to the program a list of pixels to be avoided in the fitting so that the quality of the fit is not compromised due to the presence of such features.

The minimization uses MINUIT 94.1, a multidimensional minimization package from CERN. This is written in standard FORTRAN 77 (James 1994). MINUIT allows the user to set the initial value, the resolution and the upper and the lower limits of any parameter in the function to be minimized. Values for one or more parameters to be kept fixed during a run.

MINUIT can employ several strategies to obtain the minimization. The code *fitgal* uses the routine MIGRAD which is a stable variation of Davidon-Fletcher-Powell variable metric algorithm (Press et al. 1992). It calls the user defined function (in our case χ^2_ν) iteratively, adjusting the parameters until certain criteria for a minimum are met. The code is smart

enough to avoid smaller local minima in the multi-dimensional parametric space, provided the limits and resolution are selected judiciously.

Elaborate tests on the efficiency and accuracy of the program in extracting the galaxy structural parameters under various conditions have shown that the code is highly reliable. A χ_ν^2-value less than 2 almost always suggests good recovery of parameters.

MINUIT provides the associated errors with each parameter value it obtains. In the minimization problems, two methods are commonly employed for parameter error estimation. The first is to estimate the error from the second derivative of the function being minimized with respect to the parameter under consideration. The second is to estimate the error, by gradually moving away from the minimum until a pre-determined χ^2 is obtained. This method will work fine for any single parameter fit, irrespective of whether the χ^2 function near the minimum is parabolic in shape or of a more complicated nature. MINUIT can provide errors using both estimates.

In any multi-parameter minimization process, formal errors on the parameters extracted can be estimated from the covariance matrix of the fit only if

- the measurement errors are normally distributed and

- the model is linear in its parameter space or the sample size is large enough that the uncertainties in the fitted parameters do not extend outside the region where the model could be replaced by a suitable linearized model.

Among the bulge and disk parameters that we use in the fit, two are linear ($I_b(0)$ and $I_d(0)$) and the rest are non-linear. Leaving all the parameters free results in rather large formal error bars on extracted parameters (20-30%). The χ^2 function is not parabolic near the minimum, which

causes incorrect error estimation by MINUIT when the derivative method is used. Even the method of moving away from the minimum until some χ^2 is exceeded has some limitations as ther· are multiple free parameters that correlate with one another. MINUIT is therefore unable to compute errors accurately using this technique when all parameters are free. Fixing the most non-linear parameters, i.e., the ellipticities, to their extracted values enables MINUIT to compute formal errors using this technique as the function can be approximated by a linearized model. However, the errors are still large. Fixing more parameters reduces the size of error bars. So one viable option to get a realistic estimation of errors for a particular parameter may be to run the code keeping all other parameters to their respective extracted values.

A sample output of the algorithm is shown in Figure 2.5 for the elliptical galaxy NGC 661. The image of the galaxy at the top left is the observed image and that at the top right side is the simulated one. The histogram of the difference between the two images is plotted at the bottom left corner and the extracted parameters of the galaxy is given at the bottom right side. Note that the disk parameters were kept constant at a negligible small level during the run.

In the present analysis, we have used this algorithm to extract parameters applying the de Vaucouleurs' and Sersic laws to the surface brightness profile. We compare these profiles predicted by the parameters determined by the code with those obtained by *ellipse* which are model independent. The sample and the correlations between these parameters are discussed in the next chapter.
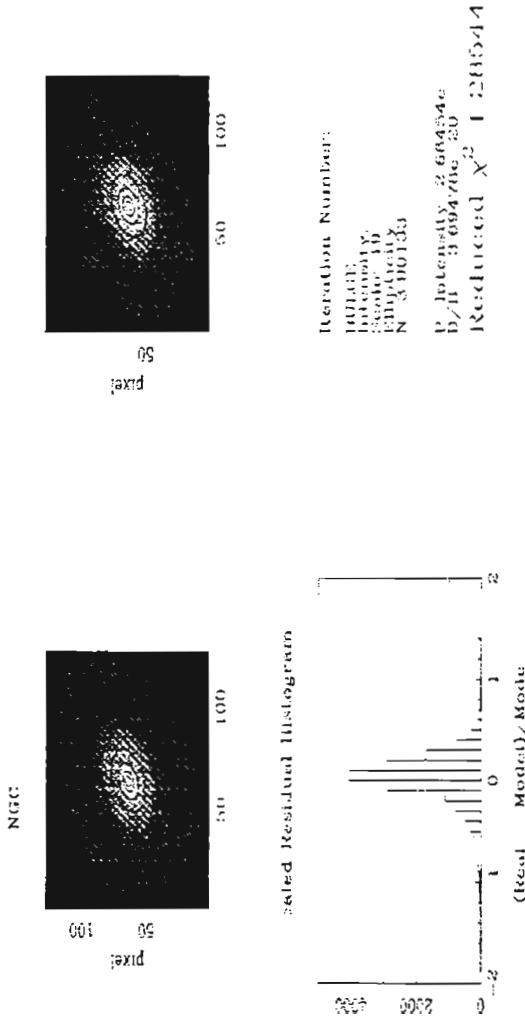
Figure 2.5: The graphical output after the decomposition of the R band image of NGC 661, using *fitgal*. Notice that the disk parameters were not extracted during this run. The intensities and effective radius are in counts and pixels respectively.

2.7   Summary

We have examined the important components of luminous matter in galaxies, viz., bulges and disks in relation to their brightness profiles. We have discussed various laws used in the literature to describe these profiles, and different one and two dimensional methods used for the quantification of surface brightness distributions. The algorithm of the decomposition procedure, *fitgal*, we used for the extraction of morphological parameters for galaxies in our sample has been discussed in some detail.

Chapter 3

Fundamental Plane Studies of Early Type Galaxies

3.1 Introduction

Elliptical galaxies form a two-parameter family, as originally discovered by Djorgovski & Davis (1987) and Dressler et al. (1987a) in the form of two-dimensional *fundamental plane* (FP) (Kormendy & Djorgovski 1989; Djorgovski 1992). The fundamental plane is usually considered in the parameter space of half-light radius r_e, the mean surface brightness within that radius $\langle\mu_b(< r_e)\rangle$, and the central velocity dispersion σ. The fundamental plane obtained for large samples of galaxies possess very small scatter (~ 0.1 dex in $\log r_e$) and hence can be used both as a distance indicator (e. g. Dressler et al. 1987b; Lynden-Bell et al. 1988; Jørgensen et al.

1995a) and to provide constraints on galaxy formation models (e. g. Bender et al. 1993; Guzmán et al. 1993, Zepf & Silk, 1996; Borriello, Salucci & Danese 2003). Also, it has been used as a tool for understanding the cosmological evolution by analysing clusters of ellipticals at high redshift (van Dokkum & Franx 1996; Kelson et al. 1997; van Dokkum et al. 1998; van de Ven, van Dokkum & Franx 2003). Historically the FP is a refinement of the Faber & Jackson (1976) relation between the luminosity and central velocity dispersion of galaxies, and the Kormendy (1977b) relation between the central surface brightness and the half-light radius.

In the present chapter we construct the fundamental plane for our sample of Abell galaxies, using structural parameters obtained for a de Vaucouleurs law bulge with or without an accompanying exponential disk, using the 2D decomposition algorithm, *fitgal*. Section 3.2 contains a description of the data and details of near infrared photometry. In the second half of this chapter, we consider various correlations and the fundamental plane relations for these galaxies.

3.2   Data and Observation

Our study is concerned with the large scale morphology of elliptical galaxies and the main part of our sample consists of elliptical galaxies from two Abell clusters; Abell 2199 ($\alpha = 16^h 28^m 38.4^s$, $\delta = 39° 33' 03''$, J2000) and Abell 2634 ($\alpha = 23^h 38^m 29.3^s$, $\delta = 27° 01' 52''$). The observations were made by B. Mobasher from United Kingdom Infra-Red Telescope using the IRCAM3 during August 7-9, 1995. The near infra-red K band (2.2 μm) of 38 galaxies were obtained with 21 galaxies from Abell 2199 and 17 galaxies from Abell 2634. The sample was selected to consist of spectroscopically confirmed members of these clusters, with available velocity dispersions from Lucey et al. (1997), which were originally chosen from published catalogues (Rood

& Sastry 1972, Strom & Strom 1978, Dressler 1980, Butchins 1983, Butcher & Oemler 1985 and Dixon, Godwin & Peach 1989). The observations were made at the United Kingdom infra-red telescope (UKIRT) during August 7-9, 1995. The near infra-red images were obtained using a 256×256 infrared array detector (IRCAM3) with a pixel scale of 0.286 arcsec. Out of these 38 galaxies, two from Abell 2199 and three from Abell 2634 were not used in the present analysis for the reasons specified in Section 3.3. This leaves a net sample of 33 galaxies in the two Abell clusters taken together. We hereafter refer to this sample simply as *Abell galaxies*.

For each galaxy, we obtained a total exposure time of nine minutes as follows: We co-added six exposures of 10 s each, and obtained nine such sequences per galaxy, with the image shifted by $\sim$ 20 arcsec around the center of the galaxy, from one sequence to another. This technique avoids the effect of bad pixels and cosmic rays, so that we can have reliable flatfields and background measurements for each frame. We also observed faint UKIRT standards on all nights and used these to monitor the accuracy of the photometry. The estimated seeing measured from the stars in the field was about one arcsec.

We have also used in our analysis a set of 48 elliptical galaxies from the Coma cluster observed in the K band by Mobasher et al. (1999), who provide morphological parameters of the galaxies obtained using de Vaucouleurs' law to describe the surface brightness profile. Forty two galaxies from this set were analyzed by Khosroshahi et al. (2000b) assuming the Sersic law for the surface brightness profile, and we use these results too in our analysis. This set of galaxies is referred to as *Coma ellipticals*. It should be noted that the Abell and Coma ellipticals used are situated in similar dense environments.

To enable us to make a comparison between the morphological parameters of ellipticals and the bulges of spiral galaxies, we have used bulge

parameters extracted by Khosroshahi et al. (2000a) from publicly available data on a sample of spiral galaxies. This set of 26 early to intermediate type spirals in the field taken from the Uppsala General Catalogue (UGC) of galaxies (Nilson 1973) was observed by Peletier & Balcells (1997) in K band and forms a complete, diameter-limited, optically selected sample. An initial set of 45 objects was compiled, comprising of all galaxies with right ascension between 13^h and 24^h, declination above $-2°$, galaxy type earlier than Sc, excluding barred objects, apparent blue magnitude brighter than 14.0, major axis diameter larger than two arcmin, absolute galactic latitude greater than $20°$ and axis ratio in B larger than 1.56 (which corresponds to disk inclinations greater than $\sim 50°$).

The near-infra red observations of Peletier & Balcells (1997) were taken on June 2-5, 1994 from UKIRT at Mauna Kea, Hawaii, using IRCAM3, a camera equipped with 256×256 InSb detector. A brief description of the observation can be found in Peletier & Balcells (1994). The details of subsequent examination, which led to a reduction in sample size to 33 can also be found in Balcells & Peletier (1994). Thirty objects from this sample were studied by Andredakis et al. (1995); the details of the observations are given in Andredakis et al. (1995) and Peletier and Balcells (1996, 1997). Using the reduced K band images of this sample publicly available at the New Astronomy website (http://www.elsevie .nl), Khosroshahi et al. (2000a) successfully decomposed 26 galaxies, which we refer to as the spiral bulges. More details on sample selection and data reduction can be had from Khosroshahi (2000) and from the references therein.

Throughout the thesis, we have used the following symbols to represent the different samples in plots. Abell galaxies are shown as stars, Coma ellipticals as filled circles, and the spiral bulges as filled triangles.

3.2.1   Data Reduction

The K band observations are useful in accurate extraction of global param-
eters of galaxies, since they provide relatively smooth and featureless light
profiles owing to the lack of absorption related features in the band. Much
of the K band light comes from low mass stars and is a good probe to trace
the bulk of the visible mass of galaxies. Here we provide the details of data
reduction carried out for the Abell galaxies observed in K' band.

We used dark frames with integration time close to the respective object
frames to carry out dark subtraction. We then median-filtered the nine
mosaic frames and normalized the resultant frame to its median pixel value
to construct the flat-field for each galaxy. Following dark-subtraction and
flat-fielding, we mosaicked the nine frames after properly registering them
in order to improve the signal-to-noise ratio S/N. We used the CCDPACK
software in the Starlink environment to carry out this data reduction. We
estimated the background sky level from the mosaicked image as the median
of intensity counts taken over several small regions located as far away as
possible from the center of the galaxy. Sky levels of individual frames in
the mosaicked image showed marginal differences, causing an uncertainty
in the measured sky values. However, these differences were always less
than 0.02 mag, and hence this is treated as the possible error arising from
sky subtraction.

We measured the point spread function (PSF), which was needed in the
analysis described below, from the stars present in the frame containing
the galaxy. When no good stars were available in a frame, we used the
average of the PSFs from other frames obtained on that night. The typical
seeing for the whole observation was about one arcsec, with a ~ 20 percent
variation overall.

We obtained the extinction relation for each night using the faint
UKIRT standards, after reducing their frames in the manner described

above. Using the standards we estimated the change in the zero points (internal photometric error) throughout the run to be 0.02 mag.

3.3   Morphological Parameters for Galaxies

If a galaxy is a pure elliptical described by the de Vaucouleurs law, then there are two parameters to be determined, while the presence of a disk brings in two other parameters. In the simplest approach, elliptical isophotes are fitted to the observed image, and the mean isophotal intensity as a function of semi-major axis length is obtained. The one dimensional profile can now be iteratively separated into bulge and disk components under certain conditions (see Chapter 2), and bulge and disk models of the type described above can be separately fitted to the two components, using some minimization technique. Another possibility is to use a combination of an exponential disk and a de Vaucouleurs or a Sersic bulge, and to obtain the best fit parameters to the observed total profile (see e. g. Mahabal et al. 1998).

Methods of the type described above involve the fitting of a model profile to the one dimensional azimuthally averaged intensity distribution. With the advent of more accurate data acquisition and high-speed reduction facilities, methods that employ two-dimensional fits to broad band galaxy images have been developed (e. g., Byun & Freeman 1995 and de Jong 1996; Wadadekar et al. 1999). In these methods a two dimensional model image, which conforms to adopted bulge and disk intensity laws, is generated and compared on a pixel-by-pixel basis with an observed image, to determine the best values of the parameters. These models provide a robust determination of the morphological parameters, as well as the shape parameters of the elliptical isophotes, and are increasingly being used in the literature. Using the decomposition algorithm *fitgal* which is described

in Chapter 2, we have obtained the best fit galaxy parameters applying a de Vaucouleurs bulge and exponential disk model. As already mentioned in Chapter 2, the code is capable of obtaining the more general Sersic fit to the bulges. A detailed comparison between the extracted parameters from de Vaucouleurs and Sersic law fits to the bulges is deferred till the next chapter. In what follows we describe the correlations arising from the assumption of structural homology of galaxies imposed in the form of de Vaucouleurs law.

Although the K band observations are advantageous for their relative lack of absorption related problems, the high sky background here poses some difficulty in extracting the global photometric parameters accurately, as it limits the region where S/N is high enough for the pixels to be used. Even a small error in the sky estimation can lead to spurious results because of the relatively low S/N in the images. For example, if the sky is underestimated, say by 5%, the residual background can lead to the detection of a large circular fake disk with a nonzero $I_d(0)$. Even when a 'bulge only' model is used, a wrong assessment of the background can lead to serious under- or over-estimation of the morphological parameters. Small fluctuations in the sky background in the individual frames in a mosaic can also lead to incorrect measurements in the mosaic at distances from the center where the S/N is poor. To limit this adverse effect we used regions where the galaxy counts per pixel are typically greater than 0.1% of the background sky in the mosaicked image for the extraction of the photometric parameters.

The code *fitgal* allows the estimation of the background simultaneously with the estimation of the morphological parameters. However, such calculation can lead to unstable values for the parameters, as the background counts are much higher than the signal (intensity from galaxy) even in the central region of the galaxies, where the galaxy counts are only 0.1% of the

sky background. To avoid the instability, we had a run for each galaxy in which the aim was to estimate the background rather than to obtain the morphological parameters. To this end, we first ran the code on the selected region of each mosaicked galaxy image, without subtracting the sky background from the image. We compared the value of the background returned by the fitting procedure, with that estimated from regions of the image frames free of the galaxy, and ensured that these values are close to each other. We then adapted the sky value returned by the code as the best representation of the sky background, since this uses information from all the relevant pixels of the image, and fixed the background parameter to this value during all subsequent runs of *fitgal*.

We fitted ellipses to the isophotes of each Abell galaxy, and obtained the one dimensional surface brightness profile along the major axis, using the IRAF task *ellipse*. For this task sky subtracted galaxy frames were used. The fits provided us with model independent surface brightness distributions, which could be compared with the surface brightness distribution predicted by our best fit models. In order to obtain good initial values for our two dimensional fits, we fitted the one dimensional profiles obtained above with de Vaucouleurs law profiles, taking care to avoid the region affected by the PSF. This provided us with approximate values of $I_b(0)$ and r_e, which we used as input to obtain a two dimensional de Vaucouleurs law fit to the galaxy. For every galaxy, we explored the presence of an exponential disk also, but found significant disks only in the two S0 galaxies; F105 in Abell 2634 and Z34A in Abell 2199. Since we did not detect significant disks in the other Abell galaxies, in these cases we used the fitted parameters obtained from a run in which the disk luminosity was set to zero.

Of the 38 Abell galaxies in our sample, we could not get satisfactory fits for three galaxies, N7720 and D76 in Abell 2634 and N6166 in Abell

Galaxy	Cluster	R_{cl} degree	cz $km\,s^{-1}$	$\log A_e$ arcsec	$\mu_b(0)$ $mag\,arcsec^{-2}$	$\log \sigma$ $km\,s^{-1}$	Mg_2 mag
BO13	A2634	0.213	9542	1.194	9.58	2.201	0.249
BO16	A2634	0.542	9337	1.338	10.71	2.351	0.325
BU32	A2634	0.562	8738	1.022	9.82	2.221	0.267
D107	A2634	0.129	9251	1.184	10.03	2.291	0.265
D119	A2634	0.249	9345	1.320	9.72	2.450	0.315
D127	A2634	0.455	9970	1.064	9.45	2.317	0.291
D38	A2634	0.149	9347	0.948	9.08	2.383	0.276
D55	A2634	0.041	9297	1.126	9.87	2.345	0.301
D57	A2634	0.053	9520	1.169	9.94	2.335	0.324
D68	A2634	0.143	9981	1.051	9.83	2.326	0.296
D75	A2634	0.015	9846	0.985	9.96	2.273	0.297
D80	A2634	0.040	9586	0.797	9.50	2.263	0.284
D93	A2634	0.373	8990	0.873	9.52	2.231	0.266
F105	A2634	0.155	9790	0.965	11.73	2.166	0.277
N7728	A2634	0.355	9498	1.600	10.16	2.519	0.333
BO73	A2199	0.064	8095	0.800	9.84	2.220	0.269
FCOM	A2199	0.014	9824	1.087	10.48	2.142	0.265
N1	A2199	0.906	9053	1.102	9.68	2.292	0.311
N6158	A2199	0.250	8914	1.348	10.24	2.280	0.277
RB130	A2199	0.336	9136	0.750	8.71	2.310	0.275
RB162	A2199	0.655	8892	1.158	10.10	2.378	0.288
RB38	A2199	0.306	9280	1.356	10.64	2.146	0.269
RB40	A2199	0.373	7840	0.813	9.27	2.220	0.248
RB72	A2199	0.742	9288	1.113	9.66	2.285	0.304
RB78	A2199	0.412	9518	1.574	12.29	2.146	0.275
RB8	A2199	0.569	8952	1.155	9.56	2.395	0.297
S18	A2199	0.302	9674	0.901	9.41	2.274	0.304
S26	A2199	0.052	8780	1.266	10.66	2.240	0.287
S30	A2199	0.018	8415	0.665	8.30	2.391	0.267
S33	A2199	0.041	8301	0.786	8.95	2.438	0.309
S34	A2199	0.033	8251	0.728	9.17	2.195	0.275
S43	A2199	0.150	8677	1.167	10.39	2.243	0.300
S44	A2199	0.169	9400	0.884	9.56	2.252	0.300
Z34A	A2199	0.323	8704	0.563	8.28	2.312	0.284
NCOM	A2199	0.008	8987	0.521	9.08	2.173	0.277

Table 3.1: Best fit values for effective diameter, $\log A_e$ and the unconvolved central brightness, $\mu_b(0)$ from de Vaucouleurs' law fitting to our Abell galaxies. The angular separation from the center of the cluster R_{cl}, the Heliocentric redshift z, the central velocity dispersion σ, and the Magnesium line strength Mg_2 for each galaxy along with their cluster membership, taken from Lucey et al. (1997), are also given.

2199. The failure occurs mainly due to the lack of two-fold isophotal symmetry expected by the code through the assumption that all isophotes are perfectly elliptical. The first two galaxies are mutually interacting, due to which isophotes in both galaxies depart significantly from elliptical shapes even in the high S/N regions near the center of the galaxies. The central region of N6166 is contaminated by three bright sources which distort the isophotes and make the fits unreliable. Further we exclude galaxies BO13 and F105, both from Abell 2634, as their structural parameters are not reliable. F105 is a small, faint lenticular galaxy because of which *fitgal* could not provide very stable results. In the case of B013, which is a normal elliptical, we could extract photometric parameters successfully, but the velocity dispersion measurement from Lucey et al. (1997) seems to be erroneous. Different observation runs provided significantly different measurements for the central velocity dispersion for B013 in Lucey et al. (1997). This is more evident from the fact that BO13 remains a serious outlier in the fundamental plane relation while in the case of Kormendy relation it is not (see Section 3.4). However, we have provided the structural parameters for galaxies F105 and B013 in our Table 3.1 with their corresponding profiles in Figure 3.1. We exclude these two galaxies also from our subsequent discussions on various correlations, thus providing us a sample of 33 galaxies. We would like to point out that inclusion of the two galaxies, BO13 and F105, does not change any conclusion made in this thesis, their effect just being limited to increasing the scatter in every correlation.

In Table 3.1, we have shown the results from fitting de Vaucouleurs' law to 35 Abell galaxies. Spectroscopic as well as some other global parameters obtained from the literature are also provided. In Figure 3.1 we show the corresponding surface brightness profiles for the Abell galaxies.   In
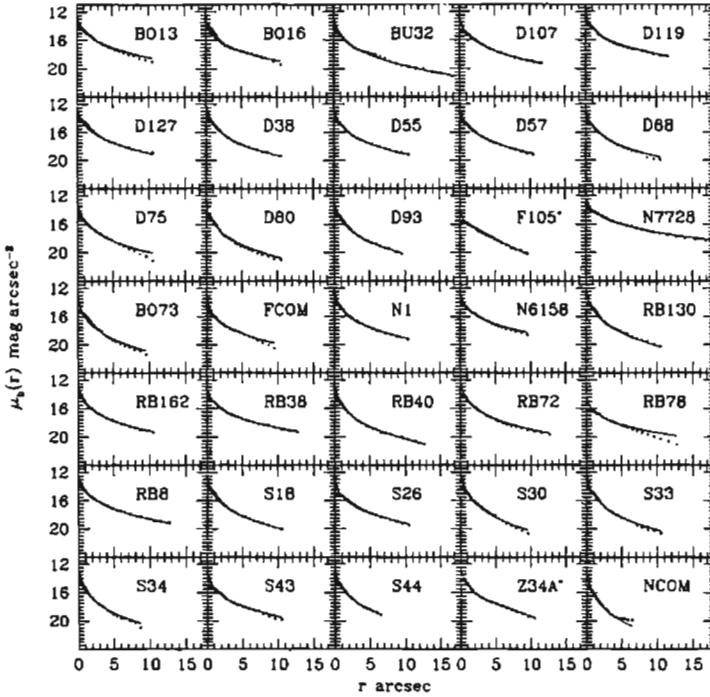
Figure 3.1: Best fit de Vaucouleurs profiles for the Abell galaxies. The points are the average isophotal intensities determined by *ellipse* and the continuous curves are the profiles generated from the best fit parameters using *fitgal*.
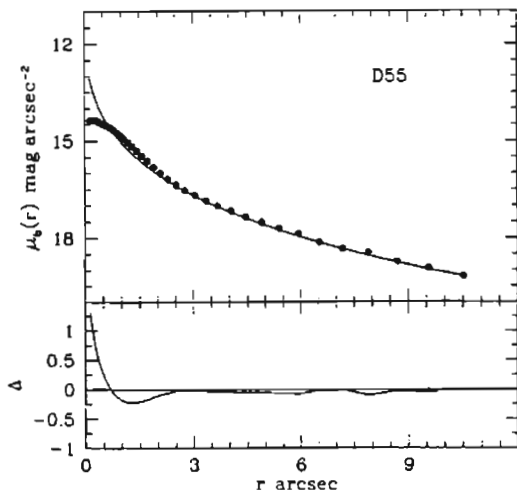
Figure 3.2: Comparison between the *ellipse* determined profile (filled dots) and the de Vaucouleurs profile generated from the best fit parameters obtained by using *fitgal*. The residual Δ is the difference between the two profiles. The larger difference at the center between the two profiles is because of the PSF, which is not taken into account in the construction of the de Vaucouleurs profile.

each window, the continuous curve shows the surface brightness profile generated using the de Vaucouleurs' law (Equation 2.2) from the best fit parameters determined by *fitgal*. The dots are from the model independent measurements using IRAF task *ellipse* obtained by fitting ellipses to the isophotes as explained in Section 2.4.

It can be seen that for many galaxies the de Vaucouleurs profile provides a reasonably good fit. In Figure 3.2 we show the profile determined using *ellipse* and the best fit de Vaucouleurs profile for the galaxy D55. The two profiles match each other very well away from the central region, but different at the centre basically because the model de Vaucouleurs profile
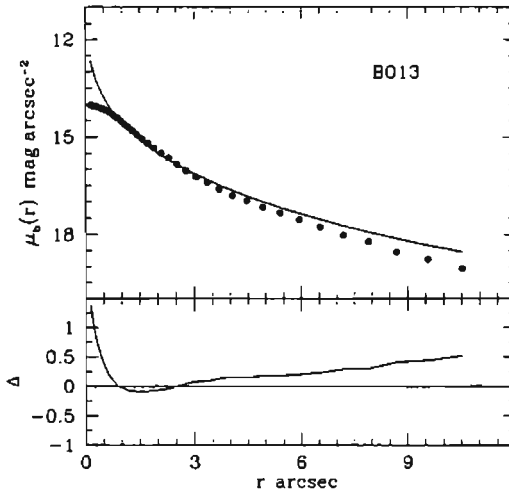
Figure 3.3: Surface brightness profiles as in Figure 3.2 for galaxy BO13.
The two profiles differ very much, showing that de Vaucouleurs law provides
a very poor fit for this galaxy.

generated has not been convolved with the point spread function. However,
not all galaxies provide such nice fits. For example, the *ellipse* and the de
Vaucouleurs' law fitted profiles for the galaxy BO13 plotted in Figure 3.3
show a mismatch over the entire range of semi-major axis length covered,
suggesting that de Vaucouleurs' law does not provide a good model for this
galaxy. This is true with several galaxies in the sample, showing that the
de Vaucouleurs law can not fit well the surface brightness profiles obtained
for all galaxies in our sample.

3.4   Correlations

Once the parameters that describe the morphology of galaxies are obtained,
it is useful to examine the various correlations existing between them, as
these help in understanding the underlying physical processes for the struc-
ture and evolution of galaxies. As already stated, these correlations can be
used in distance estimation as well as in the study of cosmological evolution
of observables. Galaxy mass measurements are extremely difficult. But em-
pirical relations such as the Tully & Fisher (1977) relation for spiral galaxies
and the fundamental plane for early- type galaxies can indicate the possible
evolution of masses of galaxies. The tightness of the fundamental plane has
provided insights into the evolution of mass and luminosity of early type
galaxies (Jørgensen et al. 1999; van de Ven et al. 2003). Since the mass-to-
light (M/L) ratio of a stellar population is expected to change with redshift,
the variation in the coefficients (slope and intercept) of the fundamental
plane provides sensitive information on the mean age and metallicity of the
stellar populations of early-type galaxies (see van Dokkum & Franx 1996).
In the next section we provide some basic correlations that exist between
the structural parameters of ellipticals using the photometric parameters
extracted assuming that the galaxies follow the $r^{1/4}$ law.

3.4.1   Kormendy Relation

One of the first purely photometric correlations was reported by Kor-
mendy (1977b). Using the structural parameters obtained by fitting de
Vaucouleurs law to the surface brightness profile, Kormendy showed that
the unconvolved central surface brightness B_0 for large ellipticals observed
in B band, correlates well with effective radius r_e.   Kormendy obtained
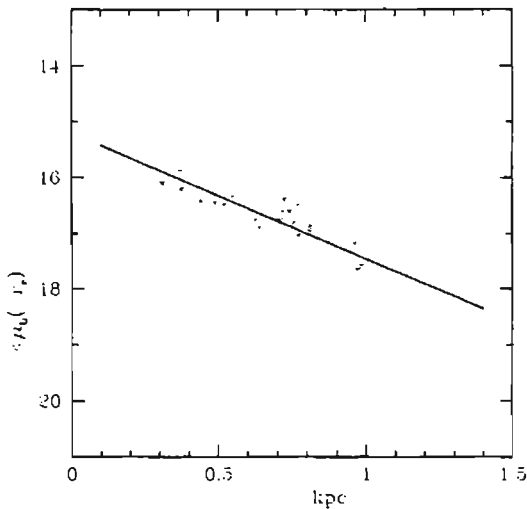
Figure 3.4: Kormendy relation with the parameters from de Vaucouleurs fit to the Abell galaxies

B_0 by least squares minimization:

$$B_0 = 3.02 \log r_e + 19.74 \,. \tag{3.1}$$

Soon the mean surface brightness within the half-light radius, $\langle I_b(< r_e) \rangle$ replaced the central surface brightness in the Kormendy relation as the former is less affected by measurement errors (e.g., Djorgovski & Davis 1987). The modified Kormendy relation has the added advantage that both $\langle I_b(< r_e) \rangle$ and r_e can in principle be operationally determined without assuming any specific intensity profile for galaxies. However, if we assume the de Vaucouleurs law, the central surface brightness and the mean surface brightness within r_e differ from each other by a simple constant.
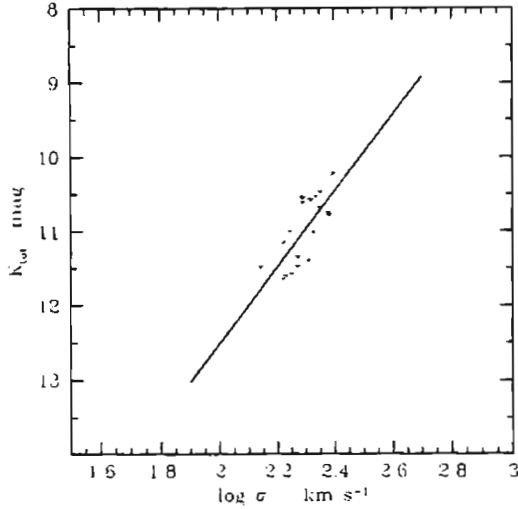
Figure 3.5: Faber-Jackson relation for Abell galaxies; de Vaucouleurs fitting.

Hence the slope of Equation 3.1 is not expected to change by this change of variables. For our Abell galaxies, we get

$$\langle \mu_b(< r_e) \rangle = (2.36 \pm 0.41) \log A_e + (14.24 \pm 0.27), \qquad (3.2)$$

where $\log A_e$ is the effective diameter expressed in arcsec [1]. The errors in the coefficients were estimated using a bootstrap technique (see Appendix A). This technique is used to estimate errors in all the subsequent relations in this thesis, unless otherwise mentioned. The best fit Kormendy relation is shown in Figure 3.4. The scatter in this relation is 0.43 mag arcsec^{-2} along the $\langle \mu_b(< r_e) \rangle$ axis. As already known, the scatter observed in the Kormendy relation is larger than the scatter expected from observational errors associated with the parameters involved in the

---

[1] Note that Equation 3.1 and Equation 3.2 are not directly comparable as the observation for the two samples are done in different bands.

fit (see e. g. Pahre et al. 1998), and we say that it possesses *cosmic scatter*. In spite of this the Kormendy relation can be used as an economical procedure to find relative distances to clusters of galaxies. Pahre (1996) used this idea to estimate the distance to two high redshift clusters and carried out an improved version of the classical Tolman test for the expansion of the Universe. As the scatter in the Kormendy relation is fairly large, it is of little use to estimate distances to individual galaxies. On the other hand, if we apply this relation to clusters of galaxies, it can be advantageous as it involves only photometric parameters and hence reduces the time spent in observation as well as data reduction. In a rich cluster, the large number of galaxies can statistically compensate to a great extent the uncertainties due to large scatter.

3.4.2 Faber-Jackson Relation

Faber & Jackson (1976) demonstrated the existence of a correlation between luminosity and central velocity dispersion for elliptical galaxies and proposed its use as a distance indicator. The presence of large scatter in the relation, however, limited its usage in measuring distances.

Figure 3.5 shows the Faber-Jackson relation for our Abell galaxies for parameters determined assuming the de Vaucouleurs law to the surface brightness profile. The best fit relation obtained using a least squares minimization treating $\log \sigma$ as the independent parameter is

$$K_{tot} = (-5.12 \pm 1.78) \log \sigma + (22.76 \pm 4.09). \tag{3.3}$$

We can use the total apparent magnitude K_{tot}, instead of the absolute magnitude, since our Abell galaxies are from clusters at very similar red shifts. The rms scatter along K_{tot} is 0.67 mag. The coefficients and the scatter of the relation reported here match those obtained in literature

for clusters of galaxies. For e. g. Mobasher et al. (1999) reported $K_{tot} = (-6.78 \pm 0.50) \log \sigma + (26.28 \pm 1.14)$ with an rms scatter of about 0.5 mag using de Vaucouleurs fits to a sample of Coma ellipticals. The larger errors in the coefficients of Equation 3.3 than that reported by Mobasher et al. may be because of the fact that the Abell galaxies are from two different clusters.

3.4.3   The Fundamental Plane

The scatter observed in both Kormendy and Faber-Jackson relations are not completely accounted for by observational errors, implying the possibility of a 'hidden' parameter. By studying large samples of elliptical galaxies (Dressler et al. 1987a; Djorgovski & Davis 1987), it was established that the central surface brightness was the parameter that caused substantial scatter in the Faber -Jackson relation. This led to the discovery that the intrinsic properties of elliptical galaxies are constrained to lie on a plane, called the fundamental plane, in the three dimensional space defined by $\log A_e$, $\langle \mu_b (< r_e) \rangle$ and $\log \sigma$, where A_e is the effective diameter expressed in arcsec. The fundamental plane, with its bi-parametric nature, was a significant improvement in the earlier understanding that ellipticals form a single parametric family manifested through the colour-magnitude and Faber- Jackson relations. Apart from providing better accuracies in measuring relative distances by studying large samples of early-type galaxies in rich clusters (e. g. Lucey & Carter 1988; Lucey et al. 1991a,b,c; Jørgensen, Franx & Kjærgaard 1993, 1996; Prugniel & Simien 1996; Hudson et al. 1997; Pahre et al. 1998; Colless et al. 2001) the small scatter in the fundamental plane provides valuable information for galaxy evolution studies (van Dokkum & Franx 1996; Pahre 1998; Kelson et al. 2000).

We have obtained the fundamental plane for our sample by minimizing the dispersion in $\log A_e$ and find that the equation for the plane is (note that
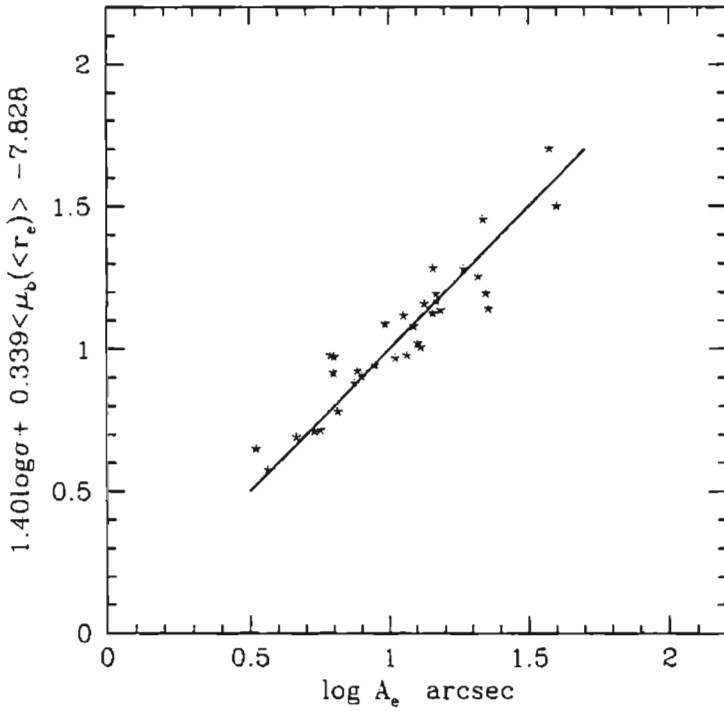
Figure 3.6: An edge on view of the de Vaucouleurs fundamental plane for Abell galaxies.

in this chapter all parameters for individual galaxies have been obtained
by using de Vaucouleurs profiles)

$$\log A_e = (1.40 \pm 0.23) \log \sigma + (0.34 \pm 0.03) \langle \mu_b(< r_e) \rangle + \gamma. \quad (3.4)$$

In Figure 3.6 an edge on view of the de Vaucouleurs fundamental plane
is shown. The scatter in this relation is about 0.092 dex along the $\log A_e$
axis, much less than that present for both Kormendy and Faber-Jackson
relations. The small scatter corresponds to an uncertainty of about 21% in
distance measurements to individual galaxies using this fundamental plane
relation. The coefficients and the errors obtained in Equation 3.4 are similar
to those reported in the literature (e. g. Pahre et al. 1998, Mobasher et al.
1999). The existence of small scatter in the fundamental plane has provided
a variety of opportunities for understanding the formation and evolution
of elliptical galaxies. The fundamental plane has been successfully used as
a distance indicator (Dressler et al. 1987a; Lucey & Carter 1988; Lynden-
Bell et al. 1988), as a cosmological evolutionary probe (van Dokkum &
Franx 1996; Kelson et al. 1997; van Dokkum et al. 1998) and to provide
constraints on models of galaxy formation and evolution (Faber et al. 1989;
Bender, Burstein & Faber 1993; Guzmán, Lucey & Bower 1993; Renzini
& Ciotti 1993; Zept & Silk 1996). In the next section we demonstrate
how the small scatter in the fundamental plane is used to constrain the
mass-to-light (M/L) ratios of elliptical galaxies.

3.5   The Fundamental Plane and M/L Ratios of Galaxies

It was Djorgovski, de Carvalho & Han (1988) who provided an elegant
interpretation of the existence of a tight fundament·l plane from simple

considerations. Assuming galaxies are in a state of virial equilibrium, or at least in a quasi-stationary one, we get,

$$\frac{GM}{R_m} = k_m \frac{\langle V^2 \rangle}{2}.$$ (3.5)

The parameter k_m is unity for a perfectly virialized galaxy. However, k_m is introduced to represent a more general situation, where galaxies evolve through quasi-equilibrium states, with different values of k_m signifying different stages of evolution of galaxies. We can obtain further constraints with the help of some assumptions on the structure of galaxies. If we assume that the gravitating mass in elliptical galaxies follow the luminous matter, we get,

$$r_e = k_r \, R_m,$$ (3.6)

where the parameter k_r allows for representing the physical radius R_m by the observed half-light radius r_e. We assume that the mass- density structure of all elliptical galaxies are the same, there by treating k_r as constant. However, it is quite possible that galaxies are formed with a characteristic mass-density distribution. It is also possible that processes like galaxy merging and tidal interactions can lead to a evolution in mass- density structure. Neglecting such variations in the mass distribution in individual galaxies can introduce systematic offsets to the characterization we employ through Equation 3.6 and hence in the construction of the (hypothetical) fundamental plane, as we can see later in the section.

We may use the central velocity dispersion for representing the kinetic energy term, as

$$\sigma^2 = k_v \, \langle V^2 \rangle,$$ (3.7)

with k_v determined by the dynamical structure within the galaxy. For simplicity, we assume k_v to be constant for all galaxies, but like the k_r term,

it might depend on various formative and evolutionary processes that have shaped the galaxy. Moreover, the anisotropies of the velocity dispersion tensor, including the differing degrees of random and circular motion in the galaxy, the differing velocity dispersion profiles, and the neglect of the rotational energy component in the calculation of kinetic energy term $\langle V^2 \rangle$ as we ignore the possible contributions from the rotational energy of each galaxy, could influence the value of k_v term for different galaxies.

By the definition of half-light radius, we have for the luminosity of a galaxy in the K band

$$L_K = 2\pi \langle I_{\mathrm{b}}(< r_{\mathrm{e}}) \rangle \, r_{\mathrm{e}}^2. \tag{3.8}$$

Note that for a de Vaucouleurs galaxy the $\langle \mu_{\mathrm{b}}(< r_{\mathrm{e}}) \rangle$ term differs from $\mu_{\mathrm{b}}(0)$ simply by a constant. If we assume that the bolometric luminosity L of ellipticals scales with their K band luminosity, we get

$$L = k_l L_K, \tag{3.9}$$

where k_l represents the luminosity structure within the galaxy.

Combining these with the virial theorem in Equation 3.5, we get

$$r_{\mathrm{e}} = k\sigma^2 \left[\langle I_{\mathrm{b}}(< r_{\mathrm{e}}) \rangle \right]^{-1} \left(\frac{M}{L} \right)^{-1} \tag{3.10}$$

with $k = k_m / (4\pi G k_r k_v k_l)$. The existence of the fundamental plane provides a relation of the form $r_{\mathrm{e}} \propto \sigma^A \left[\langle I_{\mathrm{b}}(< r_{\mathrm{e}}) \rangle \right]^B$, where A and B are observationally determined values. The tightness and stability of the FP then lead to

$$M/L \propto \sigma^{(2-A)} \left[\langle I_{\mathrm{b}}(< r_{\mathrm{e}}) \rangle \right]^{-(1+B)} \tag{3.11}$$

For the best fit A and B values in Equation 3.4, $M/L \propto$

$\sigma^{0.60}\left[\langle I_b(<r_e)\rangle\right]^{-0.15}$ This result is important as there is a large spectrum of parameters that determines the evolution of M/L of galaxies, like age and metallicity of the stellar populations and the dark matter. In star forming disks aging of the stellar population can be compensated by the formation of new stars, and various models indicate little or slightly negative evolution of M/L with time (e. g. Pozzetti, Bruzual, & Zamorani 1996; Ferraras & Silk 2001) with some support from the studies on the evolution of Tully-Fisher relation (Vogt et al. 1996; van Dokkum & Stanford 2001; Ziegler et al. 2002). On the other hand, the M/L ratios of early- type galaxies as well as bulges of other Hubble types are expected to increase with age as the vanishing of massive stars causes their stellar populations to go fainter (Tinsley & Gunn 1976). From fundamental plane studies, cluster ellipticals show a gradual increase in M/L ratios with redshift (e. g. van Dokkum & Franx 1996; Kelson et al. 1997; van Dokkum et al. 1998).

3.6   Summary

In this chapter, we have provided discussions on observation of the sample and reduction of data. Assuming a de Vaucouleurs profile for the surface brightness of bulges, we have determined the photometric structural parameters using the decomposition algorithm *fitjal*. The extracted parameters are used to examine various correlations including the fundamental plane. In the next chapter we will compare the results described here with those obtained by using the more general Sersic law.

Chapter 4

Sersic Fundamental Plane for Galaxies

In Chapter 2, we have seen that a large variety of approximations, numerical as well as analytical, is used by various authors to describe the surface brightness profiles. After the discovery of de Vaucouleurs' $r^{1/4}$ law (de Vaucouleurs, 1948), it was extensively used to describe the light distribution in elliptical galaxies and in the bulges of spiral galaxies (e. g. de Vaucouleurs, 1959). In the previous chapter we showed that de Vaucouleurs law provides reasonably good fits to many galaxies in our Abell clusters, but it was noted that not all galaxies obey the $r^{1/4}$ law.

While de Vaucouleurs' law seemed to be adequate when it was first introduced, the scenario changed considerably with the availability of more sensitive and accurate data from sophisticated CCDs. Detailed analysis of larger samples of bulges from different types of galaxies, like dwarf and giant ellipticals, showed the existence of systematic deviations of the intensity profiles from the $r^{1/4}$ law (Michard 1985; Schombert 1986; van den Berg

1989; Bingelli & Cameron 1991). Sersic (1968) proposed a generalization for the de Vaucouleurs' law, replacing the $r^{1/4}$ term by $r^{1/n}$, with n as free parameter, expecting the modified form to represent better the observed profiles in ellipticals.

The Sersic law, Equation 2.5, was used to fit bulges of different types of galaxies. Caon et al. (1993) obtained large values of n for some galaxies from a sample of ellipticals and bulges of S0 galaxies. They also noticed that the Sersic index n is correlated with the effective radius and total luminosity of the galaxy. Andredakis et al. (1995), in their study of spiral galaxies, found that n varies systematically with a value of around one to six as the galaxy type changes from late- to early-type bulges. Khosroshahi et al. (2000b) observed from their study of ellipticals in Coma cluster that the distribution of n showed a wide variation with values ranging from around one to five, with a clear peak around four. This explained the fact that de Vaucouleurs' law could fit well many ellipticals, but not all of them. On the other hand, they noticed that n values for the bulges of early-type spiral galaxies covered almost uniformly about the same range as in the case of ellipticals. Hubble Space Telescope (HST) observations also showed a marked deviation from $r^{1/4}$ profiles for a sample of bulges in spirals and S0 galaxies (Balcells et al. 2003). However, structural parameters are still extracted using $r^{1/4}$ law, especially at high redshifts, for ellipticals (Kelson et al. 1997, 2000; Dressler et al. 2000) as well as bulges of different Hubble types (e. g. Simard et al. 2002, Seigar et al. 2002).

The present chapter deals with detailed comparison of structural parameters determined by applying two different distribution laws, namely the de Vaucouleurs' law and the more generalised Sersic law to the Abell clusters sample. As explained in Chapter 2, we extract the photometric parameters for the galaxies in the Abell clusters using the full 2D code *fitgal*. The extracted parameters are used to construct profiles for these

galaxies, and are compared with that obtained from the model indepen-
dent estimation using *ellipse.* The comparison revealed that though the
de Vaucouleurs' law could provide reasonable representation to the surface
brightness profile of many galaxies, the Sersic law provided better fits to
the observed profile in all cases. It is also shown that enforcing the de Vau-
couleurs' law to all cases actually leads to serious and systematic under- or
over-estimation of the global photometric parameters. The more deviant
the Sersic index n of the galaxy from four, the greater the discrepancies
in the estimated parameters are. Finally, we move on to examine vari-
ous correlations involving these parameters to see whether there are any
systematic deviations arising because of the choice of the inherent surface
brightness profile one adopts.

4.1   Sersic Profiles

The three parameters in the Sersic law, the central surface brightness $\mu_b(0)$,
half-light radius r_e and the Sersic index n, completely specify a smooth
and monotonically decreasing profile. To a first approximation, the $\mu_b(0)$
determines how bright the galaxy is, r_e provides an estimation of how
far the galaxy extends to outer space while n decides the steepness of
the profile. In Figure 4.1 we show a series of Sersic profiles, for different
shape parameters $(1 \leq n \leq 10)$ taking an arbitrary central brightness of
12 magnitude and r_e of 20 units. As can be seen, for $n = 1$ we get an
exponential profile, and as n increases the steepness of the profile within
r_e increases. Analytically it is easy to show that the surface brightness at
the effective radius is given by

$$\mu_b(r_e) = \mu_b(0) + 2.5 \, b_n \qquad (4.1)$$
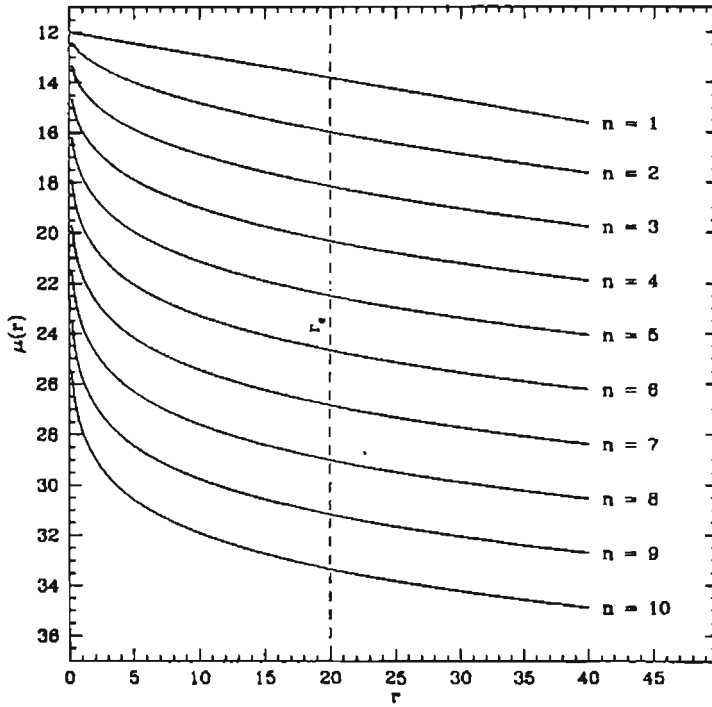
Figure 4.1: Sample Sersic profiles with different shape parameters. The central surface brightness and the effective radius for all profiles are kept at $12\,\mathrm{mag\,arcsec}^{-2}$ and 20 units respectively.

where b_n is linearly dependent on n within the range specified (see Equation 2.7). Hence large values of the Sersic index ($n > 6$) are to be treated with caution, as this combined with a reasonable r_e (i. e., greater than a few times the PSF) would mean extremely large dynamic ranges for the surface brightness of galaxies. For example, for a bulge with $n = 12$, which is not uncommon in some studies (e. g. Graham et al. 1996; Bertin, Ciotti & Del Principe 2002), the difference of magnitudes between the centre (unconvolved) and at r_e is more than 25 mag. However, any extra central light could result in detecting large n values. Inner disks, very compact sources, and excessive star formation in galactic nuclei (e. g. Phillips et al. 1996; Rest et al. 2001; Carollo et al. 2002; Pizzela et al. 2002) can contribute to the bulge intensity which is difficult to disentangle from the bulge using ground-based observations (Ravindranath et al. 2001).

We show in Figure 4.2 the surface brightness profiles of Figure 4.1 as a function of $r^{1/4}$ It should be noted that almost all the profiles near $n = 4$ provide an approximately straight line region close to r_e. Methods that assume de Vaucouleurs' law, in general, used the straight line region, avoiding regions affected by the PSF and sky brightness, to estimate the photometric parameters. Hence it is not surprising that de Vaucouleurs law could provide reasonable approximations to the observed profiles for bulk of the less sensitive photographic data. However, this is not without pitfalls, as we show in the next section where we analyse the photometric parameters extracted assuming de Vaucouleurs and Sersic profiles separately.

4.2   Analysis

As already mentioned in Section 2.6, the bulge-disk decomposition algorithm *fitgal*, can be used to determine the photometric parameters of galaxies assuming de Vaucouleurs or the general Sersic law to the surface bright-
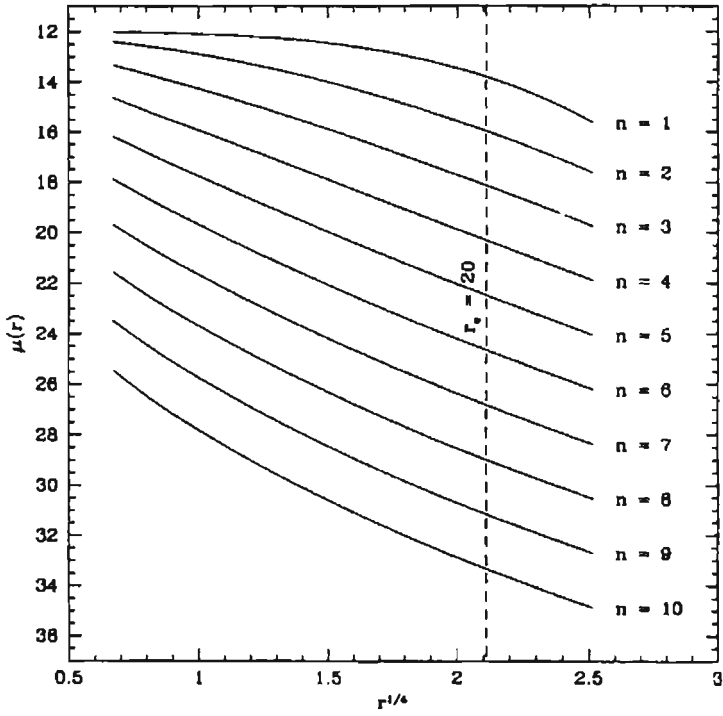
Figure 4.2: Sersic surface brightness profiles as a function of $r^{1/4}$

ness profiles. In the previous chapter we discussed de Vaucouleurs' fits to the Abell galaxies and showed that not many galaxies could be represented well using the $r^{1/4}$ law. Here we report the best fit parameters obtained from another run of *fitgal* for the Abell galaxies assuming Sersic profiles. For easy comparison, we have shown in Table 4.1 the best fit de Vaucouleurs and Sersic parameter values for all the 35 Abell galaxies in the sample, and in Figure 4.3 the corresponding surface brightness profiles. The galaxies BO13 and F105 are avoided in the following discussion for reasons already given in Section 3.3. In the figure, the de Vaucouleurs profiles have been shifted (made fainter) by two magnitudes for clarity. In each window, the model independent profile obtained by fitting ellipses to the isophotes has been shown as a series of points. The de Vaucouleurs and the Sersic profiles were generated using Equation 2.2 and Equation 2.5 respectively from the best fit parameters obtained from the corresponding two-dimensional fits to the images using *fitgal*. We wish to emphasize here that the model independent profile for each galaxy has been introduced only as an aid in the comparison between the observed surface brightness distribution and the best fit profiles and that it was *not* used to determine the structural parameters.

It can be seen from Figure 4.3 that de Vaucouleurs law provides a satisfactory fit in many cases but not all. In all cases the fit is improved when the Sersic law is used, which also reflects in a reduced value of χ^2 for the Sersic case. It is interesting to note that when the best fit n value for the $r^{1/n}$ fit is close to 4, i.e., in the range $3.5 \lesssim n \lesssim 4.2$, de Vaucouleurs law also provides a good fit which is not surprising given the description in the previous section. In Figure 4.4 the different profiles for galaxy D55 are shown. As already noted in the previous chapter for the galaxy D55, the de Vaucouleurs law profile generated from *fitgal* (the dashed curve, made fainter by two magnitudes for clarity) matches well with the   observed

Galaxy	de Vacouleurs		Sersic				
	$\log A_e$	$\mu_b(0)$	n	$\log A_e$	$\mu_b(0)$	$\langle \mu_b(<r_e) \rangle$	K_{tot}
	arcsec	mag/$\Box$		arcsec	mag/$\Box$	mag/$\Box$	mag
BO13	1.194	9.58	2.71	0.948	11.32	15.74	10.51
BO16	1.338	10.71	4.87	1.479	9.42	18.16	10.28
BU32	1.022	9.82	4.78	1.152	8.69	17.26	11.01
D107	1.184	10.03	2.74	0.984	11.85	16.32	10.91
D119	1.320	9.72	4.00	1.319	9.72	16.71	9.63
D127	1.064	9.45	3.38	0.963	10.34	16.10	10.80
D38	0.948	9.08	3.87	0.933	9.30	16.03	10.88
D55	1.126	9.87	3.65	1.095	10.39	16.68	10.72
D57	1.169	9.94	3.52	1.081	10.61	16.63	10.74
D68	1.051	9.83	3.50	0.974	10.58	16.58	11.22
D75	0.985	9.96	2.31	0.757	12.52	16.14	11.86
D80	0.797	9.50	3.30	0.766	11.00	16.59	12.27
D93	0.873	9.52	3.62	0.834	10.09	16.33	11.67
F105	0.965	11.73	3.61	0.968	12.50	18.71	13.38
N7728	1.600	10.16	2.40	1.275	12.23	16.02	9.16
BO73	0.800	9.84	2.19	0.640	12.90	16.27	12.58
FCOM	1.087	10.48	3.00	0.872	11.78	16.78	11.93
N1	1.102	9.68	3.47	1.001	10.40	16.33	10.84
N6158	1.348	10.24	3.37	1.139	10.83	16.58	10.40
RB130	0.750	8.71	4.36	0.788	8.14	15.86	11.42
RB162	1.158	10.10	2.83	0.931	11.67	16.33	11.18
RB38	1.356	10.64	2.76	1.145	12.46	16.99	10.77
RB40	0.813	9.27	3.54	0.737	10.05	16.13	11.95
RB72	1.113	9.66	4.21	1.056	9.10	16.53	10.76
RB78	1.574	12.29	1.90	1.041	14.97	17.77	12.07
RB8	1.155	9.56	3.62	1.095	10.10	16.35	10.38
S18	0.901	9.41	3.60	0.847	9.99	16.19	11.47
S26	1.266	10.66	3.78	1.189	10.69	17.25	10.81
S30	0.665	8.30	3.07	0.656	10.26	15.41	11.63
S33	0.786	8.95	3.10	0.676	10.27	15.47	11.60
S34	0.728	9.17	3.00	0.651	10.90	15.90	12.15
S43	1.167	10.39	2.62	0.930	12.35	16.58	11.44
S44	0.884	9.56	3.70	0.838	10.01	16.40	11.72
Z34A	0.563	8.28	2.66	0.350	10.41	14.74	12.50
NCOM	0.521	9.08	4.78	0.648	8.07	16.62	12.89

Table 4.1: Photometric structural parameters obtained from de Vaucouleurs and Sersic fitting. For $n = 4$, $\langle \mu_b(<r_e) \rangle = \mu_b(0) + 6.935$; $K_{tot} = \langle \mu_b(<r_e) \rangle - 5 \log A_e - 0.490$. Note: The symbol $\Box$ is used to show the unit arcsec^2.
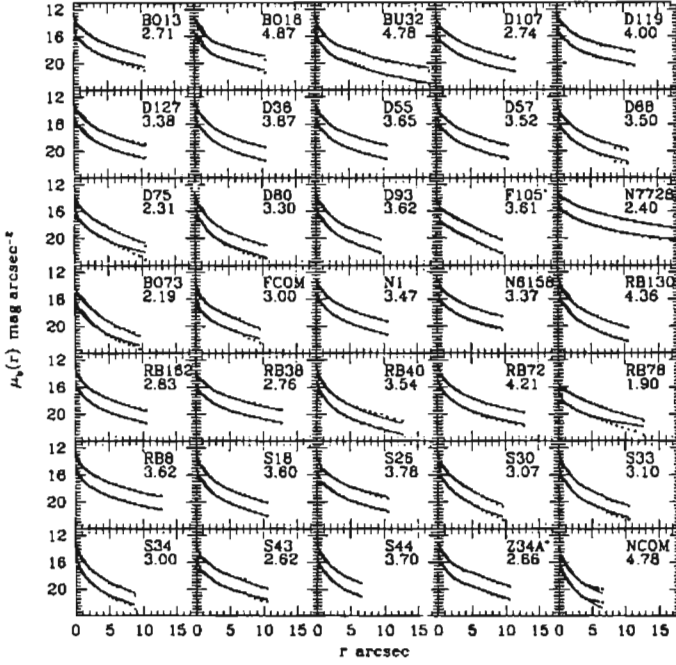
Figure 4.3: Best fit de Vaucouleurs & Sersic profiles for the sample Abell galaxies. In each window, the upper and lower curves are from the Sersic and the de Vaucouleurs fits respectively, obtained from separate runs of *fitgal*, with the latter made fainter by two magnitudes for clarity. The curves represent the unconvolved surface brightness along the major axis for the corresponding model. The points indicate the model free surface brightness distribution obtained using the *ellipse* task. The galaxy name and the best fit Sersic parameter value are shown in the upper right hand corner of each window.
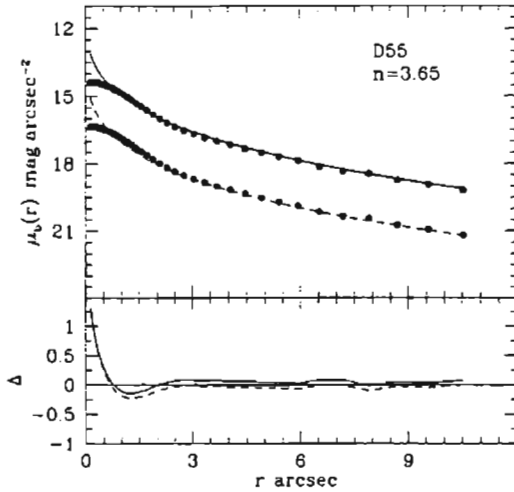
Figure 4.4: Best fit de Vaucouleurs (dashed curve) and Sersic (continuous curve) profiles for galaxy D55. The profile fits are nearly equally good, as the Sersic index is close to 4. In the bottom window the corresponding residual profiles from the *ellipse* estimation are shown.

profile determined by *ellipse* (shown as filled circles). The Sersic index for the galaxy obtained is close to 4 as shown in the upper right hand corner of the figure. For an easy comparison the Sersic profile generated from best fit parameters obtained from *fitgal* is also shown (the continuous curve). The residuals of both the profiles from the *ellipse* profile are shown in the lower window. Clearly, both de Vaucouleurs and Sersic profiles provide reasonably good fits to the observed profile. On the other hand for the galaxy BO13 the Sersic profile provides a much better fit, as can be seen from Figure 4.5. It is also worth noting that in this case the best fit n value is quite different from four.
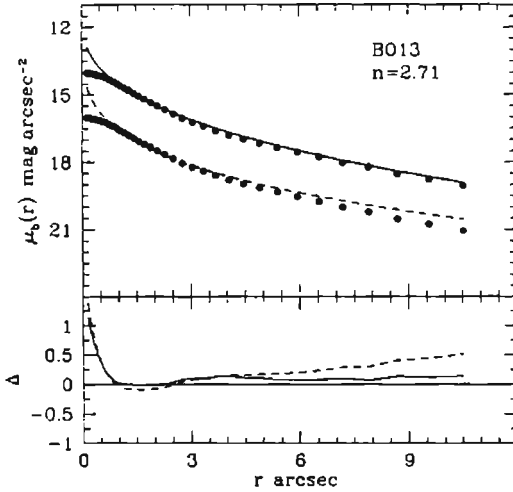
Figure 4.5: The Sersic law fits the observed profile better for the galaxy BO13. The curves and symbols are used as in Figure 4.4.

The distribution of best fit n values for the Abell galaxies is shown in Figure 4.6, along with the same for the Coma sample and the spiral bulges. It is seen that a fair number of the Abell and Coma ellipticals have best fit n values close to 4, which explains why de Vaucouleurs law has worked well with ellipticals in the past. The distribution of n values for bulges of spiral galaxies is flat and favors neither the value $n = 4$, nor the value $n = 1$ (Khosroshahi et al. 2000b). The latter means that it is not a good approximation to assume that bulge intensity profiles have an exponential form, as has sometimes been done in the literature.

In the top panel of Figure 4.7, we have plotted the logarithmic ratio of the best fit effective radii for the Sersic and de Vaucouleurs laws respectively for each galaxy in the Abell clusters, against the best fit Sersic value n, for the same galaxy.   In the middle we have shown a similar plot of
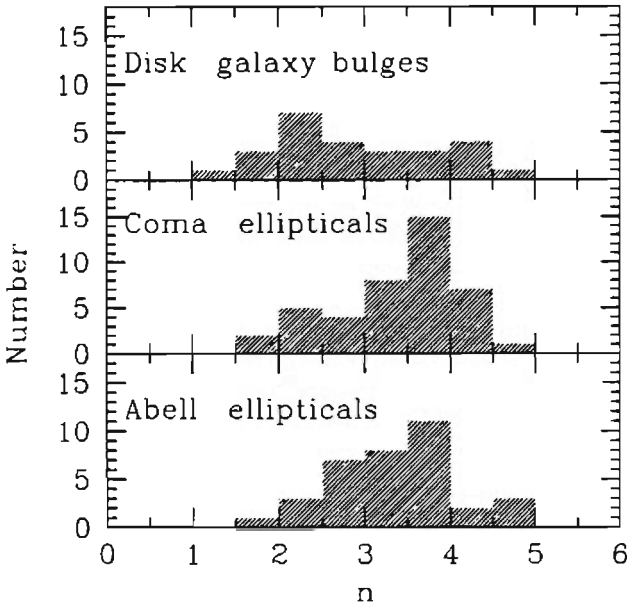
Figure 4.6: Distribution of Sersic index n for different samples of galaxies.

$\mu_b(0)_n - \mu_b(0)_4$, and in the lower panel a plot of $\langle\mu_b(< r_e)\rangle_n - \langle\mu_b(< r_e)\rangle_4$ for the sample. These plots enable us to estimate the deviation of the best fit parameters from their Sersic value, when the de Vaucouleurs law is used to fit the profile. The plots help us answer the question "How good is to use de Vaucouleurs law instead of the more general Sersic law?"

It is seen that usage of de Vaucouleurs law leads to an over-estimation of the effective radius for $n < 4$, and an under-estimation for $n > 4$. The deviation of the central surface brightness, upon using de Vaucouleurs law, is in the opposite direction as a function of n. This is a reflection of the underlying correlations between the parameters, which we describe later.

The dependence of $\langle\mu_b(< r_e)\rangle_n - \langle\mu_b(< r_e)\rangle_4$ on n follows from the
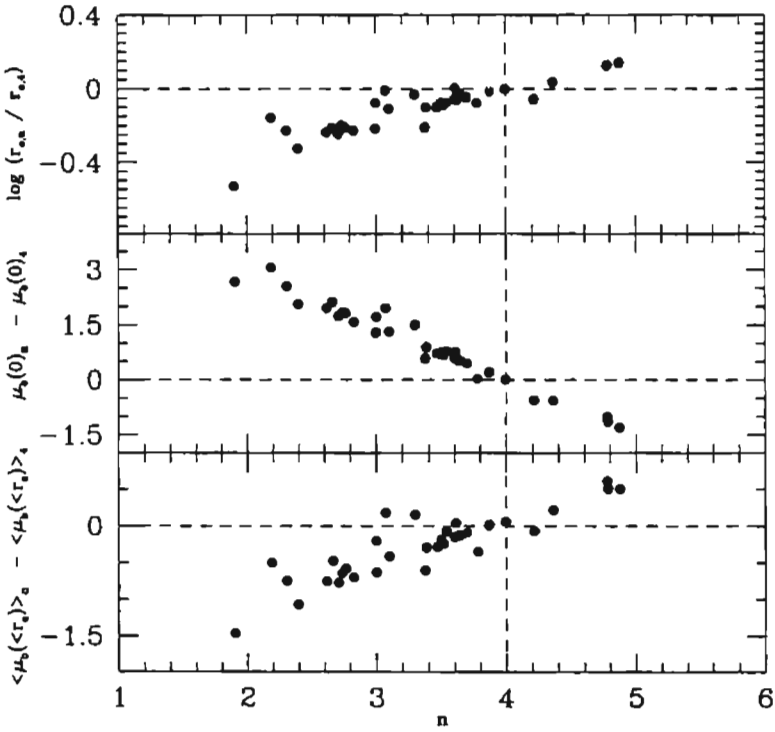
Figure 4.7: Comparison of best fit de Vaucouleurs and Sersic parameters. There is a systematic under- or over-estimation of the best fit de Vaucouleurs parameters, relative to the best fit Sersic parameters, when the best fit n differs from 4, as explained in the text.
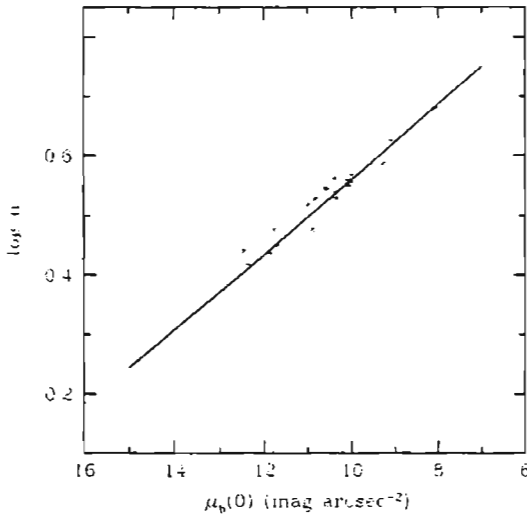
Figure 4.8: Logarithm of the Sersic index n as a function of unconvolved bulge central surface brightness. The linear correlation coefficient is -0.92 with a significance level > 99.99%.

the behaviour of the other two deviations. It is seen that the value of $\langle \mu_b(< r_e) \rangle$ is less sensitively dependent on the fitting model used than the value of $\mu_b(0)$.

4.3   Correlations

In the last section we showed that the Sersic law describes better the surface brightness profile of the galaxies than de Vaucouleurs one. Hence in our analysis, we will be using results obtained from the Sersic fits, citing the deviations introduced, if any, by the use of de Vaucouleurs fits. We first look at the bi-parameter correlations for the   Sersic fits for the 33
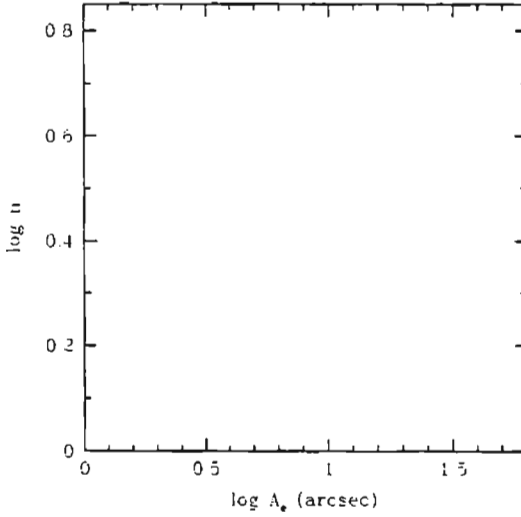
Figure 4.9: $\log n$ as a function of $\log A_e$. There is no significant correlation.

galaxies in the Abell sample. The central surface brightness is well corre-
lated with $\log n$ (Figure 4.8), with a linear correlation coefficient of -0.92 at
a significance level of greater than 99.99%. We find that $\log A_e$ and $\log n$
are poorly correlated; there is large scatter, the correlation coefficient being
0.27 with a significance level of 87% (Figure 4.9). Since higher values of
n imply steeper surface brightness profiles, these correlations suggest that,
in general, higher values of n are expected for brighter galaxies.

In Figure 4.10, we show the variation of K_{tot} magnitude with n for our
Abell sample. The expected trend is clearly seen, but the linear correlation
coefficient is only 0.22 at a significance of 78%. But removing the two
outliers, N7728 and NCOM the correlation   coefficient and significance
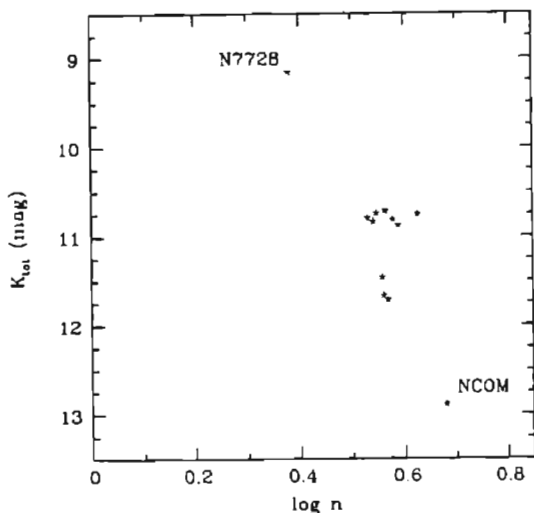
Figure 4.10: Variation of n with K_{tot} magnitude. There is a clear trend suggesting brighter galaxies move towards the higher side of n axis.

improves to 0.57 and 99.9% respectively. Such a correlation was proposed by Young & Currie (1998) for measuring distances to galaxies.

We have seen in Section 4.2 that imposing the de Vaucouleurs' law to the surface brightness profile of bulges leads to serious under- or over- estimation of their structural parameters. Hence it is worth studying how the well-known correlations like Kormendy, Faber-Jackson and the fundamental plane change when we use the more accurate parameters obtained from the Sersic law fits.

4.3.1   Kormendy Relation from Sersic Law Fits

It is interesting to note that the correlation suggested by Kormendy (1977) is lost when we introduce n in the profile fitting. In Figure 4.11 we show the variation between the central surface brightness and effective diameter,
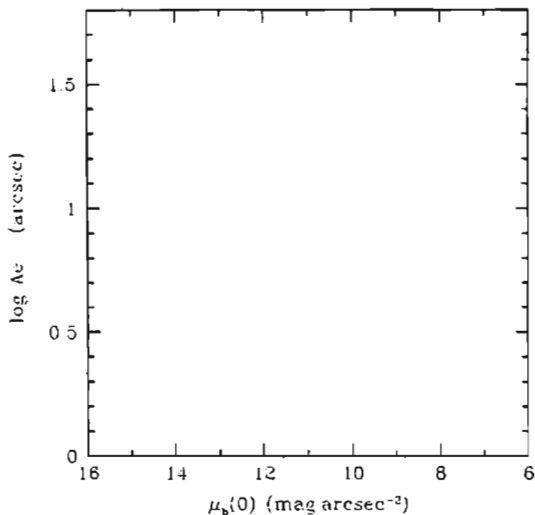
Figure 4.11: No significant correlation between effective diameter and the unconvolved bulge central intensity for our Abell galaxies.

and clearly there is no correlation. However, for the modified Kormendy relation, where one replaces $\mu_b(0)$ by $\langle\mu_b(<r_e)\rangle$, an excellent correlation is seen (Figure 4.12) similar to Figure 3.4 of Chapter 3. When n is introduced, the relation between $\mu_b(0)$ and $\langle\mu_b(<r_e)\rangle$ is strongly dependent on n (see Appendix B) and hence no correlation is seen between $\mu_b(0)$ and $\langle\mu_b(<r_e)\rangle$ (Khosroshahi et al. 2000b).

Using least squares minimization we have obtained the Kormendy relation for the Sersic law fitted parameters for the Abell galaxies as

$$\langle\mu_b(<r_e)\rangle = (1.99 \pm 0.35)\log A_e + (14.57 \pm 0.32). \tag{4.2}$$
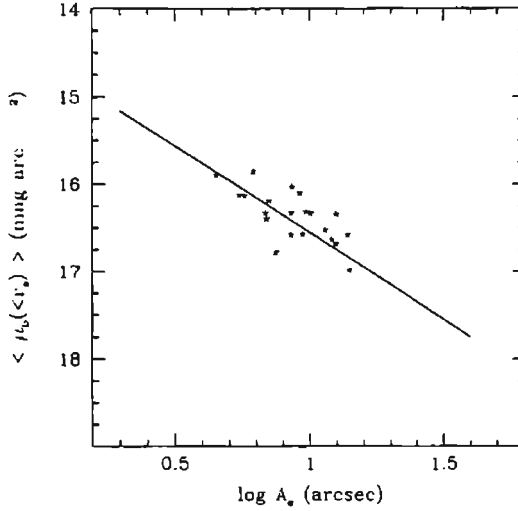
Figure 4.12: Kormendy relation for the Abell galaxies.

The relation has an rms scatter of 0.43 $\mathrm{mag\,arcsec}^{-2}$ in mean surface brightness and is plotted in Figure 4.12. The errors in the coefficients were estimated using a bootstrap technique. The coefficients and the scatter in Equation 4.2 are similar to those observed by Khosroshahi et al. (2000b) for a sample of Coma ellipticals. It is interesting to note that the slope and scatter of the Equation 4.2 is not significantly different from Equation 3.2 obtained using $r^{1/4}$ law fitted parameters.

4.3.2 Faber-Jackson Relation

For the Sersic parameters, we obtain the Faber-Jackson relation as

$$K_{tot} = (-5.71 \pm 1.52)\log\sigma + (24.35 \pm 3.48). \tag{4.3}$$

A plot is shown in Figure 4.13. The rms scatter in this relation is about
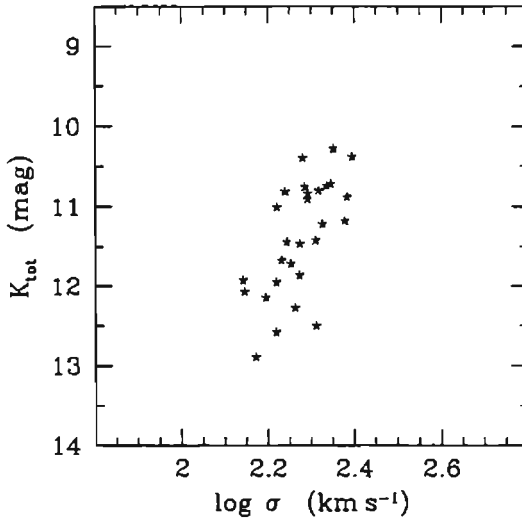
Figure 4.13: Faber-Jackson relation for Abell galaxies, for Sersic parameters.

0.64 mag along the K_{tot} axis. Here too the relation does not differ much from the corresponding relation in Equation 3.3 obtained from de Vaucouleurs' law fitted parameters. Here the correlation is preserved possibly because the under- and over- estimations induced in the $\langle \mu_b(< r_e) \rangle$ due to $r^{1/4}$ fit is almost canceled by a corresponding over- and under- estimation of effective radius in the other direction.

4.3.3 Sersic Fundamental Plane

Even though the structural parameters change systematically, and significantly in some cases, depending on the assumption of underlying distribution of the surface brightness, the fundamental plane for the Sersic parameters, like the Kormendy and Faber-Jackson relations, does not differ
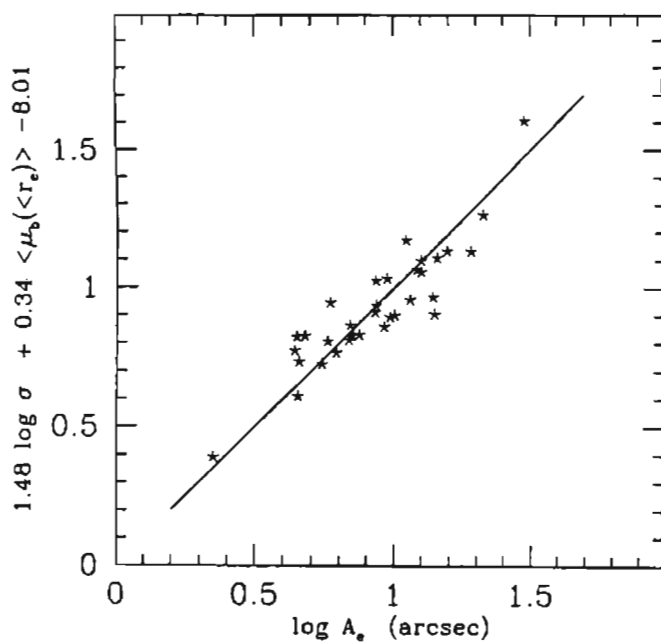
Figure 4.14: An edge-on view of the best fit Sersic fundamental plane for Abell galaxies.

significantly from the corresponding Equation 3.4. For the best fit Sersic fundamental Plane we have

$$\log A_e = (1.48 \pm 0.25)\log\sigma + (0.34 \pm 0.04)\langle\mu_b(< r_e)\rangle + \gamma, \quad (4.4)$$

where γ is a constant which mainly depends on the distance to the cluster of the sample concerned. An edge-on view of the relation is shown in Figure 4.14.

4.4   Summary

In this chapter we have studied the parameters extracted using different laws to the surface brightness profile of galaxies. We have shown that the Sersic law provides better fits, than the de Vaucouleurs law, to the observed surface brightness profiles of elliptical galaxies. The imposition of de Vaucouleurs law, which is done even today, actually introduces serious and systematic deviations in the estimated photometric parameters. However, these systematic under- or over -estimations do not change the well-known correlations like Kormendy, Faber-Jackson and the Fundamental plane significantly. Hence the $r^{1/4}$ law can be used where the objectives of the study are on the underlying correlations. But it is necessary to use the Sersic law when the best fit parameters of individual galaxies are important, as in the estimation of relative distances to individual galaxies in clusters.

A detailed study on correlations involving higher dimensions is deferred to the next chapter, where we analyse the fundamental and photometric plane relations for the early type galaxies and show that there exists a 4D hyper-plane for early-type galaxies.

Chapter 5

The Hyper-Plane for Early-Type Galaxies

5.1 Introduction

As already noted, the parameters that describe the morphology and internal dynamics of elliptical galaxies, and correlations between them, provide valuable information on the structure, formation and evolution of these objects. In this chapter we pay attention to two such three dimensional correlations, the photometric and fundamental planes, known for their very small inherent scatter, and show that there also exists a four dimensional correlation between n, σ, r_e, and $\mu_b(0)$. The lower dimensional photometric plane forms a simple projection of the hyper plane, where the displacements along the $\log \sigma$ axis in the definition of the hyper plane are not taken care of. It is also shown that the fundamental plane, by way of selection of variables, forms an unusual projection of the hyper plane. We then move on to discuss how the mass-to-light ratios (M/L) of early type galaxies is

influenced by the hyper plane relation.-

5.2   The Near-IR Photometric and Fundamental Planes

The photometric plane (PP), defined as the relation between the Sersic index (n)- effective radius (r_e)- central surface brightness ($I_b(0)$) has been studied at near-infra-red wavelengths for a sample of ellipticals in the Coma cluster by Khosroshahi et al. (2000a,b) and at optical wavelengths for a sample of early type galaxies in the Virgo and Fornax clusters (Graham 2002) and has been successfully extended to bulges of spirals, both early-type (Khosroshahi et al. 2000a) and late-type (Mölenhoff & Heidt 2001). A less obvious variant of the photometric plane can be traced in the study of a sample of dwarf ellipticals and dwarf S0s in the Virgo cluster by Binggeli & Jerjen (1998). The similarity of the PPs between ellipticals and bulges of different Hubble types is used as evidence that the underlying physical processes for the formation of these objects may be the same.

An edge-on view of the best fit near-IR PP for the galaxies in the two Abell clusters is presented in Figure 5.1. This is obtained by least squares minimization along the $\log n$ axis from the PP and is given as

$$
\begin{aligned}
\log n \;=\; & (0.122 \pm 0.021) \log A_e - (0.064 \pm 0.003)\mu_b(0) \\
& + (1.08 \pm 0.05).
\end{aligned} \tag{5.1}
$$

The rms scatter in $\log n$ is 0.024 dex. The errors in the coefficients were estimated using a bootstrap technique.

As already noted in the previous chapter, the Sersic fundamental plane Equation 4.4, possesses a scatter of 0.099 dex in $\log A_e$. The lesser inherent scatter of the PP is useful in examining the underlying correlations between
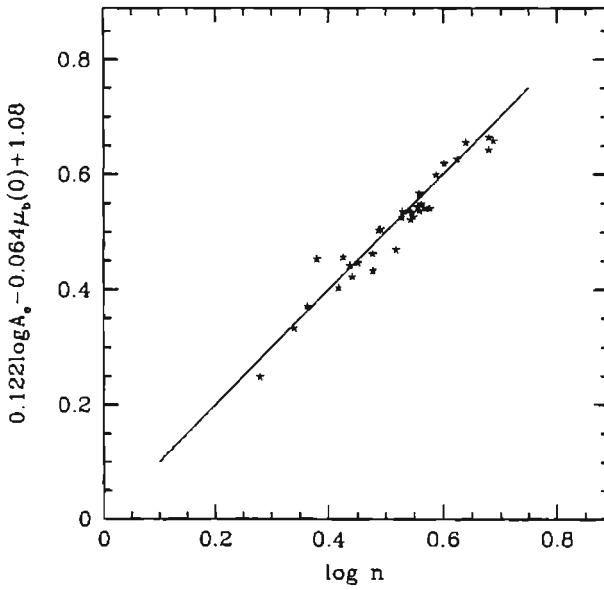
Figure 5.1: An edge on view of the best fit photometric plane for our galaxies in the two Abell clusters.

the structural parameters and can be used in simulations of formation and evolution of galaxies.

5.2.1 Scatter and Distance Estimation Error

Tight correlations between parameters that characterize the large scale morphology of galaxies provide information about underlying physical relationships and the origin and evolution of these complex systems. However, observed scatter in a relationship, which cannot be completely attributed to measurement error alone, provides important insights. The existence of such cosmic scatter in a correlation between a certain number of parameters is evidence for the existence of one or more other parameters which are 'hidden' in the present study. Accounting for these parameters, in general, results in an increase in the number of dimensions required for the best fit representation of the underlying correlation.

The colour- magnitude (de Vaucouleurs 1961, Sandage 1972, Sandage & Visvanathan 1978) and Faber-Jackson relations, each of which relates two parameters, independently suggested that ellipticals may be considered as a structurally and chemically homogeneous, single- parameter family. The correlations were useful in the study of galaxies, but the large scatter suggested the need for the study of higher dimensional correlations. This led to the establishment of the Fundamental Plane and the closely related $D_n - \sigma$ relation (Dressler et al. 1987a) [1], which involved three parameters. The new relations had lesser scatter, and the older relations with fewer parameters could be derived from them. The fundamental plane and $D_n - \sigma$ relations showed that the elliptical galaxies must be at least a bi-parametric family (there could be other underlying parameters which could become evident through the cosmic scatter as the data quality improved). The smaller

---

[1] D_n is the angular diameter of that central circular region of a galaxy with a pre-determined average surface brightness, like 20.75 mag arcsec^{-2} for B band.

scatter in the three dimensional relations makes the effects of any underlying observational biases less important; it also leads to an improvement in the accuracy in distance measurements to early type galaxies in rich clusters. FP measurements have been made in this way to redshifts $z \approx 1.3$ (van Dokkum & Stanford, 2003; van de Ven, van Dokkum & Franx, 2003), though individual cluster peculiar velocities are derivable only at $z \leq 0.05$ (Blakeslee et al. 2002). Since the angular size of an object is inversely proportional to its distance, the rms scatter along the $\log A_e$ axis is directly proportional to the percentage error in distance r,

$$\frac{\Delta r}{r} = \ln 10 \; \mathrm{rms}_{\log A_e}, \tag{5.2}$$

where $\mathrm{rms}_{\log A_e}$ is the rms scatter along the $\log A_e$ axis. When the best fit plane is not obtained taking $\log A_e$ as the independent variable, as in the case of the PP, we determine the distance measurement errors by obtaining another fit among the same variables but with $\log A_e$ as the independent variable. Even though the scatter in PP is smaller than that in FP, the distance measurement uncertainties are less for the FP (22.7%) than that for the PP (34.2%). This is not surprising as the PP contains only photometric parameters and the uncertainty obtained here is comparable to other purely photometric methods.

5.3 $n - \sigma$ Correlation?

The fundamental and photometric planes represent two separate three dimensional correlations between the four basic parameters r_e, $\mu_b(0)$, n and σ. It may be noted that the surface brightness term used in the PP ($\mu_b(0)$) differs from that in FP ($\langle \mu_b(< r_e) \rangle$). For a Sersic bulge, it is easy to see that $\langle \mu_b(< r_e) \rangle$ is a separable function of $\mu_b(0)$ and n (see Appendix B).
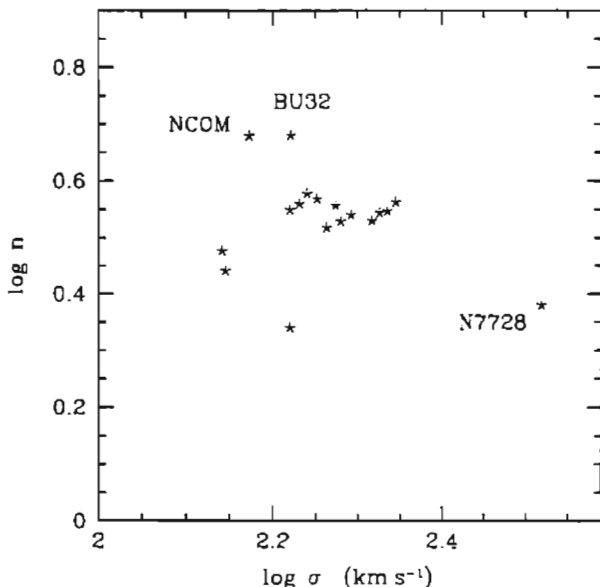
Figure 5.2: Sersic index n vs. velocity dispersion σ for Abell galaxies. The three outliers, the removal of which improves the correlation significantly, are marked.

The question now is: Are the two planes independent correlations, or are they different representations of just one relation between these four parameters? If the latter were to be true, we should expect an excellent correlation (i.e., without any cosmic scatter) between the Sersic parameter n and central velocity dispersion σ, which would allow a transformation from one plane to the other which preserves the observed scatter in the two planes.

Figure 5.2 shows the n - σ plot for the Abell galaxies in our sample.

No significant correlation is found between the two parameters, the linear correlation coefficient being $r = 0.11$, with a confidence level of 44%. If we remove the three outliers, BU32, N7728 and NCOM, the correlation coefficient improves to $r = 0.43$ with a confidence level of 98%, but still with large scatter. For a sample of early-type galaxies in the Virgo and Fornax clusters, Graham (2002) has found a significant correlation between n and σ. The values of both n and σ reported by Graham span a greater range than ours, and limiting his sample to our more limited range reduces the correlation significantly, and therefore there is no inconsistency in our results with Graham's correlation. But both in our sample and Graham's, the scatter about the best fit line is such that mapping from the FP to PP using the correlation would not preserve the small scatter observed in the PP.

5.4   The Hyper Plane

The observed scatter in the correlation between n and σ implies that one cannot simply map from the fundamental to the photometric planes and we should consider the possibility that these two planes derive from a higher dimensional entity. If the four parameters, r_e, $\mu_b(0)$, n and σ, are indeed correlated, we expect a trend between the scatter in the photometric plane and the velocity dispersion, which is not included in the definition of PP. Figure 5.3 shows the correlation between deviations along the $\log n$ axis of the PP for individual galaxies, $\delta_{PP} = (\log n - a \, \log A_e - b \, \mu(0) - c)$, and $\log \sigma$. A clear anti-correlation is present with the linear correlation coefficient -0.73, which is significant at more than 99.99% level. This suggests the existence of a higher dimensional and tighter correlation than the PP involving $\log \sigma$. We refer to this four dimensional correlation as the hyper plane (HP).
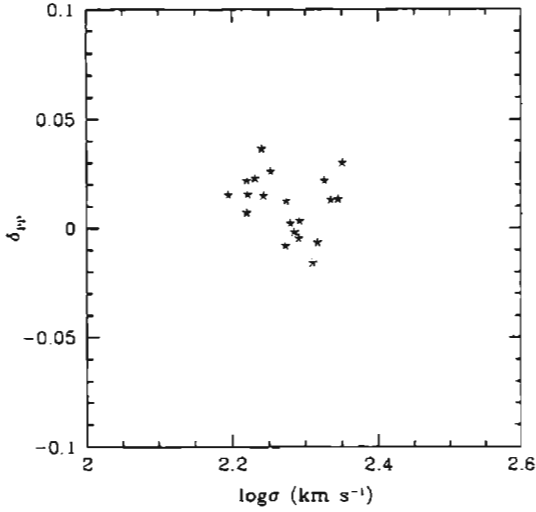
Figure 5.3: Variation of δ_{PP} with $\log \sigma$. The correlation coefficient is -0.73 at a significance level greater than 99.99%.

In Figure 5.4, we show the hyper plane relation for the Abell galaxies. We obtain the HP using a least squares fit to the four parameters, taking $\log n$ as the independent variable,

$$\begin{aligned}
\log n &= (0.144 \pm 0.014) \log A_e - (0.067 \pm 0.002)\mu_b(0) \\
&\quad - (0.221 \pm 0.043) \log \sigma + (1.60 \pm 0.11).
\end{aligned} \qquad (5.3)$$

The rms scatter along the $\log n$ axis is only 0.015 dex, corresponding to a derived distance error of 21.6%, which is significantly less than that for the photometric plane (34.2%), and comparable to that of the (Sersic) fundamental plane(22.7%).
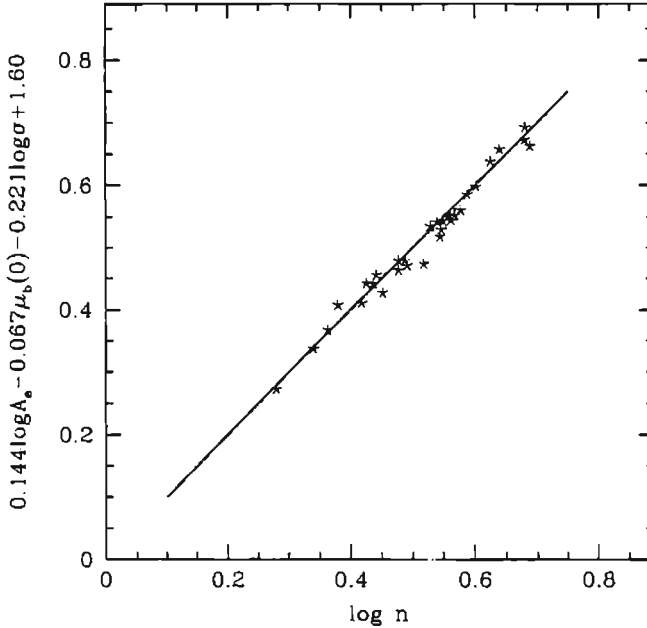
Figure 5.4: The best-fit hyper plane for the Abell cluster galaxies seen edge-on.

5.4.1 Fundamental and Photometric Planes as Projections of the Hyper Plane

It is instructive to study the 4-dimensional HP in relation to the two lower-dimensional planes, PP and FP. The PP and HP are both derived using the same independent variable of the fit (viz., $\log n$), but in the case of the former we neglect the variations along the $\log \sigma$ axis. The coefficients of the $\mu_b(0)$ and $\log A_e$ terms in Equations 5.1 and 5.3 are similar,   and
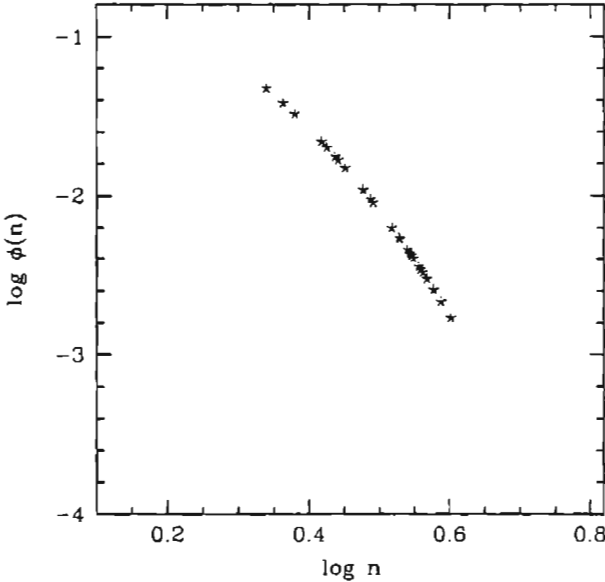
Figure 5.5: Variation of $\log \phi(n)$ with $\log n$.

we can derive the PP from HP by simply averaging over the $\log \sigma$ term, and combining the average value with the constant in Equation 5.3, to get $1.60 - 0.22 \langle \log \sigma \rangle = 1.10$. This is close to the observed zero-point term in Equation 5.1, showing that PP is a projection of HP.

However, it is not easy to show the relation between the HP and the FP for two reasons. Firstly, as already mentioned, the n dependence of FP is not estimated along the $\log n$ axis, but along the $\log \phi(n)$ axis through the definition of $\langle \mu_b(< r_e) \rangle$. Hence for Sersic bulges, FP itself forms a correlation with four dimensions, two of which, $\mu_b(0)$ and $\log n$ are contracted through the $\langle \mu_b(< r_e) \rangle$ axis to give a three dimensional correlation.   The
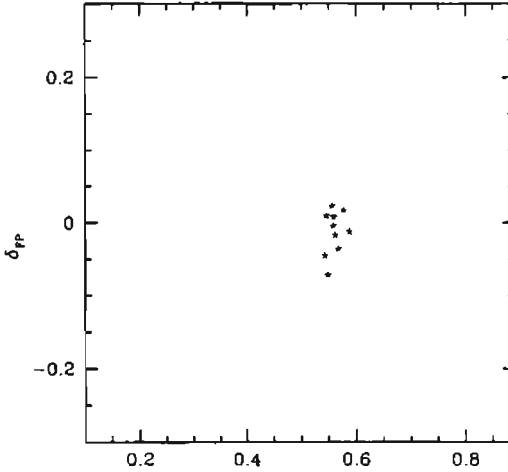
Figure 5.6: Variation of δ_{FP} with n.

modified four dimensional FP for our Abell galaxies can be obtained from a least squares fit as

$$\log A_e = (1.48 \pm 0.25) \log \sigma + (0.34 \pm 0.04)\mu_b(0)$$
$$- (0.83 \pm 0.09) \log \phi(n) - (7.88 \pm 1.06) \qquad (5.4)$$

which is very similar to Equation 4.4. This shows that the FP has a concealed n dependence, and therefore one may not expect a strong correlation between δ_{FP} and $\log n$. This explains why earlier studies (Graham & Colless 1997, Graham 2002) remained unsuccessful in obtaining a hyper plane relation by adding a $\log n$ axis to the fundamental plane; The scatter simply did not reduce enough to warrant the formulation of a higher dimensional plane. One can expect a strong correlation between δ_{FP} and $\log n$ only if $\log \phi(n)$ is linearly dependent on $\log n$. In Figure 5.5 we show the variation

of $\log \phi(n)$ as a function of $\log n$. Clearly $\log \phi(n)$ is *not* linearly dependent on $\log n$ and hence one may not expect a strong $\delta_{FP} - \log n$ correlation (see Figure 5.6).

Secondly, even after allowing for the transformation from $\log n$ to $\log \phi(n)$, it is not straight forward to obtain the FP from HP because of the statistical uncertainties (see Isobe et al. 1990) introduced by the change in the independent variable of the fit to the planes. However, a comparison between the HP and FP can still be achieved by constructing a variant of the HP by treating $\log A_e$ as the independent variable, and averaging out the n dependent terms in it. Applying the least squares minimization along the $\log A_e$ axis, we get the modified HP for our Abell galaxies as

$$
\begin{aligned}
\log A_e \;=\; & (1.39 \pm 0.27)\log \sigma + (0.38 \pm 0.03)\mu_b(0) \\
& + (5.70 \pm 0.40)\log n + (9.28 \pm 0.80).
\end{aligned} \tag{5.5}
$$

Rewriting the equation in $\langle \mu_b(< r_e) \rangle$ using Equation B.12 from Appendix B, we get that

$$
\begin{aligned}
\log A_e \;=\; & 1.39 \log \sigma + 0.38 \langle \mu_b(< r_e) \rangle \\
& +5.70 \log n - 0.77n - 8.90.
\end{aligned}
$$

Now averaging the n dependent terms (For our Abell galaxies, $\langle \log n \rangle = 0.52$; $\langle n \rangle = 3.38$) the constant term gets modified to give us

$$
\log A_e \;=\; 1.39 \log \sigma + 0.38 \langle \mu_b(< r_e) \rangle - 8.54, \tag{5.6}
$$

which is well within the errors expected for the Sersic fundamental plane (Equation 4.4) showing that FP can also be derived from the HP.

5.5   Mg$_2$ index

In the case of gas-poor systems such as elliptical galaxies and bulges of spirals the measured colours and integrated spectra depends heavily on the stellar population. Several line features in the integrated spectra are sensitive to metallicity, the hydrogen abundance ratio relative to iron [Fe/H]. However, to interpret the line features, several assumptions about the age of the stars (and its uniformity) and about the spread in metallicity are required. Sometimes the spread in metallicity is considered negligible or predicted from a theoretical population synthesis model.

One important feature that has provided useful information is the Mg triplet, accompanied by the MgH molecular bands. Studying the galactic globular clusters for which the metallicity can be measured for individual stars, this feature can be calibrated. Following Spinard & Taylor (1969), Faber, Burstein & Dressler (1977) defined the Mg$_2$ index which can be measured in stellar magnitudes. Bender, Burstein & Faber (1993) have provided the calibration

$$\text{Mg}_2 \simeq 0.1 \left[\frac{Z}{Z_\odot} t \, (\text{Gyr}) \right]^{0.41} \tag{5.7}$$

where $\log(Z/Z_\odot)$ is more or less equivalent to [Mg/H].

We have compiled the Mg$_2$ line index measured for the Abell galaxies. The correlation between Mg$_2$ index and velocity dispersion is well-known (e.g. Burstein et al. 1988, Bender et al. 1993, Jørgensen et al. 1996). For our Abell galaxies, we get the best fit relation as

$$\text{Mg}_2 = (0.139 \pm 0.027) \log \sigma - (0.030 \pm 0.06). \tag{5.8}$$

Figure 5.7 shows the strong correlation between Mg$_2$ index and central velocity dispersion for the Abell galaxies. The coefficients reported here
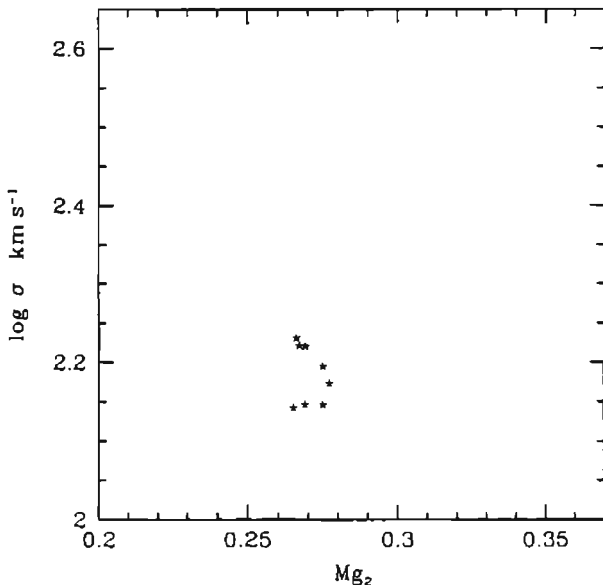
Figure 5.7: Mg₂ index Vs velocity dispersion for Abell ;alaxies.

differs slightly from those given by Jørgensen et al. (1996) for a sample of early type galaxies in clusters. The limited range of both Mg_2 and σ we obtained for our galaxies in the Abell clusters could be a possible reason for this discrepancy.

5.5.1   Residual Diagrams

As discussed before, when the scatter of individual points from a best fit relation, like the FP, is higher than that expected on statistical grounds, then the deviations contain important information about underlying   pa-
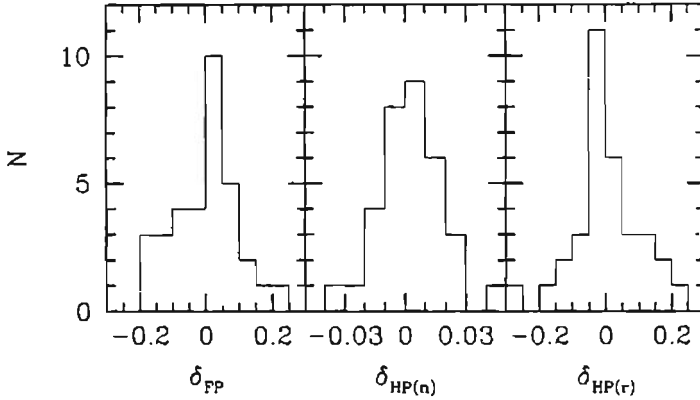
Figure 5.8: Histogram of residuals for Sersic fundamental plane (δ_{FP}), hyper plane ($\delta_{HP(n)}$) and for the modified hyper plane ($\delta_{HP(r)}$).

rameters and relationships. Deviations from the FP and other relations which follow from it have been used to make predictions about stellar populations and evolution in galaxies. However, these predictions are highly model dependent, and in most cases it becomes very difficult to provide a unique interpretation for the results (Worthey 1994, Jørgensen et al. 1996). Here we consider the correlation of such deviations with the Mg$_2$ index.

We have shown the histogram of the residuals of the fundamental plane (Equation 4.4), hyper plane (Equation 5.3) and for the modified hyper plane (Equation 5.5) for the Abell galaxies, in Figure 5.8. In Figure 5.9 the Mg$_2$ index for our Abell galaxies is plotted against the residuals in the different planes. In the fundamental plane case, the residuals are not correlated with Mg$_2$. In the case of the residuals from the hyper plane too there appears to be no correlation for the sample of the 33 Abell galaxies. The linear correlation coefficient r is only 0.11 at a significance of 44%.
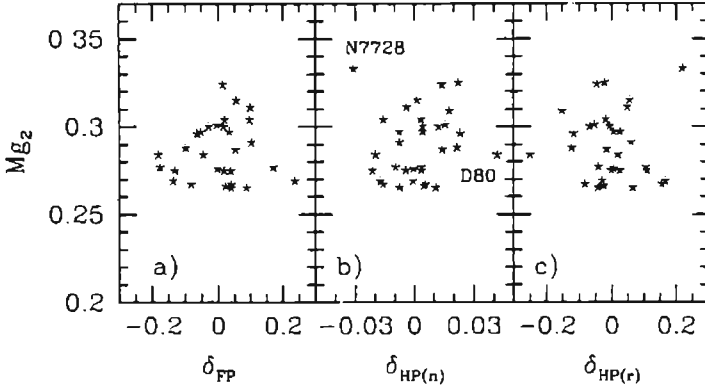
Figure 5.9: Mg_2 index vs residual in Sersic fundamental plane (a), hyper plane (b) and the modified hyper plane (c).

But the correlation improves significantly to 0.37 and 96% respectively, on removal of the two outliers shown in Figure 5.9b. It is difficult to judge why the two galaxies, N7728 and D80, are outliers in the plot. The large scatter in the $Mg_2 - \sigma$ relation (Figure 5.7) does not allow for a detection of measurement error in the former.

We explored the possibility of reducing the scatter in the HP, by adding Mg_2 index to it, as there is a $\delta_{HP(n)} - Mg_2$ correlation. However, at least at present the results are not promising with the scatter remains unaffected. For the 31 galaxies, (obtained by removing N7728 and D80 from the original sample of 33 galaxies), we get a significant Mg_2 dependence as

$$\log n = 0.065\mu_b(0) - 0.193\log\sigma + 0.148\log A_e$$
$$+0.176Mg_2 + 1.47 \tag{5.9}$$

The rms scatter along the $\log n$ axis is 0.011 dex which is very similar to that

for the HP relation for the same 31 galaxies. However, this could be just a reflection of the fact that our sample consists of limited range in Mg$_2$ and σ compared with the reported values observed for large samples of galaxies. Only a detailed study with a larger sample to estimate the Malmquist bias induced in the selection of our sample will resolve the issue.

5.6   M/L Ratios

One of the most important applications of the of tight FP was to provide strong constraints on M/L ratios for galaxies (see e. g. Djorgovski, de Carvalho & Han 1988). This was achieved through the assumptions that galaxies are virialized and that they obey homologous relations (see Chapter 3). Generalization of de Vaucouleurs' $r^{1/4}$ law to the Sersic law for the surface brightness allows for estimating the M/L ratios, even when there is no homology in the luminosity distribution (see Graham & Colless 1997). The lower scatter in the hyper plane can be effectively used for better constraining the M/L ratios of galaxies. Combining the hyper plane relation with the virial theorem and velocity structural homology (Equations 3.5 to 3.7), we get the mass of a galaxy as

$$M = \frac{k_m}{2Gk_r k_v}\sigma^2 r_{\rm e}. \qquad (5.10)$$

For a galaxy with the Sersic law surface brightness profile, the bolometric luminosity is

$$L = k_l L_K = k_l 2\pi I_{\rm b}(0)\phi(n)r_{\rm e}^2. \qquad (5.11)$$

Putting the two together, we get for the M/L ratio,

$$\frac{M}{L} \quad \propto \sigma^2 r_{\rm e}^{-1}\langle I_{\rm b}(< r_{\rm e})\rangle^{-1}$$

$$\propto \sigma^2 r_e^{-1} \left[I_b(0) \right]^{-1} \left[\phi(n) \right]^{-1} \qquad (5.12)$$

If M/L ratios were a constant for all galaxies, this would suggest the existence of a planar relation $r_e \propto \sigma^2 \langle I_b(< r_e) \rangle^{-1}$ But the fundamental plane observed in all pass bands deviates from this slightly and the deviation is considered as a 'tilt' in the fundamental plane. Using the Sersic fundamental plane, Equation 4.4, to eliminate r_e terms in the above proportionality, as shown in the Section 3.5 for de Vaucouleurs' fundamental plane, we get

$$\left(\frac{M}{L} \right)_{SFP} \propto \sigma^{0.52 \pm 0.25} \left[\langle I_b(< r_e) \rangle \right]^{0.16 \pm 0.09} \qquad (5.13)$$

It is evident from Equation 5.12 that, the M/L ratios could also depend on n However, the usage of $\langle I_b(< r_e) \rangle$ conceals the n dependence. If we use the hyper plane (Equation 5.3) in combination with Equation 5.12 to eliminate r_e dependent terms, we get for the Abell galaxies,

$$\frac{M}{L} \propto \sigma^{0.47 \pm 0.34} \left[I_b(0) \right]^{0.16 \pm 0.12} \left[\phi(n) \right]^{-1} n^{-6.76 \pm 0.69} \qquad (5.14)$$

This suggests that the M/L ratios are not very sensitive to the central surface brightness. Figure 5.10 demonstrates variation of the function $\left[\phi(n) \right]^{-1} n^{-6.76}$ with n. It clearly shows that for most of the ellipticals in our sample with n values around four, the M/L dependence on n is little or negligible. M/L increases for smaller values ($n < 2$), and it will be interesting to see whether the ratio for $n \lesssim 1$ is similar to the ratio in disk galaxies, where too the intensity distribution has an exponential form.

It is interesting to see what one can expect if the modified HP in Equation 5.5 is used instead of Equation 5.3. Ideally one should get the same results as above, but because of the scatter in the correlations, we get in
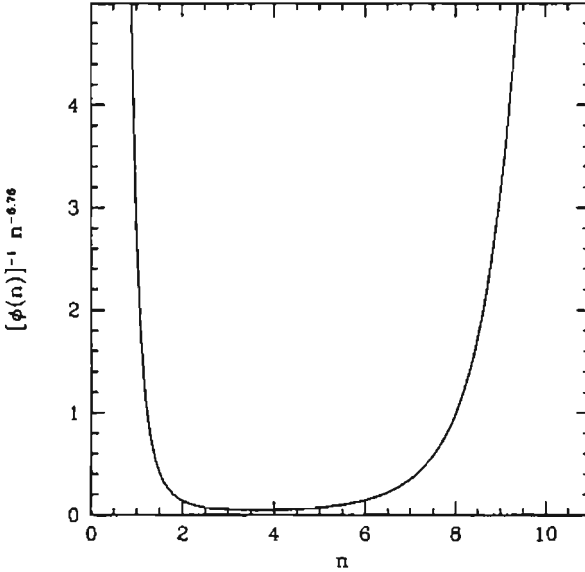
Figure 5.10: Dependence of M/L on Sersic index n for Abell galaxies.

this case

$$\frac{M}{L} \propto \sigma^{0.61\pm0.68} \left[I_b(0)\right]^{0.04\pm0.07} \left[\phi(n)\right]^{-1} n^{-5.70\pm0.40}. \tag{5.15}$$

There is no significant difference from Equation 5.14, and the larger error bars in the exponents here are expected from the larger scatter of the modified hyper plane. The dependence of M/L on the central surface brightness is even less in this case.

Sample	a	b	c	N	rms dex
Coma	1.28 ± 0.16	0.23 ± 0.02	-6.17 ± 0.50	42	0.105
Abell	1.48 ± 0.25	0.34 ± 0.04	-8.40 ± 0.91	33	0.099
Both	1.26 ± 0.13	0.25 ± 0.01	-6.47 ± 0.37	75	0.110

Table 5.1: Coefficients of the fundamental plane relation, $\log r_e = a \log \sigma + b \langle \mu_b(< r_e) \rangle + c$, for early type galaxies in Coma and Abell clusters.

5.7 Bulges and Ellipticals on Fundamental and Hyper Planes

In Table 5.1 we show the fundamental plane relation for the Abell and Coma ellipticals taken separately and together. In order to compare different clusters (at different redshifts), we have converted the effective diameter from angular units to physical units (kpc). The coefficients differ significantly across the samples. However, this can be a manifestation of selection effects applied for the two samples. This is clear from two facts: 1) the error estimates in the Abell sample is larger than that for the Coma sample and 2) the coefficients obtained for the combined plane is closer to that for Coma, which is a statistically complete sample. Treating the two samples of early type bulges together, we examine how the bulges of early type spirals are distributed over the fundamental and hyper planes.

In Figure 5.11 the combined fundamental plane relation for bulges of early type galaxies in Abell and Coma clusters are shown. Clearly, at least in the near neighbourhood, the plane seems to be 'universal', suggest-

Name	$\log r_e$	$\mu_b(0)$	n	σ	σ_{FP}	σ_{HP}	σ_m	$\log M_{bh}$
NGC 5326	-0.2007	11.83	1.66	164.4	157.4	191.2	174.3	7.890
NGC 5422	-0.1487	10.87	2.41	160.3	145.7	146.3	146	7.581
NGC 5475	-0.4437	11.69	2.02	91.2	103.1	115.9	109.5	7.078
NGC 5587	-0.1739	12.32	2.11	92.68	111.3	122	116.6	7.189
NGC 5689	0.3385	9.76	3.3	142.9	208.6	195.7	202.1	8.149
NGC 5707	-0.1549	13.08	1.77	140.9	110.2	134.1	122.2	7.269
NGC 5719	-0.04096	12.12	1.61	108.1	178.3	218.7	198.5	8.117
NGC 5838	-0.02687	10.66	2.66	255.3	154.3	150.2	152.3	7.654
NGC 5854	-0.1367	9.19	3.57	96.83	123.7	124.4	124.1	7.297
NGC 5879	-0.699	11.56	2.19	57.68	73.27	82.25	77.76	6.481
NGC 5965	0.5051	9.56	3.94	162.2	185	186.5	185.7	8.001
NGC 6010	-0.3098	10.6	2.19	143.5	148.2	153.4	150.8	7.637
NGC 6504	0.4698	10.19	3.2	184.5	227.1	210.3	218.7	8.286
NGC 7332	-0.2076	6.89	4.18	112.5	154	160.8	157.4	7.711
NGC 7457	0.1523	8.65	4.8	55.34	97.97	122.1	110	7.087
NGC 7537	-0.3665	14.23	1.43	41.59	75.18	112.6	93.89	6.81
IC 1029	-0.03152	10.96	2.19		182.7	185.5	184.1	7.986
NGC 5362	0.1335	12.92	2.31		118.8	125.3	122	7.267
NGC 5675	0.1492	10.37	2.9		178.6	169.1	173.8	7.885
NGC 5866	-0.08619	9.83	4		85.42	94.54	89.98	6.735
NGC 5908	0.3304	9.21	4.47		123.6	141.4	132.5	7.411
NGC 5987	0.2945	9.13	3.53		208.3	197.6	202.9	8.155
NGC 6368	0.4594	9.83	4.15		144.4	154.4	149.4	7.621
NGC 6757	-0.4089	10.31	2.68		109.9	110.5	110.2	7.089
NGC 7311	0.1847	10.25	2.65		220.6	206.3	213.4	8.243
NGC 7711	0.3838	10.21	3.06	...	221.9	205.2	213.6	8.245

Table 5.2: The morphological parameters for Bulges of early type spirals. The photometric parameters effective radius (r_e, in kpc), unconvolved central surface brightness ($\mu_b(0)$, in mag arcsec^{-2}) and Sersic index (n) are from Khosroshahi (2000) while the velocity dispersion (σ in km s^{-1}) are from the measurements by Falcón-Borosso et al. (2002). The σ_{FP} and σ_{HP} are the velocity dispersion estimates from the photometric parameters using the fundamental plane and hyper plane respectively, and the σ_m is their mean. M_{bh} is the black hole mass estimate (in $M_\odot$).
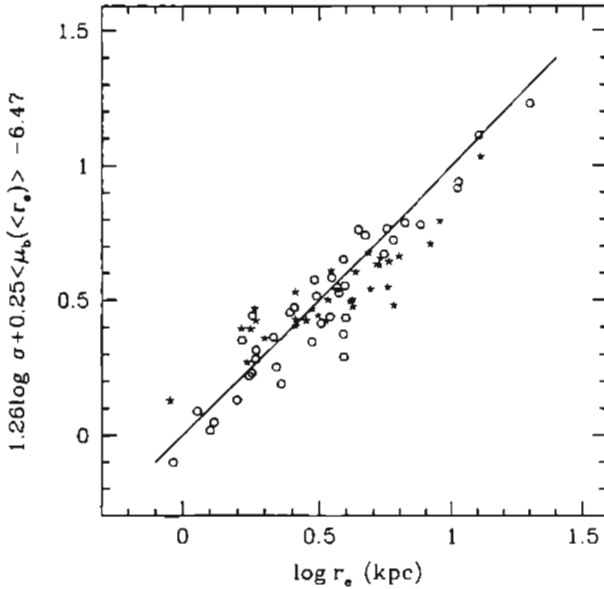
Figure 5.11: Sersic Fundamental plane for both Abell and Coma ellipticals

ing the common scenario for the formation and evolution of these bulges. It is interesting to see whether the bulges of spirals are also distributed evenly over the fundamental plane. For this we use the sample of bulges of Spiral galaxies described in Section 3.2. Table 5.2 shows the morphological parameters obtained by Khosroshahi (2000) for the 26 galaxies. Of these, 15 galaxies have velocity dispersion measurements reported by Falcón-Borroso, Peletier, & Balcells (2000), and their values are shown in the Table. In Figure 5.12 we have plotted the spiral bulges over the common Sersic fundamental Plane for ellipticals. The good distribution of spiral bulges around the best fit line suggest that they also obey the same fundamental plane relation for early type galaxies.
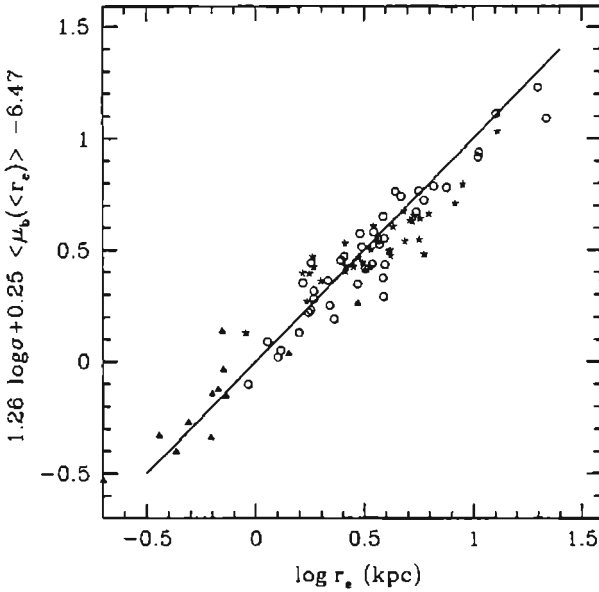
Figure 5.12: Bulges of Spiral galaxies on the Sersic Fundamental plane for ellipticals in Abell and Coma clusters

Similar results are obtained from the study of hyper plane for early type galaxies. The hyper plane coefficients for the Abell and Coma cluster galaxies are given in Table 5.3. We show the hyper plane for both Abell and Coma galaxies in Figure 5.13. Here also the bulges of spirals are well distributed over the hyper plane defined by early type galaxies (Figure 5.14). This suggests that the bulges of different Hubble types can be treated as of the same class as ellipticals for studying their formation and evolution. Also this provides a simpler way for estimating the velocity dispersion measurements for bulges of spirals, which is more difficult to obtain because of the difficulty in separating the bulge and disk velocity components.
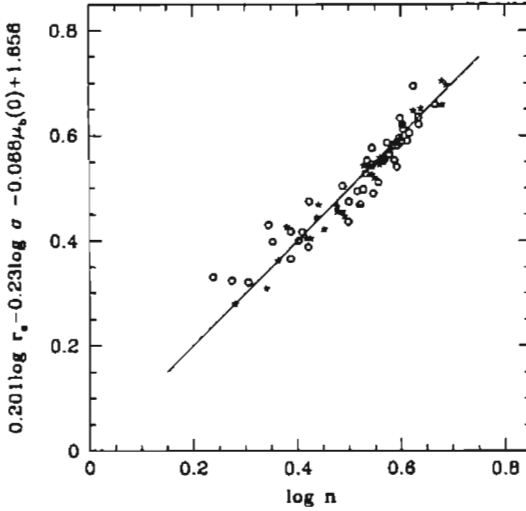
Figure 5.13: Hyper plane for Abell and Coma galaxies

5.7.1 Estimation of σ from Photometry of Galaxies

Determination of central velocity dispersion is very important as it provides information regarding the dynamics of galaxies. It is the study of velocity distribution of stars in the galaxy that led to the understanding that bulges are less supported by rotation, while the stars in disks show much more ordered rotation. Assuming the stellar systems to be virialized it is possible to estimate the mass of the black hole M_{bh}, situated at the centre of every galaxy. The observed tight correlation between M_{bh} and σ (see Appendix C) suggests the strong interplay between the black hole potential and the bulk matter in the galaxies. However, determination of central velocity dispersion becomes difficult as we go for distant galax-
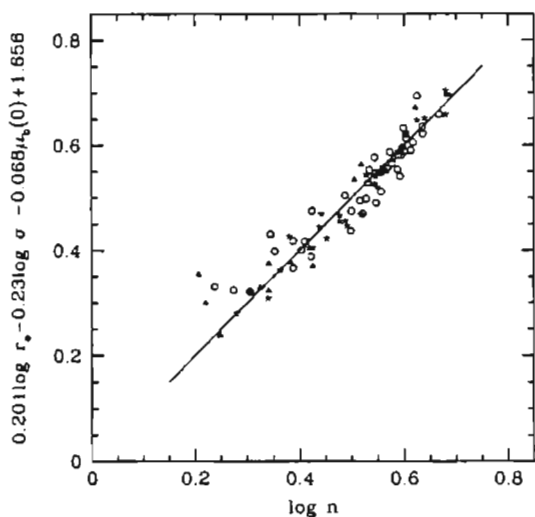
Figure 5.14: Bulges of Spirals over plotted on the hyper plane for Abell and Coma galaxies.

Sample	a	b	c	d	N	rms dex
Coma	0.243 ±0.027	-0.273 ±0.065	-0.072 ±0.0)5	1.770 ±0.164	42	0.034
Abell	0.144 ±0.014	-0.221 ±0.043	-0.067 ±0.002	1.659 ±0.115	33	0.015
Both	0.201 ± 0.020	-0.231 ±0.038	-0.068 ± 0.003	1.656 ± 0.098	75	0.030

Table 5.3: Coefficients of hyper plane, $\log n = a \log r_e + b \log \sigma + c \mu_b(0) + d$, for early type galaxies in Coma and Abell clusters.
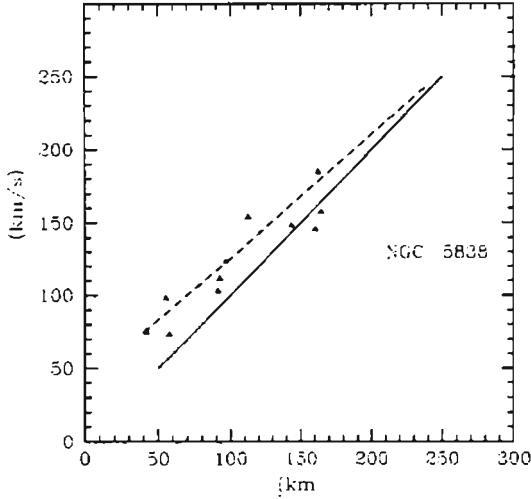
Figure 5.15: Comparison between observed σ and that predicted using the Sersic fundamental plane for Abell and Coma galaxies.

ies. Even for the nearby galaxies, it is difficult to disentangle the bulge dynamics from that of the disks, like in edge-on spirals and lenticulars, and to obtain the central velocity dispersion for the bulges. The fact that the bulges of different Hubble types obey common fundamental and hyper planes can be used to estimate the velocity dispersion measurements. For this we have determined the fundamental and hyper plane relations for the combined sample of galaxies in our Abell and Coma clusters treating $\log \sigma$ as the independent variable to minimize the statistical uncertainties. The modified fundamental plane is:

$$\log \sigma = (0.485 \pm 00.038) \log r_e - (0.122 \pm 0.012) \langle \mu_b (< r_e) \rangle$$
$$+ (4.019 \pm 0.189). \tag{5.16}$$
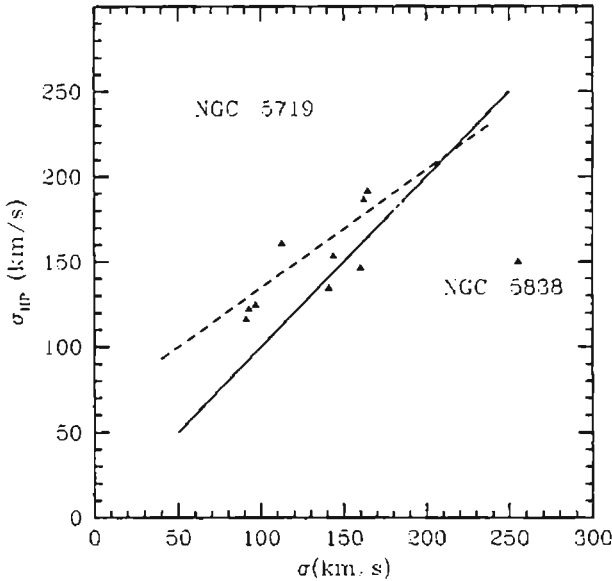
Figure 5.16: Comparison between observed σ and that predicted using the hyper plane for Abell and Coma galaxies.

The rms scatter in this relation is about 0.068 dex suggesting a fractional error of about 16% for velocity dispersion measurements. In Figure 5.15 we show the comparison between the σ estimates from Equation 5.16 and observation. We get the bold straight line when both the σ values are equal. The dashed line is the straight line fit for σ_{FP} obtained avoiding the outlier NGC 5838. Similarly using the the modified hyper plane for the ellipticals with $\log \sigma$ as independent variable,

$$\begin{aligned}
\log \sigma \;=\;& -(1.486 \pm 0.246)\log n + (0.434 \pm 0.046)\log r_e \\
& -(0.106 \pm 0.017)\mu_b(0) + (3.950 \pm 0.285),
\end{aligned} \qquad (5.17)$$

we can determine the σ values using the photometrically obtained morpho-

logical parameters. Figure 5.16 shows a plot between the estimates using Equation 5.17 and actual observation. The bold straight line is what we get when both the σ values are equal while the dashed line is the straight line fit for σ_{HP} obtained avoiding the outliers NGC 5838 and NGC 5719. In Table 5.2 we show the different σ estimates. This velocity dispersion estimates can be used for determining black hole masses, using the tight $M_{bh} - \sigma$ correlation, Equation C.5. In Appendix C we provide a description on the various techniques used for the estimation of M_{bh} and the $M_{bh} - \sigma$ correlation.

5.8   Summary

We have established the existence of a hyper plane for elliptical galaxies in the log space of the three photometric variables n, r_e, $I_b(0)$ and the central velocity dispersion σ. The fundamental and photometric planes, whose existence are independently known, can both be derived from the hyper plane. Here we would like to mention that our definition of the hyper plane differs from that proposed by Graham & Colless (1997) and later by Graham (2002). They considered the existence of a hyper plane constructed using n, A_e, $\langle I_b(< r_e) \rangle$ and σ. But since this lead to no significant reduction in the scatter about the plane, they concluded that no hyper plane was warranted. When the Sersic law is assumed for galaxy surface brightness profiles, the mean surface brightness within r_e necessarily depends on n, since $\langle I_b(< r_e) \rangle = I_b(0)\ \phi(n)$. n is therefore already included implicitly in the FP, and therefore no clear correlation is seen when the residuals are plotted against n. But when another projection of the hyper plane, i. e., PP, is considered, the correlation between the residuals and the fourth parameter, σ, is immediately apparent as discussed in Section 5.4. A need for a higher dimensional plane is also apparent from the reduction in

scatter which occurs when, instead of a correlation between n and σ, three dimensional correlations between n, σ and $\mu_b(0)$, or between n, σ and A_e are considered. It is then natural to tie together the four parameters in a single correlation. The decreased scatter in the hyper plane should provide better constraints for modeling galaxy formation and evolution.

The existence of the hyper plane leads to the dependence of the M/L ratio of elliptical galaxies on the Sersic parameter n, besides other morphological parameters. It has been shown (Khosroshahi et al. 2000b) that a single photometric plane provides a good fit to ellipticals as well as to the bulges of early type spiral galaxies, with this result further extended to the bulges of late type spirals as well (Möllenhoff & Heidt 2001). If the photometric plane is the projection of a hyper plane, then it is plausible that ellipticals and bulges will lie on the same hyper plane, allowing us to predict bulge central velocity dispersions. This applies to the bulges of lenticular galaxies as well (S. Barway et al. in preparation), so that we can estimate central velocity dispersions over a broad range of the Hubble sequence, knowing only their photometric parameters. This provides us with estimations of useful parameters like the mass of super-massive black holes now believed to be existing at the centers of most galaxies.

Chapter 6

Results and Conclusion

6.1 Results

In this thesis we have presented detailed results on the surface photometry in near infra red K band for a sample of 33 early type galaxies from two rich clusters, Abell 2199 and Abell 2634, both of which are at a redshift $z \approx 0.03$. Using a full two dimensional bulge-disk decomposition algorithm (Wadadekar et al. 1999). we determined the large scale morphological parameters of the bulge and disk components of galaxies in our sample. In this simultaneous bulge and disk determination, we have obtained separate fits for the bulge by successively applying de Vaucouleurs and Sersic laws to the surface brightness while an exponential profile was fit to the disk component each time.

Studying the quality of fits showed that the Sersic law provided better representation of the observed surface brightness profile than the de Vaucouleurs law. It was also shown that even though the de Vaucouleurs law could fit well the galaxies with $3.5 \lesssim n \lesssim 4.2$, applying it to galaxies

with n out side this range resulted in serious under or over-estimation of structural parameters. The more different n is from four, the larger are the systematic errors. However, the famous Kormendy, Faber-Jackson and the fundamental plane relations did not seem to depend so much on the choice of the approximation we used to fit the surface brightness distributions. This can be exploited to explore the inherent correlations, like the evolution of M/L for galaxies, at high redshifts using de Vaucouleurs law, which is comparatively easier and faster than applying the generalised Sersic law. However, caution must be taken when such correlations are used for determining the structural property of individual galaxies, like the determination of individual (relative) distances from the de Vaucouleurs fundamental plane (e. g. Jørgensen et al. 1996) or the estimation of velocity dispersion for individual galaxies using the fundamental plane (Woo & Urry 2002).

The three parameter correlations, photometric and Sersic fundamental plane relations for the sample were studied in detail. The scatter in the photometric plane is found to correlate strongly with velocity dispersion. This is important as it suggests a tight correlation between the observables $\mu_b(0)$, r_e, n and σ. We show that the scatter in the hyper plane is considerably less than that in the photometric plane. However, the correlation between the scatter in the Sersic fundamental plane and n is very poor, as already reported by other studies (Graham & Colless 1997; Graham 2002). On closer examination, it can be realised that the fundamental plane contains n dependence in the surface brightness term $\langle \mu_b(< r_e) \rangle$ used. We also show that we can derive the fundamental plane from the hyper plane relation. Thus hyper plane provides the link between fundamental and photometric plane relations.

The smaller scatter in the hyper plane is used for better constraining the M/L relation for the galaxies in the Abell sample. Using the hyper

plane the n dependence of M/L ratio is also derived, which is not possible with conventional fundamental plane studies. It shows for our Abell sample that higher M/L ratios are expected for galaxies with $n \leq 1$ or for those with $n > 4$. It will be interesting to see how metallicity varies for these galaxies.

The bulges of early type spirals are found to follow the same fundamental and hyper plane relation. This provides an easier and quicker method to estimate the central velocity dispersion for bulges of spiral galaxies, where it is difficult to apply conventional observational techniques because of the 'shielding' of the bulge dynamics by the surrounding disk. Apart from the dynamics, velocity dispersion estimates are important because of its observed tight correlation with the mass of the central black hole and that of the bulge.

6.2   Future Prospects

One of the important things one would like to know is the possible evolution of the hyper plane with redshift. It is equally important to know how the hyper plane varies with samples containing galaxies of different morphological types. For such a study an intermediate to high redshift cluster data set in the near infra red window will be ideal.

In a forgoing study we are analysing high quality multi-band data on nearby lenticular galaxies. It will be interesting to see how the bulges of lenticulars are distributed along the different planar relations. Any systematics in such correlations will provide significant inputs to the understanding of the lenticulars as a class. The analysis of scalelengths of bulge and disk components help in differentiating the different models of galaxy formation and evolution.

Appendix A

Bootstrapping Technique

In the statistical analysis it is generally assumed that the data are distributed normally. There are a lot of statistical methods that are guaranteed to work well in almost all cases, especially when we are mainly interested in linear functions in random variables. As we know, the mean or average of a data set is a linear combination of the random variables, and according to the central limit theorem, we can expect the observed mean to approach the 'true mean' as the sample size increases. However in some cases we may be left with a small sample. To add the complexity, we may wish to consider ratios of random variables, which are obviously nonlinear combinations making the conventional statistics unreliable.

Bootstrapping is a relatively recent development which can be employed in such complicated situations also. This method was devised by Efron (1979) and has been used in a variety of fields (Efron 1982; Efron & Tibshirani 1993; Mooney and Duval 1993). The word 'bootstrapping' was coined, according to Efron & Tibshirani (1993), from the phrase 'to pull oneself by ones bootstrap', i. e., to accomplish a physical impossibility. This method

was preceded by 'jackniffing', a means developed by Quenouille (1956) to study bias in estimators, but was named so by John Tukey (1958) for its all-purpose applicability.

One of the important advantages of the bootstrapping is that it is extremely simple so long as the user can implement the calculations using computers which contain essentially a random number generator algorithm. It can be used when the objective of the test is to draw a conclusion about a population based on a random sample. In bootstrap methods artificial samples are generated by random selection (with replacement) from the original sample itself (Efron 1982; Noreen 1989).

Let us suppose that there exists a true set of parameters x_t which we do not know as an observer. These 'true' parameters are statistically realized, along with random measurement errors, as a measured data set symbolized as D_0. Because of the random nature of the measurement errors, let us suppose that one might obtain a series of data sets D_i; $i = 1, 2, 3, \ldots$. Each one, had it been realized, would have provided a slightly different set of parameters a_i; $i = 1, 2, 3, \ldots$. The actual measured data set a_0 is one member drawn from this ensemble. These parameter sets a_i therefore occur with some probability distribution in the M dimensional space of all possible parameter sets a. The distribution of the difference $a_i - a_t$ is of more importance (Press et al. 1992). The bootstrapping provides a method for estimating or approximating the probability distribution of $a_i - a_t$ without knowing a_t and having an infinite universe of hypothetical datasets.

The bootstrap method uses the actual data set D_0^S with its N data points, to generate a large number of synthetic data sets D_i^S, each with N data points. The procedure is simply to draw N points at a time with replacement from the set D_0^S. Because of replacement we don't get back our own original data set each time. Treating each of these drawn data sets

as independent realizations of observations, various statistics is performed to give the parameters a_i^S, which will be distributed around a_0 in close to the same way that a_0 is distributed around a_t. In this thesis we have adopted this method to estimate errors in coefficients of different correlations, like the fundamental plane, obtained by means of the least squares minimization.

Appendix B

Sersic Bulge and Exponential Disk: Formulae

B.1 Introduction

Elliptical galaxies in classical catalogues were noticed for their simple and continuous distribution of surface brightness, with little evidence for morphological peculiarities and dust. Though later observations using sensitive CCD detectors revealed an array of substructures, the luminosity structure in most galaxies can still be considered smooth enough to a great extent and different laws, empirical or motivated from theory, were used to represent the observed luminosity profile of different components of galaxies. Here we derive the equations relating the morphological parameters assuming that the bulge follows the Sersic law while the intensity distribution of

the disk component is exponential.

B.2   Sersic Bulge

For a bulge obeying Sersic law (Equation 2.5), the total light contained by the bulge within a radius r_1 is given by,

$$
\begin{aligned}
I_b(r \leq r_1) &= \int_0^{r_1} I_b(r)\, 2\pi\, r dr \\
&= 2\pi I_b(0) \int_0^{r_1} e^{-2.303 b_n (r/r_e)^{1/n}} r dr
\end{aligned}
\tag{B.1}
$$

Employing a change of variable, $x = 2.303 b_n\, (r/r_e)^{1/n}$ we get,

$$
I_b(r \leq r_1) = \frac{2\pi\, I_b(0) r_e^2 n}{(2.303 b_n)^{2n}} \int_0^{x_1} e^{-x} x^{2n-1} dx,
\tag{B.2}
$$

where $x_1 = 2.303 b_n\, (r_1/r_e)^{1/n}$ The integral in the Equation B.2 forms part of the incomplete Gamma function $P(a, x)$ (Press et al. 1992) and hence we get,

$$
I_b(r \leq r_1) = \frac{2\pi\, I_b(0) r_e^2 n}{(2.303 b_n)^{2n}} \Gamma(2n)\, P(2n, x_1),
\tag{B.3}
$$

where $\Gamma(x) = \int_0^\infty e^{-x} x^{2n-1} dx$ is the usual Gamma function.
Or

$$
I_b(r \leq r_1) = 2\pi\, I_b(0) r_e^2\, \phi(n)\, P(2n, x_1),
\tag{B.4}
$$

where

$$
\phi(n) = \frac{n\Gamma(2n)}{(2.303 b_n)^{2n}}.
\tag{B.5}
$$
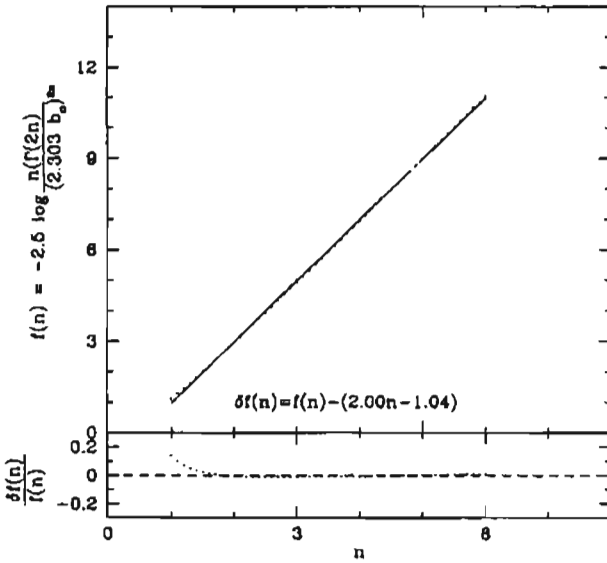
Figure B.1: The upper window shows the variation of $-2.5 \log \phi(n)$ for $1 \geq n \geq 6$ and in the lower one its fractional residual from the straight line fit is shown.

The total light contained by the bulge is given by,

$$B \equiv I_b(r \leq \infty) = 2\pi\, I_b(0) r_e^2\, \phi(n) \tag{B.6}$$

Also, the light contained within r_e is given by

$$
\begin{aligned}
I_b(< r_e) &\equiv I_b(r \leq r_e) \\
&= 2\pi\, I_b(0) r_e^2\, \phi(n)\, P(2n, 2.303 b_n). \tag{B.7}
\end{aligned}
$$

By the definition of half light radius r_e, the light contained by the circular region of radius r_e is half of the total light emitted by the bulge. i.e.,

$$I_b(< r_e) = \frac{1}{2} B. \tag{B.8}$$

Using Equations B.6, B.7 and B.8 we get,

$$. P(2n, 2.303 b_n) = \frac{1}{2}. \tag{B.9}$$

This equation is used for determining the value of b_n.

Now the mean surface brightness within r_e is given by

$$
\begin{aligned}
\langle I_b(< r_e) \rangle &\equiv \frac{\int_0^{r_e} I_b(r)\, 2\pi\, r dr}{\int_0^{r_e} 2\pi\, r dr} \\
&= I_b(0)\, \phi(n) \tag{B.10}
\end{aligned}
$$

It is important to note that $\langle I_b(< r_e) \rangle$ depends on $\mu_b(0)$ and n. In magnitudes, Equation B.10 becomes

$$\langle \mu_b(< r_e) \rangle = \mu_b(0) - 2.5 \log \phi(n). \tag{B.11}$$

In Figure B.1 we have shown the variation of $-2.5 \log \phi(n)$ with n. In

the upper panel it can be seen that the curve is very close to being a straight line. We have applied a straight line fit to the curve and in the lower panel its fractional residual is shown. Thus we can write, to an accuracy of a few percents,

$$\langle \mu_b(< r_e) \rangle \approx \mu_b(0) + 2n - 1 \tag{B.12}$$

B.3 Exponential Disk

For the disk component, we assume that the surface brightness follows an exponential form as given in Equation 2.9. Then the total light contained by the disk,

$$
\begin{aligned}
D &\equiv \int_0^\infty I_d(r)\, 2\pi\, r dr \\
&= 2\pi\, I_d(0)\, r_d^2 \int_0^\infty e^{-y} y dy \\
&= 2\pi\, I_d(0)\, r_d^2. \tag{B.13}
\end{aligned}
$$

In the above derivation, we change the variable r to y through $y = r/r_d$.

Appendix C

Black Hole Mass Estimation Across the Hubble Sequence

C.1 Introduction

The existence of massive black holes at the centres of galaxies, once considered a fanciful imagination, has become a reality with recent observations. A detailed description on the early searches for 'massive dark objects (MDO)' at the centers of galaxies using stellar and gas dynamics studies is summarised in Kormendy & Richstone (1995) and the references therein. Black holes have long been proposed as the main source to power AGNs by accretion of matter on to it (e. g. Salpeter 1964; Zel'dovich 1964; Lynden-Bell 1969, 1978; Rees 1984; Begelman et al. 1984; Blandford 1990; Blandford & Rees 1992), supported with a broad array of circumstantial evidence.

With the availability of reliable M_{bh} estimations increasing rapidly, mainly due to advanced *Hubble Space Telescope (HST)* observations, all spheroidal bulges are expected to contain central black holes (see Magorrian et al. 1998). This idea is emphasized by the detection of the presence of a black hole at the centre of our own Galaxy from Keplerian motion of stars near the Galactic centre. Various studies proposed that the black hole mass M_{bh} is proportional to the galaxy mass or luminosity, but with large scatter (Kormendy 1993; Kormendy & Richstone 1995; Magorrian et al. 1998). There appears to be a stronger and probably more fundamental correlation between M_{bh} and the velocity dispersion of the host galaxy (Ferrarese & Merrit 2000; Gebhardt et al. 2000a,b; Merrit & Ferrarese 2001a,b; Ferrarese 2002). These followed a series of attempts to explain the observed range of slope of the M_{bh} - σ relation for different studies with theoretical modeling (Ostriker 2000; Haehnelt & Kauffmann 2000; Adams, Graff, & Richstone 2001; Burkert & Silk 2001; Nipoti, Londrillo, & Ciotti 2003) and systematics in observations (Tremaine et al. 2002).

The correlation between the mass of the central black hole and the bulge luminosity suggests a strong interplay between the black hole and the formation of bulges. The Eddington limit, the maximum luminosity for an idealised spherical accretion is set by the black hole mass and is given by

$$L_{Edd} = 1.25 \times 10^{38} M_{bh}/M_{\odot} \, \text{ergs s}^{-1}. \tag{C.1}$$

However, direct estimation of the black hole mass from kinematic observations is limited by finite spatial resolution available as at a typical redshift of 2 one would require nanoarcsecond resolution to explore the sphere of influence of the black hole. Hence various less direct methods have also been devised and are out lined in the next section. In the reverberation mapping technique (Blandford & McKee 1982; Peterson 1993), the time lag between continuum and emission lines is used to derive distance of the

broad-line region (BLR) from the black hole. Then the mass of the black hole is estimated assuming that the BLR is gravitationally bound by the black hole potential. One can adopt to a less costly alternative by estimating the BLR size from the optical or ultraviolet luminosity (McLure & Dunlop 2001; Vestergaard 2002). There is yet other method for estimating the black hole mass which exploits the tight correlation between velocity dispersion and M_{bh} for near by normal galaxies. Since stellar velocity dispersion measurement by itself is difficult for higher redshift galaxies, it is worth exploring the possibility of using the fundamental and hyper plane relations for estimating the stellar velocity dispersions.

C.2   Estimation of M_{bh}

As already mentioned, because of the very high spatial resolution demanded, it is extremely difficult to explore the the presence of black holes, even for near by galaxies. Studying the Kepler motion of stars near the center of our own galaxy, it was shown that the Milky Way contains a massive black hole at the centre. The AGN activity of galaxies provides the estimation of M_{bh} using spatially resolved maser dynamics near the black hole (Miyoshi et al. 1995; Greenhill et al. 1997). Studying the broad line regions provide less direct methods for the estimation of black hole masses.

C.2.1 M_{bh} from Virialised Motion

Studies on the dynamics of the broad line clouds support the idea that most of them, if not all, form virialised systems (Krolik et al. 1991; Wandel, Petrerson & Makkan 1999; Krolik 2001). Assuming the virial theorem for

the system, we can estimate the black hole mass as

$$M_{bh} = \frac{R_{BLR}v^2}{G} \tag{C.2}$$

where R_{BLR} and v trace the radial distance from the black hole and the rotational velocity respectively of the broad line region. The velocity v under this assumption can be estimated from the width of the broad lines emitted by the BLR.

However, it may be noted that the virial assumption may not be completely correct. The radiation pressure and/or the magnetic fields modify the dynamics significantly (Krolik 2001). Moreover, out flows or jets or winds can cause the observed line widths to deviate from what is expected by the black hole potential. In all such cases the black hole mass determined using Equation C.2 would provide serious over estimations.

M_{bh} from Reverberation mapping

In the reverberation mapping method, the BLR size (R_{BLR}) is estimated by measuring the time lag between the ionizing continuum and the broad line emissions (Peterson 1993; Wandel et al. 1999; Ho 1999; Kaspi et al. 2000; Onken & Peterson 2002). As can be seen from Equation C.2, the assumptions used for the determination of BLR orbits and their velocities contribute to the uncertainty in the estimated black hole mass. In the literature two methods are used for the determination of velocity of BLR region from the observed spectra. One derives v from the mean of the FWHM (frequency width at half maximum) derived from each line or the FWHM of the rms spectrum (Peterson1988). Even though both the velocity estimates are reported to be similar (Kaspi et al. 2000), the difference in the estimated M_{bh} can some times be as large as a factor of 10 (Woo & Urry 2002). Additional uncertainties are introduced by the assumptions about

the shape and inclination of the broad-line clouds. In Equation C.2, the velocity is taken as

$$v = f \times \text{FWHM}. \tag{C.3}$$

Assuming an isotropic distribution of broad line clouds with random inclinations Netzer (1990) derived $f = \sqrt{3}/2$. However, McLur & Dunlop (2001) were able to reproduce the FWHM distribution of Seyfert galaxies and quasars with two disk components and showed that the average relationship between observed FWHM and the actual orbital velocity with $f = 3/2$. The two methods thus, for the same AGN, differ by a factor of three in the black hole mass estimates. If one considers the orbital shape alone, the uncertainty of the M_{bh} estimates can be of the order of two magnitudes (Krolik 2001; Woo & Urry 2002). Even though the reverberation mapping can provide a robust estimation of M_{bh}, it is highly resource intensive and time consuming. It has the additional disadvantage that it is not applicable to systems that do not emit broad lines, as is the case with most AGNs, limiting the number of black holes with mass estimation using this method.

M_{bh} from BLR size - Luminosity Relation

Several studies on the BLRs suggest that the R_{BLR} (determined from reverberation mapping) correlates well with ultra- violet (UV) as well as optical luminosity (Koratkar & Gaskell 1991; Kaspi et al. 1996, 2000; Wandel et al. 1999). Wandel et al. (1999) reported $R_{BLR} \propto L_{opt}^{0.5}$ but later studies modified it to $R_{BLR} \propto L_{5100\mathring{A}}^{0.7}$ (Kaspi et al. 2000; Vestergaard 2002; McLure & Jarvis 2002). Combining this with the assumption of random isotropic orbits, we can determine the black hole mass as,

$$M_{bh} = 4.817 \times \left[\frac{\lambda L_\lambda (5100\mathring{A})}{10^{44}\,\text{ergs s}^{-1}} \right]^{0.7} \text{FWHM}^2. \tag{C.4}$$

However, apart from the large scatter, the $R_{BLR} - L$ correlation is crippled with the fact that it is valid only in a limited range of luminosities. Hence the uncertainties in the black hole mass estimation using Equation C.4 is larger than those from the reverberation mapping, the differences being of the order of a magnitude or so (Woo & Urry 2002). Still this method can be employed in the determination of M_{bh} considering that the more precise methods are difficult and time consuming (McLure & Dunlop 2001; Gu, Cao, & Jiang 2001; Oshlack, Webster, & Whiting 2002).

C.2.2 M_{bh} from Stellar Velocity Dispersion

For the near by galaxies there is an important connection between the central black hole and the bulge kinematics which is evident from the tight correlation between M_{bh} and the stellar velocity dispersion. Gebhardt et al. (2000a) noticed $M_{bh} \propto \sigma^{3.75}$ while Ferrarese & Merrit (2000) reported $M_{bh} \propto \sigma^{4.8}$. Tremaine et al. (2002) studied the large differences in the slope of the correlation and found the systematics employed in the observation and data reduction of the velocity dispersion responsible and modified the relation as

$$M_{bh} = 1.349 \times 10^8 M_{\odot} \left(\frac{\sigma}{200 \text{ km s}^{-1}} \right)^{4.02} \qquad (C.5)$$

The scatter in this relation is surprisingly small with a dispersion which is less than < 0.3 dex in $\log M_{bh}$ at any given value of σ. This result is important as it implies that formation and evolution of bulges are closely related to the black hole potential. In other words, the mass of the central black hole, situated in a very small region of $\leq 10^{-4}$ pc, is almost *completely* determined by the bulk properties of the galaxy. Though the slope of the correlation is somewhat controversial and the exten; of intrinsic scatter is yet to be estimated accurately, the $M_{bh} - \sigma$ correlation seems to be well established. The galaxies with reliable M_{bh} estimations are still very

limited. More estimates of M_{bh} are needed, over the widest possible of host galaxy types and velocity dispersions, in order to understand the black hole demography better.

For a sample of Seyfert galaxies (Wu & Han 2001) for which both velocity dispersions and reverberation mapped BLR sizes are available, the M_{bh} estimated from Equation C.5 agrees well with those from Equation C.2, the scatter being well within an order of magnitude (Woo & Urry 2002).

C.3 Indirect Estimation of σ for Bulges of Spirals

As the distance to galaxies increases, determination of velocity dispersion becomes very difficult. Even for nearby late type galaxies, measuring stellar velocity dispersion for their bulge components is not easy as it is difficult to disentangle the disk dynamics from that of the bulges. However, the existence of fundamental and hyper planes can be exploited for the estimation of σ for bulges from their morphological parameters, albeit with additional scatter. It will be of great use if a reasonably accurate calibration becomes available, as this method requires simple imaging of galaxies rather than complicated spectroscopy, and that it can be applied to a wide spectrum of galaxies over different Hubble types and at larger red shifts.

Woo & Urry (2002) estimated black hole masses for a sample containing BL Lac and radio galaxies using the velocity dispersion values determined by this technique. They used the fundamental plane relation obtained by Jørgensen et al. (1996) for early type galaxies obtained in Gunn r band. They report a difference of about 10% between the M_{bh} estimates using this method and that obtained from more accurate reverberation mapping.

References

[1] Adams F. C., Graff D.S., & Richstone D.O., 2001, *Astrophys. J.* 551, L31

[2] Agurri J.A.L., Balcells M., & Peletier R.F., 2001, *Astro. Astrophys.* 367, 428

[3] Andredakis Y. C., Peletier R.F., & Balcells M., 1995, *Mon. Not. Roy. Astr. Soc.* 275, 874

[4] Baade W., 1944, *Astrophys. J.* 100, 137

[5] Balcells M., Graham A.W., Domíngues-Palmero, & Peletier R.F., 2003, *Astrophys. J.* 582, L79

[6] Balcells M. & Peletier R.F., 1994, *Astron. J.* 107, 135

[7] Barnes J. E. & Hernquist L., 1992, *Nature.* 360, 715

[8] Barnes J. H, 1988, *Astrophys. J.* 331 699

[9] Baum W.A., 1959, *Proc. Astr. Soc. Pacific.* 71, 106

[10] Beers T.C., & Tonry J.L., 1986, *Astrophys. J.* 300, 557

[11] Begelman M.C., Blandford R.D., & Rees M.J., 1984, *Rev. Mod. Phys.* 56, 225

[12] Bender R., Burstein D., & Faber S. M. 1993, *Astrophys. J.* 411, 153

[13] Bertin G., Ciotti L., & Del Principe M., 2002, *Astro. Astrophys.* 386, 149

[14] Bertin G. & Stavelli M., 1984, *Astro. Astrophys.* 137, 26

[15] Bertin G. & Stavelli M., 1989, *Astrophys. J.* 338, 723

[16] Bertola F & Capacciolli M., 1975, *Astrophys. J.* 200, 439

[17] Bingelli B. & Cameron L. M., 1991, *Astro. Astrophys.* 252, 27

[18] Bingelli B. & Jerjen H., 1998, *Astro. Astrophys.* 333, 17

[19] Binney J., 1976, *Mon. Not. Roy. Astr. Soc.* 177, 19

[20] Binney J., 1982, *Mon. Not. Roy. Astr. Soc.* 200, 951

[21] Binney J. & Tremaine S., 1994, *Galactic Dynamics*, Princeton Uty Press, 3rd edition.

[22] Blakeslee J.P. et al. 2002, *Mon. Not. Roy. Astr. Soc.* 330, 443

[23] Blandford R.D., 1990, in *Active Galactic Nuclei, Saas-Fee Advanced Cource 20*, ed. T.J.L. Courvoisier & M. Mayor. p. 161. Berlin: Springer-Verlag

[24] Blandford R.D. & McKee C.F., 1982, *Astrophys. J.* 255, 419

[25] Blandford R.D., & Rees M.J., 1992, in *Testing the AGN Paradigm*, ed. S.S. Holt, S.G. Neff, & C.M. Urry, p 3. New York: Am. Inst. Phys.

[26] Borriello A., Salucci P., & Danese L., 2003, *Mon. Not. Roy. Astr. Soc.* 349, 1109

[27] Bower R. G., Lucey J. R. & Ellis R. S., 1992, *Mon. Not. Roy. Astr. Soc.* 254, 589

[28] Burkert A., 1993, *Astro. Astrophys.* 278, 23

[29] Burkert A., & Silk J., 2001, *Astrophys. J.* 554, L151

[30] Burstein D., 1979, *Astrophys. J.* 234, 435

[31] Burstein D. et al. 1988, in *Towards understanding Galaxies at high redshifts*, eds. Kron R.G., Renzini A., Kluwer Academic Publishers, Dordrecht

[32] Butcher H.R. & Oemler A., 1985, *Astrophys. J. Suppl.* 54, 33

[33] Butchins S.A., 1983, PhD Thesis, Oxford University

[34] Byun Y. I. & Freeman K. 1995, *Astrophys. J.* 448, 563

[35] Caon N., Capaccioli M., & D'Onofrio M. 1993, *Mon. Not. Roy. Astr. Soc.* 265, 1013

[36] Carollo C.M., Stiavelli M., Seigar M., de Zeeuw P.T., & Dejonghe H., 2002, *Astron. J.* 123, 159

[37] Carlberg R.G., 1984, *Astrophys. J.* 286, 403

[38] Colless M., Saglia R. P., Burstein D., Davies R.L., McMahan R.K., Wegner G., 2001, *Mon. Not. Roy. Astr. Soc.* 321, 277

[39] Dehnen W., 1993, *Mon. Not. Roy. Astr. Soc.* 265, 250

[40] de Jong R. S., 1996, *Astron. Astrophys. Suppl.* 118, 557

[41] de Vaucouleurs G., 1948, *Ann. Astrophys.* 11, 247

[42] de Vaucouleurs G., 1956, *Occasional Notes on Roy. Astron. Soc.* 3,129

[43] de Vaucouleurs G., 1959, *Handbuch der Physik*, 53, 275

[44] Djorgovski S. & Davis M. 1987, *Astrophys. J.* 313, 59

[45] Djorgovski S., 1992, in ASP Conf. Proc. 24, Cosmology and Large-Scale Structure in the Universe, ed. R.R. de Carvalho (San Francisco:ASP), 73

[46] Djorgovski S., de Carvalho R., & Han M.S. 1988, in ASP Conf. Ser. 4, The Extragalactic Distance Scale, ed. S. van den Bergh & C. J. Prichet (San Francisco:ASP), 329

[47] Dixon K.L., Godwin J.G., & Peach J.V., 1989, *Mon. Not. Roy. Astr. Soc.* 239, 459

[48] Dressler A., 1980, *Astrophys. J.* , 236, 351

[49] Dressler A., 1984, *Ann. Rev. Astron. Astrophys.* 22, 185

[50] Dressler A., Lynden-Bell D., Burstein D., Davies R. L., Faber S.M.,Terlevich R.J., & Wegner G. 1987a, *Astrophys. J.* 313, 42

[51] Dressler A., Faber S.M., Burstein D., Davies R. L., Lynden-Bell D., Terlevich R.J., & Wegner G. 1987b, *Astrophys. J.* , 313, L37

[52] Efron B., 1979, *Annals of Statistics*, 7, 1

[53] Efron B., 1982, in *The Jacknife, the bootstrap and other resampling plans*, Soc. for Ind. & Appl. Maths.

[54] Efron B., & Tibshirani R.J., 1993, in *An introduction to the Bootstrap*, New York: Chapman & Hall

[55] Faber S.M. & Jackson R.E. 1976, *Astrophys. J.* 204,668

[56] Faber S.M., Wegner G., Burstein D., Davies R. L., Dressler A., Lynden- Bell D., & Terlevich R.J. 1989, *Astrophys. J. Suppl.* 69, 763

[57] Falcón-Borroso J., Peletier R.F., Balcells M., *Mon. Not. Roy. Astr. Soc.* 2002, 335, 741

[58] Ferraras I. & Silk J., 2001, *Astrophys. J.* 557, 165

[59] Ferrarese L. 2002, in *Current High Energy Emission around Black Holes*, ed. C.H. Lee & H. Y. Chang, Singapore:WSP, p 3

[60] Ferrarese L. & Merrit, D., 2000, *Astrophys. J.* 539, L9

[61] Freeman K. 1970, *Astrophys. J.* 160, 811

[62] Gebhardt K., et al. 2000a, *Astrophys. J.* 539, L13

[63] Gebhardt K., et al. 2000b, *Astron. J.* 119, 1157

[64] Graham A.W., 2002, *Mon. Not. Roy. Astr. Soc.* 334, 859

[65] Graham A., Lauer T.R., Colless M., & Postman M., 1996, *Astrophys. J.* 465, 534

[66] Graham A. & Colless M., 1997, *Mon. Not. Roy. Astr. Soc.* 287, 221

[67] Gu M., Cao X., & Jiang D.R. 2001, *Mon. Not. Roy. Astr. Soc.* 327, 1111

[68] Guzmán R., Lucey J.R., & Bower R.G. 1993, *Mon. Not. Roy. Astr. Soc.* 265, 731

[69] Haehnelt M.G. & Kauffmann G. 2000, *Mon. Not. Roy. Astr. Soc.* 318, L35

[70] Hernquist L., 1990, *Astrophys. J.* 356, 359

[71] Hubble E. P., 1922, *Astrophys. J.* 56, 162

[72] Hubble E. P., 1926, *Astrophys. J.* 64, 321

[73] Hubble E. P., 1929, *Proc. Nat. Acad. Sci.* (Wash.), 15, 168

[74] Hubble E. P., 1930, *Astrophys. J.* 71, 231

[75] Hubble E. P., 1936, *The Realm of the Nebulae*, (New Haven: Yale University Press).

[76] Hubble E. P. & Humason M.L., 1931, *Astrophys. J.* 74, 43

[77] Hudson M.J., Lucey J. R., Smith R.J., & Steel J., 1997, *Mon. Not. Roy. Astr. Soc.* 291, 488

[78] Illingworth G., 1977, *Astrophys. J.* 218, L43

[79] Isobe T., Feigelson E. D., Akritas M. J., & Babu G.J. 1990, *Astrophys. J.* 364, 104

[80] Jaffe W., 1983, *Mon. Not. Roy. Astr. Soc.* 202, 995

[81] James F. 1994, MINUIT: *Function Minimization and Error Analysis*, (CERN Program Libr. Long Writeup D506) (Version 94.1; Geneva: CERN)

[82] Jedrzejewski R. I., 1987, *Mon. Not. Roy. Astr. Soc.* 226, 747

[83] Jørgensen I., Franx M., Hjorth J., & van Dokkum P.G., 1999, *Mon. Not. Roy. Astr. Soc.* 308, 833

[84] Jørgensen I., Franx M., & Kjærgaard P. 1993, *Astrophys. J.* 411, 34

[85] Jørgensen I., Franx M., & Kjærgaard P. 1995a, *Mon. Not. Roy. Astr. Soc.* 273, 1097

[86] Jørgensen I., Franx M., & Kjærgaard P. 1995b, *Mon. Not. Roy. Astr. Soc.* 276, 1341

[87] Jørgensen I., Franx M., & Kjærgaard P. 1996, *Mon. Not. Roy. Astr. Soc.* 280, 167

[88] Kaspi S., Smith P.S., Maoz D., Netzer H. & Jannuzi B.T., 1996, *Astrophys. J.* 471, L75

[89] Kaspi S. et al. 2000, *Astrophys. J.* 533, 631

[90] Kent S. M., 1984, *Astrophys. J. Suppl.* 56, 105

[91] Kent S. M., 1985, *Astrophys. J. Suppl.* 59, 115

[92] Kelson D. D., Illingworth G.D., van Dokkum P.G., Franx M., Fabricant D., 1997, *Astrophys. J.* 478, L13

[93] Kelson D. D., van Dokkum P.G., Franx M., Illingworth G.D., 2000, *Astrophys. J.* 531, 184

[94] Khosroshahi H.G., 2000, Phd Thesis, Institute for Advanced Studies in Basic Sciences, Iran

[95] Khosroshahi H.G., Wadadekar Y., & Kembhavi A., 2000a, *Astrophys. J.* 533, 162

[96] Khosroshahi H.G., Wadadekar Y., Kembhavi A., & Mobasher B., 2000b, *Astrophys. J.* 531, L103

[97] Knapen J. H., & van den Kruit P. C., 1991, *Astro. Astrophys.* 248, 57

[98] Koratkar A.P. & Gaskell C.M., 1999, *Astrophys. J.* 370, L61

[99] Kormendy J., 1977a, *Astrophys. J.* 217, 406

[100] Kormendy J., 1977b, *Astrophys. J.* 218, 333

[101] Kormendy J., 1993, in *The Nearest Active Galaxies*, ed. J. Beckman, L. Colina, & H.Netzer (Madrid: CSIC), 197

[102] Kormendy J. & Djorgovski S., 1989, *Ann. Rev. Astron. Astrophys.* 27, 235

[103] Kormendy J. & Richstone D., 1995, *Ann. Rev. Astron. Astrophys.* 33, 581

[104] Kodaira K., Watanabe M., & Oamura S., 1987, *Astrophys. J.* 62, 703

[105] Krolik J.H., 2001, *Astrophys. J.* 551, 72

[106] Krolik J.H. et al. 1991, *Astrophys. J.* 371, 541

[107] Larsen R. B., 1969, *Mon. Not. Roy. Astr. Soc.* 145, 405

[108] Larsen R. B., 1975, *Mon. Not. Roy. Astr. Soc.* 173, 671

[109] Larsen R. B., 1990, *Proc. Astr. Soc. Pacific.* 102, 709

[110] Lima Neto G.B., Gerbal D., & Márquez I., 1999, *Mon. Not. Roy. Astr. Soc.* 309, 481

[111] Lucey J.R.& Carter D., 1988, *Mon. Not. Roy. Astr. Soc.* 235, 1177

[112] Lucey J.R., Bower R.G., & Ellis, R.S., 1991a, *Mon. Not. Roy. Astr. Soc.* 249, 755

[113] Lucey J.R., Gray P. M., Carter D., & Terlvich R.J., 1991b, *Mon. Not. Roy. Astr. Soc.* 248, 804

[114] Lucey J.R., Guzmán R., Carter D., & Terlvich R.J., 1991c, *Mon. Not. Roy. Astr. Soc.* 253, 584

[115] Lucey J.R., Guzmán R., Steel J., & Carter D. 1997, *Mon. Not. Roy. Astr. Soc.* 287, 899

[116] Lynden-Bell D., 1969, *Nature.* 223, 690

[117] Lynden-Bell D., 1978, *Phys. Scr.* 17, 185

[118] Lynden-Bell D., Faber S. M., Burstein D., Davies R. L., Dressler A., Terlevich R.J., & Wegner G., 1988, *Astrophys. J.* 326, 19

[119] Magorrian et al. 1998, *Astron. J.* 115, 2285

[120] Mahabal A., 1998, PhD Thesis, University of Pune, India

[121] Márquez I., Lima Neto G. B., Capelato H., Durret F., Lansoni B., & Gerbal D., 2000, *Astro. Astrophys.* 379, 7ż7

[122] McLure R.J. & Dunlop J.S., 2001, *Mon. Not. Roy. Astr. Soc.* 327, 199

[123] McLure R.J. & Jarvis M.J., 2002, *Mon. Not. Roy. Astr. Soc.* 337, 109

[124] Melnick J. & Sargent W.L.M., 1977, *Astrophys. J.* 215, 401

[125] Merrit D. & Ferrarese L., 2001a, *Astrophys. J.* 459, L57

[126] Merrit D. & Ferrarese L., 2001b, in *ASP Conf. Ser. 249, The Central Kiloparsec of Starbursts* and AGNs, ed. J.H. Knapen, J.K. Beckman, I. Shlosman, & T.J. Mahoney, (Sanfrancisco: ASP), 335

[127] Michard R., 1985, *Astro. Astrophys.* 59, 205

[128] Mobasher B., Guzmán R., Aragón-Salamanca A., & Zepf S., 1999, *Mon. Not. Roy. Astr. Soc.* 304, 225

[129] Möllenhoff C., & Heidt J., 2001, *Astro. Astrophys.* 368, 16

[130] Mooney C.Z., Duval R.D., 1993, in *Bootstrapping: A Nonparametric Approach to Statistical Inference*, Newbury Park, CA: Sage Publications

[131] Nilson P., 1973, Uppsala General Catalogue of Galaxies (Uppsala: Astronomiska Obs.)

[132] Nipoti C., Londrillo P., & Ciotti L., 2003, *Mon. Not. Roy. Astr. Soc.* 342, 501

[133] Noreen E., 1989, *Computer Intensive Methods for Testing Hypothesis*. New York: Wiley

[134] Oemler A., 1974, *Astrophys. J.* 194, 1

[135] Oshlack A., Webster R., & Whiting M., 2002, *Astrophys. J.* 576, 81

[136] Osterbrock D. E., 1960, *Astrophys. J.* 132, 325

[137] Ostriker J.P., 2000, *Phys. Rev. Lett.* 84, 5258

[138] Patterson F S., 1940, *Harvard Bull.* 914, 9

[139] Pahre M. A., 1996, *Astron. Astrophys. Suppl.* 189, 2905

[140] Pahre M. A., Djorgovski S. G., & de Carvalho R. R. 1998, *Astron. J.* 116, 1591

[141] Peletier R. F & Balcells M., 1996, *Astron. J.* 111, 2238

[142] Peletier R. F. & Balcells M., 1997, *New Astronomy.* 1, 349

[143] Peterson B.M., 1993, *Proc. Astr. Soc. Pacific.* 100, 18

[144] Phillips A. C., Illingworth G.D., MacKenty J.W., & Franx M., 1996, *Astron. J.* 111, 1566

[145] Pizzela A., Corsini E.M., Morelli L., Sarzi M., Scarlata C., Stiavelli M., & Barota F., 2002, *Astrophys. J.* 573, 131

[146] Pozzetti Bruzual, & Zamorani, 1996, *Mon. Not. Roy. Astr. Soc.* 281, 953

[147] Press W. H., Teukolsky S.A., Vetterling W., T., & Flannery B. P. 1992, *Numerical Receipes in C*, CUP, Cambridge.

[148] Prugniel P. & Simien F., 1996, *Astro. Astrophys.* 309, 749

[149] Quenouille M.H., 1956, *Notes on Bias Estimation.* Biometrika, 61, 353

[150] Ravindranath S., Ho L.C., Peng C.Y., Filippenko A.V., & Sargent W.L.W., 2001, *Astron. J.* 122, 653

[151] Rees M.J., 1984, *Ann. Rev. Astron. Astrophys.* 22, 471

[152] Renzini, A., & Ciotti, L. 1993, *Astrophys. J.* 416, L49

[153] Rest A., van den Bosch F.C., Jaffe W., Tran H., Tsvetanov, Z., Ford H.C., Davies J., & Schafer J., 2001, *Astron. J.* 121, 2431

[154] Reynolds J. H., 1913, *Mon. Not. Roy. Astr. Soc.* 74, 132

[155] Rood H.J., & Sastry G.N., 1972, *Astrophys. J.* 77, 451

[156] Salpeter E.E., 1964, *Astrophys. J.* 140, 796

[157] Sandage A., 1972, *Astrophys. J.* 178, 1

[158] Sandage A. & Visvanathan N., 1978a, *Astrophys. J.* 223, 707

[159] Sandage A. & Visvanathan N., 1978b, *Astrophys. J.* 225, 742

[160] Schechter P. L. & Dressler A., 1987, *Astron. J.* 94, 563

[161] Schombert J. M. & Bothun G. D., 1987, *Astron. J.* 93, 60

[162] Schombert J. M., 1986, *Astrophys. J.* 60, 603

[163] Schweizer F., 1982, *Astrophys. J.* 252, 455

[164] Schweizer F., 1983, *Astrophys. J.* 252, 455

[165] Seigar M., Carollo C.M., Stiavelli M., de Zeeuw P.T., & Dejonghe H. 2002. *Astron. J.* 123, 184

[166] Sersic J. L., 1968, *Atlas de Galaxies Australes*, (Cordoba; Observatorio Astronomica)

[167] Silk J., 1978, *Astrophys. J.* 220, 390

[168] Simard et al. 2002, *Astrophys. J. Suppl.* 142, 1

[169] Simien F., 1989, *The World of Galaxies*, ed. H. G. Corwin, Jr., & L. Bottinelli (New York: Springer), 293

[170] Slipher V M., 1914, *Lowell Obs. Bull.* 2, 62

[171] Strom K.M., & Strom S.E., 1978, *Astron. J.* 83, 1293

[172] Tinsley B. M. & Gunn J.E., 1976, *Astrophys. J.* 203, 52

[173] Tinsley B. M. & Larsen R. B., 1979, *Mon. Not. Roy. Astr. Soc.* 186, 503

[174] Tonry J. L., & Davis M., 1981, *Astrophys. J.* 246, 680

[175] Toomre A., 1977, *The Evolution of Galaxies and Stellar Populations*, ed. Tinsley B. M. & Larson R. B. (New Haven: Yale University Press), p. 401

[176] Tremaine S. et al. 2002, *Astrophys. J.* 574, 740

[177] Tukey J.W., 1958, *Exploratory Data Analysis*. Addison Wesley

[178] Tully R. B. & Fisher J.R., 1977, *Astro. Astrophys.* 54, 661

[179] van de Ven G., van Dokku P.G., & Franx, M., 2003, *Mon. Not. Roy. Astr. Soc.* 344, 924

[180] van den Bergh S., 1989, *Proc. Astr. Soc. Pacific.* 101, 1072

[181] van Dokkum P.G. & Franx M. 1996, *Mon. Not. Roy. Astr. Soc.* 281, 985

[182] van Dokkum P.G. & Stanford S.A., 2001, *Astrophys. J.* , 562, L101

[183] van Dokkum P.G. & Stanford S.A., 2003, *Astrophys. J.* , 585, 78

[184] van Dokkum P.G., Franx M., & Kelston D. D., & Illingworth G.D.1998, *Astrophys. J.* 504, L17

[185] van Houten C. J., 1961, *Bull. Astron. Inst. Netherlands.* 16, 1

[186] Vestergaard M., 2002, *Astrophys. J.* 571, 733

[187] Visvanathan N. & Sandage A., 1977, *Astrophys. J.* 216, 214

[188] Vogt N. P., Forbes D.A., Philips A. C., Gronwall C., Faber S.M., Illingworth G.D., & Koo D.C., 1996, *Astrophys. J.* 465, L15

[189] Wadadekar Y., Robbason R., & Kembhavi A., 1999, *Astron. J.* 117, 1219

[190] Wandel A., Peterson B.M., & Makkan M.A., 1999, *Astrophys. J.* 526, 579

[191] White S. D. M. & Rees M. J., 1978, *Mon. Not. Roy. Astr. Soc.* 183, 341

[192] Worthey G., 1994, *Astrophys. J. Suppl.* 95, 107

[193] Woo J. & Urry M., 2002, *Astrophys. J.* 579, 530

[194] Wu X-B. & Han J.L., 2001, *Astro. Astrophys.* 380, 31

[195] Yoshizawa M. & Wakamatsu K., 1975, *Astro. Astrophys.* 44, 363

[196] Young C.K. & Currie M.J., 1998, *Astro. Astrophys.* 333, 795

[197] Young P. J., 1976, *Astron. J.* 81, 807

[198] Zel'dovich Ya.B., 1964, *Sov. Physi. Dokl.* 9, 195

[199] Zepf. S., & Silk, J. 1996, *Astrophys. J.* 466, 114

[200] Ziegler B.L., et al. 2002, *Astrophys. J.* 564, L69